

Ministry of Science and Higher Education of the Russian Federation
Far Eastern Federal University

**The 11TH ANNUAL STUDENT SCIENTIFIC
CONFERENCE IN ENGLISH**

Vladivostok

May 2024

CONFERENCE PROCEEDINGS

Scientific electronic publication

Vladivostok
Far Eastern Federal University 2024

**THE 10th ANNUAL STUDENT SCIENTIFIC CONFERENCE IN ENGLISH
Vladivostok, May 2023**

UDC 082
LBC 94.3
T44

Editorial board:

Chief editor – V.Y.Ermachenko

Scientific editors – K.R. Frolov, I.L. Artemeva, K.V. Gorobets,

L.G. Moskovchenko, A.V. Shirokova, E.A. Elsykova.

Editors - G.L. Ardeeva, V.B. Kolycheva, E.V. Kravchenko, I.N. Lazareva,
O.K. Titova, I.F. Veremeeva, A.V. Shtramilo, Y.O. Kamornaya.

The 11th annual student scientific conference in English,
Vladivostok, May 2024 [Electronic resource]: conference
proceedings / Chief editor V.Y.Ermachenko. – Electr. dat. –
Vladivostok: Far Eastern Federal University, 2024. Uniform Resource
Locator: https://www.dvfu.ru/institute_of_high_technologies_and_advanced_materials/Conferences/. – Title screen.

ISSN 2686-9454

The collected volume contains proceedings of the contest of scientific
reports in English and the results of scientific studies made by students,
master's degree students and postgraduate students of the FEFU May 2024.

UDC 082

LBC 94.3

Text electronic edition

Minimum System Requirements:

Минимальные системные требования:

Web browser Internet Explorer 6.0 or higher,

Opera version 7.0 or higher,

Google Chrome version 3.0 or higher

a computer with Internet access

Volume 9.8 MB

Far Eastern Federal University
690922, Vladivostok, Russky Island, 10 Ajax Bay,

© FEFU, 2024

CONTENTS

Section I BIOLOGY AND ECOLOGY.....	6
Alaverdov E.S., Degtyarenko A.I. BETAINES AS FACTORS OF PLANT RESISTANCE: ACHIEVEMENTS AND PROSPECTS	6
Brak G.M. SPECIES OF THE GENUS <i>ERRINOPORA</i> FISHER, 1931 (CNIDARIA: HYDROZOA: STYLASTERIDAE) FROM THE WATERS OF THE KURIL ISLANDS	7
Burylova A.L. Sabutsky Y.E. BIOLOGICAL ACTIVITY OF NEW THIOGLYCOSIDE DERIVATIVES OF 1,4-NAPHTHOQUINONE	9
Variushina K.I. COMMUNITY-FORMING ROLE OF BROWN ALGAE OF THE GENUS SACCHARINA IN MARINE ECOSYSTEMS OF THE BOREAL BELT	11
Gerasimova V.Yu. <i>CECINA TATARICA</i> (GASTROPODA, POMATIOPSIDAE) – A NEW SPECIES OF MOLLUSKS FOR RUSSKY ISLAND (SEA OF JAPAN, PETER THE GREAT BAY)	13
Dmitrenko G.D. Zhankov G.V. Ardeeva G.L. CONTENT OF AVAILABLE PHOSPHATES IN SOILS OF DIFFERENT MANUFACTURERS.....	15
Zhankov G.V., Dmitrenko G.D., Ardeeva G.L pH PROPERTIES OF SOILS FROM VARIOUS MANUFACTURERS.....	16
Zamurueva V. V. THE FIRST STAGES OF OVERGROWTH OF GAPS IN THE CANOPY OF A STAND IN BLACK FIR-CEDAR-DECIDUOUS FORESTS	18
Katugina L.O. PHYLOGENETIC RELATIONSHIPS OF THE MOLLUSCS <i>KOREOLEPTOXIS</i> <i>AMURENSIS</i> (SEMISULCOSPIRIDAE) BASED ON MOLECULAR MARKERS	19
Kashina A.A., Zavalnaia E.G. IDENTIFICATION OF PIWI PROTEIN AS A STEM CELL MARKER IN SOMATIC TISSUES OF SEA CUCUMBER <i>APOSTICHOPUS JAPONICUS</i>	20
Nagornaya O.A. EFFICIENCY OF CARBON FOOTPRINT ABSORPTION IN VLADIVOSTOK DUE TO MARINE SUBMERGENT VEGETATION OF PETER THE GREAT BAY	22
Oskerko S.E. THE ROLE OF EELGRASS (<i>ZOSTERA MARINA</i> L.) IN MARINE COMMUNITIES AND ITS POTENTIAL FOR CLIMATE CHANGE MITIGATION.....	22
Rostovtseva M.O. DESCRIPTION OF <i>RHODYMENICHTHYS DOLICHOGASTER</i> LARVAE FROM PETER THE GREAT BAY	24
Rudenko D.A., Shkryl Y.N. THE INFLUENCE OF THE <i>ROLB</i> AND <i>ROLC</i> GENES ON THE COMPOSITION OF SECONDARY METABOLITES OF <i>ARISTOLOCHIA MANSURIENSIS</i> AND STUDY OF THEIR ANTICANCER ACTIVITY	25
Ryabtseva S.D. <i>SACHALINOCETUS CHOLMICUS</i> (ODONTOCETI: SQUALODONTIDAE): SKULL MORPHOMETRY AND CRANIAL RECONSTRUCTION.....	27
Teshchina Z.V., Pianova A.S., Kameneva L.A., Berdasova K.S. INTRODUCTION OF <i>ASTRAGALUS</i> <i>ULIGINOSUS</i> L. (FABACEAE) INTO IN VITRO CULTURE	28
Thai H.N., Tsarenko N.A., Zorina E.V. THE POLLEN GRAIN VIABILITY OF THE GARDEN ROSE COLLECTION OF THE BOTANICAL GARDEN-INSTITUTE FEB RAS	30
Yachmen L.P., Biklibayeva A.R., Gilyov A.M., Sukhin D.V., Sotskaya A.A., Lapshina N.V., Ardeeva G.L DYNAMICS OF SWEET BASIL (<i>OCIMUM BASILICUM</i>) DEVELOPMENT ON VARIOUS SUBSTRATES WITH THE APPLICATION OF MINERAL FERTILIZER IN A HYDROPONIC SETUP	31
Section II CHEMISTRY AND CHEMICAL TECHNOLOGY.....	34
Artemov P.M., Frolov K.R. PHYSICOCHEMICAL MODELING OF DALNRGORSK DISTRICT ACID MINE DRAINAGE	34

THE 11th ANNUAL STUDENT SCIENTIFIC CONFERENCE IN ENGLISH
Vladivostok, May 2024

Vashchenko M.V. THE STUDY OF METABOLITES OF 2,3,6,-TRIHYDROXY-7-METHYLNAPHTHAZARIN, A FUNCIONAL ANALOGUE OF ECHINOCHROME USING A DEUTERIUM LABEL	35
Gavrik A.E., Kovshun A.A. COMPARISON OF SCHEMES FOR UTILIZATION OF ALKALINE HYDROLYSATES OF RICE HULLS TO OBTAIN SOLID PRODUCTS	36
Emelianova V. G., Shchitovskaya E. V., Kolzunova L. G. ELECTROCHEMICAL SYNTHESIS OF POLYMER COMPOSITES WITH INCLUSION OF NOBLE METAL NANOPARTICLES	37
Ivanov N.P., Rastorguev V.L., Marmaza P.A., Seroshtan A.I., Dran'kov A.N., Shichalin O.O. HYDROPHOBIZATION OF MAGNETIC SORPTION MATERIALS BASED ON LAYERED DOUBLE HYDROXIDES FOR SELECTIVE OIL REMOVAL.....	40
Ivanov N.P., Gurin M.S., Seroshtan A.I., Shichalin O.O. ELECTROCHEMICAL ACTIVITY OF Ti ₂ AlC/TiC MAX-PHASE COMPOSITE CERAMICS OBTAINED BY SPARK PLASMA SINTERING	43
O. V. Kapustina, Ya. G. Zernov, S. M. Pisarev COMPONENT RATIO EFFECT ON THE BIOCOMPOSITE PROPERTIES FOR BONE REGENERATION	45
Marmaza P.A., Ivanov N.P., Kaptakov V.O. HYDROTHERMAL SYNTHESIS OF DUAL-CATION GRACE TITANOSILICATE FOR EFFICIENT ¹³⁷ Cs REMOVAL FROM LIQUID WASTE WITH HIGH SALINITY	47
Marchenko A.V. EXPLORATION OF THE ACTIVE SPECIES IN THE PHOTOCATALYTIC DEGRADATION OF METHYL ORANGE UNDER UV LIGHT IRRADIATION	48
Orinicheva P.D., Kharchenko V.G., Tsyganok V.S., Frolov K.R. TAILING DUMPS OF DALNEGORSK MINING AND PROCESSING PLANT: WASTE CHARACTERIZATION, IMPACT ON THE HYDROSPHERE.....	50
Pisarev S.M., Lembikov A.O., Kolodeznikov E.S. , Marmaza P.A. STRENGTHENING OF TITANIUM COMPOSITE BY MICRO- AND NANO-ENTROPIC SYSTEMS OBTAINED BY SPARK PLASMA SINTERING METHOD.....	51
Savelyeva N.Yu., Balybina V.A., Kuular J.S., Kokorina N.G. SYNTHESIS AND STUDY OF FERROCYANIDE-BASED COMPOSITE MATERIALS FOR CESIUM RECOVERY FROM LIQUID MEDI	52
Section III EARTH SCIENCE.....	54
Grebennik P.V. THE COMPARISON OF THE HYDROLOGICAL CHARACTERISTICS OF THE SOUTHEASTERN AND SOUTHWESTERN COASTAL WATERS OF THE KAMCHATKA PENINSULA OBTAINED DURING CTD-SENSING ON CRUISE 23/4 OF THE RV "PROFESSOR MULTANOVSKY"	54
Denga V.S. FEATURES OF THE QUATERNARY GLACIATION OF THE EASTERN FLANK OF THE BUREINSKOYE HIGHLANDS (SOUTH OF THE FAR EAST)	55
Kuzmina N.A. THE INFLUENCE OF COMFORT INDICATORS ON THE COST OF RENTING A ONE-ROOM APARTMENT ON THE EXAMPLE OF SOVETSKY DISTRICT, VLADIVOSTOK.....	57
Malitskii S.I. SPATIAL DIFFERENTIATION OF THE SOCIO-ECONOMIC COMPLEX OF THE COASTAL ZONE OF PRIMORSKY KRAI	59
Potapov L.O., Makarchuk I.M. ASSESSMENT OF THE MICROCLIMATE OF THE FEFU CAMPUS	60
Section IV MATHEMATICS AND COMPUTER SCIENCES	64
Alekseitceva N.D. ANALYSIS AND MODEL CONSTRUCTION FOR DISTRIBUTION OF ANTI-THEFT SYSTEMS SUBJECT AREA	64
Bakhtin K.E. GENERALIZATIONS OF KARLSSON-MINTON SUMMATION FORMULAS FOR HYPERGEOMETRIC FUNCTIONS OF THE IPD TYPE	66
Cherkasov M.D. THE PRINCIPLE OF OPERATION OF THE PARALLEL TEMPERING ALGORITHM IN THE ISING MODEL	67

THE 11th ANNUAL STUDENT SCIENTIFIC CONFERENCE IN ENGLISH
Vladivostok, May 2024

Daquan Yu THE METHOD OF TORQUE CONTROL FOR UPPER LIMB REHABILITATION ROBOT	69
Dranov S.V., Afanasyeva S.D. NUMERICAL SIMULATION OF NAVIER-STOKES BLOOD FLOW MODEL IN AN ARTERY WITH A NARROWING CHANNEL USING NEURAL NETWORKS AND FINITE ELEMENT METHOD.....	72
Frolov A.A. AI-BASED CHEATING PREVENTION ON E-LEARNING PLATFORMS.....	75
Gerus P.A., Protsenko D.V. DEVELOPMENT OF A PROTOTYPE SOFTWARE SYSTEM FOR TEACHING WRITTEN ENGLISH	76
Kobzar D.A. THE USE OF AUGMENTED REALITY IN APPLICATIONS WITH MOVABLE CAMERA	78
Kuchapina S.S. THE DEVELOPMENT OF A RECOMMENDATION SYSTEM FOR PREDICTING THE OCCURRENCE OF FOREST FIRES USING METEOROLOGICAL DATA	80
Lobanova E.A., Strongin V.S. ENERGY DISTRIBUTION OF APAMEA LATTICE VERTICES FOR SPIN ICE	82
Malikov V. P. MODEL OF AUTONOMOUS DRIVING USING OBSTACLE DETECTION BASED ON RAY TRACING AND NEURAL NETWORK	83
Moiseev D.A., Vayay M.S. DEVELOPMENT OF A SOFTWARE TOOL FOR ANALYSING ARBITRAGE SITUATIONS ON FINANCIAL MARKETS OF "ARBITRUM"	84
Moskovchenko Z.A. DEVELOPMENT OF A PROGRAM FOR CONTROLLING A ROBOTIC TRAINER USING ROBOTICS OPERATING SYSTEM	86
Nazarov M.S., Kurbanov M.M., Pestryak N.E. VST PLUGIN FOR AUTOMATIC EQUALIZATION.....	87
Sakharov I.A. DEGREES OF SEMANTIC AND SYNTACTIC RIGIDITY OF CONNECTED UNARS WITHOUT LEAVES.....	88
Shutov K.S. CREATING AN ARCHITECTURAL SOLUTION FOR DRONE CONTROL IN AUTONOMOUS AND REMOTE MODES	90
Simakov V.K. ČECH COHOMOLOGIES OF A SINGLE-ELEMENT FAMILY	91
Vasileva N.B., Pugach P.A. TRAINING OF THE APPLIED AI "RAZUM AI" ALGORITHMS FOR FINDING THE SHORTEST SPANNING TREES	92
Section V PHYSICS	95
Amelkina N.O. META-SUBJECT PHYSICAL TASKS	95
Bunkov V.V. SEMANTIC STRUCTURING OF THE HALL EFFECT AND ELECTRICAL CONDUCTIVITY	97
Gordienko Y.D. ON THE CONCEPTS OF INERTIA AND INERTNOST IN SCHOOL PHYSICS TEXTBOOKS BY DIFFERENT AUTHORS	98
Didenko Y. P., Shut M. V., Sorokin M. A. HYDROLOGY INHOMOGENEITY INFLUENCE ON SOUND PROPAGATION IN SHALLOW SEA WAVEGUIDES	100
Sokirkina D. V., Tkachenko P. D., Skorobogatov D. E., Sorokin M. A. BATHYMETRY INHOMOGENEITY INFLUENCE ON SOUND PROPAGATION IN SHALLOW SEA WAVEGUIDES	101
Lisovitckii.A.S. POSSIBLE EARTHQUAKE PRECURSORS IN THE EARTH'S CRUST MICRO DEFORMATIONS	102
Stepanov D. V. INVESTIGATION OF THE DIRAC OPERATOR SPECTRUM IN TWO PHASES OF MATTER	105
Pochinok A.S., Goy V.A. PARAMETRIZATION OF COUPLE CONSTANTS IN THE ANISOTROPIC LATTICE MODEL	107
Tsuranova M.E. PHOTOMETRIC STUDIES OF THE CATACLYSMIC VARIABLE YZ CNC STAR....	109

Section I

BIOLOGY AND ECOLOGY

Alaverdov E.S.¹, Degtyarenko A.I.²

BETAINES AS FACTORS OF PLANT RESISTANCE: ACHIEVEMENTS AND PROSPECTS

¹Far Eastern Federal University, Institute of the World Ocean, FEFU

²Federal Scientific Center of the East Asia Terrestrial Biodiversity FEB RAS

³Far Eastern Federal University, Oriental Institute School of Regional and International Studies

Scientific adviser – Y.A. Yugay³

Scientific consultant – G.L. Ardeeva³

An increasing number of areas are affected by drought due to climate change and anthropogenic pollution increases soil salinization, making them unsuitable for cultivation [1]. The ability to accumulate betaines, being trimethyl derivatives of amino acids, is one of the most important mechanisms providing the possibility of plant growth in adverse conditions. A significant amount of betaine is contained by members of the families Plumbaginaceae [2] and Poaceae [3] Members of the families Plumbaginaceae [2], and Poaceae [3] contain significant amounts of betaines. The use of betaines significantly increases plant resistance to cold [4, 5], osmotic [6], salt [7], water [8] stress as well as cell freezing stress [5], drought [9], and heavy metal salts [10]. All these positive grounds give reason to speak about the high efficiency of using betaines in national economy both applied exogenously and as a strategy of varieties improvement by genetic engineering methods. Betaines stabilize the tertiary structure of proteins [11], protect cell membranes [12], support photosynthesis under stressful conditions [13], reduce reactive oxygen species (ROS) [12], activate ROS detoxification systems [14] and affect gene expression [14] resulting in increased stress tolerance and plant productivity.

Despite the large number of publications confirming the link between adaptive changes and osmolyte accumulation, the data available today are insufficient to form a mechanistic understanding of the action of betaine on genetic and enzymatic systems. The mechanisms of betaine impact on cell membrane stability and enzyme activity under adverse environmental conditions remain incompletely studied. To date, the causes of changes in the expression levels of some genes associated with the accumulation of glycine betaine are unknown. The efficiency of the metabolic pathway of choline oxidation compared to the use of glycine methylation enzymes in the development of genetically modified crop varieties also requires more detailed study. Despite the discovery of the β-alanine methylation pathway [15, 16], there are no experimental data on the use of β-alanine betaine, including by genetic engineering of plants to increase crop yield and stress resistance.

References

1. Smith, P. Which practices co-deliver food security, climate change mitigation and adaptation, and combat land degradation and desertification? / P. Smith et al. // Global Change Biology . – 2020. – №3. – C. 1532-1575.
2. Hanson, A.D. Osmoprotective compounds in the Plumbaginaceae: A natural experiment in metabolic engineering of stress tolerance / A.D. Hanson et al. // Proceedings of the National Academy of Sciences of the United States of America. – 1994. – №1. – C.306–310.
3. Servillo, L. The betaine profile of cereal flours unveils new and uncommon betaines / L. Servillo, et al. // Food Chemistry. – 1994. – №1. – C. 234-241.
4. Kishitani, S. Accumulation of glycine betaine during cold acclimation and freezing tolerance in leaves of winter and spring barley plants / S. Kishitani et al. // Plant Cell Environ. – 1994. – №17. – 89–95.
5. Allard, F. Betaine improves freezing tolerance in wheat / F. Allard et al. // Plant and Cell Physiology. –

**THE 11th ANNUAL STUDENT SCIENTIFIC CONFERENCE IN ENGLISH
Vladivostok, May 2024**

1998. – №11. – C.1194-1202.

6.Gibon, Y. Is glycine betaine a noncompatible solute in higher plants that do not accumulate it? / Y. Gibon et al. // *Plant Cell Environ.* – 1997. – №20. – C.329–340

7.Wang, Y., Changes in chlorophyll, ribulose bisphosphate carboxylase - oxygenase, glycine betaine content, photosynthesis and transpiration in *Amaranthus tricolor* leaves during salt stress./ Y.Wang,Nii, N. // *The Journal of Horticultural Science and Biotechnology.* – 2000. – №75– C.623–627.

8.Chołuj, D. Influence of long-term drought stress on osmolyte accumulation in sugar beet *Betavulgaris* L. plants./D.Chołuj et al. //*Acta Physiologiae Plantarum.* – 2008. – №30 – C.679–687.

9.Díaz-Zorita, M. Applications of foliar fertilizers containing glycine betaine improve wheat yields./M. Díaz-Zorita et al //*Journal of Agronomy and Crop Science.* – 2001. – №186 – C.209–215.

10.Shafaqat, A. Glycine Betaine Accumulation, Significance and Interests for Heavy Metal Tolerance in Plants/ A. Shafaqat et al.// *Cryo Letters.* – 2020. – №9 – C.896.

11.Incharoensakdi, A. Effect of Betaine on Enzyme Activity and Subunit Interaction of Ribulose-1,5-Bisphosphate Carboxylase / Oxygenase from *Aphanothecce halophytica*. / A. Incharoensakdi et al. //*Plant Physiologia.* – 1986. – №81 – C.1044-1049.

12.Chen W.P. Glycine betaine increases chilling tolerance and reduces chilling-induced lipid peroxidation in *Zea mays* L. / W. P. Chen et al.//*Plant, Cell & Environment.* – 2001.

13.Hidenori, H. Transformation of *Arabidopsis thaliana* with the *codA* gene for choline oxidase; accumulation of glycine betaine and enhanced tolerance to salt and cold stress/ H. Hidenori et al. //*The Plant Jornal*– 2003– №2.

14.Weijuan, F. Improved tolerance to various abiotic stresses in transgenic sweet potato *Ipomoea batatas* expressing spinach betaine aldehyde dehydrogenase / F. Weijuan.et al. //*PLoS One.* – 2012. – №5.

15.Rathinasabapathi, B. β-Alanine Betaine Synthesis in the Plumbaginaceae. Purification and Characterization of a Trifunctional, S-Adenosyl-L-Methionine-Dependent *N*-Methyltransferase from *Limonium latifolium* Leaves / B. Rathinasabapathi et al.// *Plant Physiologia.* – 2001. – №126 – C. 1241–1249.

16.Suresh B. β-alanine N-methyltransferase of *Limonium latifolium*. cDNA cloning and functional expression of a novel N-methyltransferase implicated in the synthesis of the osmoprotectant beta-alanine betaine/Suresh Babu Raman et al// *Plant Physiologia.* – 2003. – №132 – C. 1642-1651.

Brak G.M.¹

SPECIES OF THE GENUS *ERRINOPORA* FISHER, 1931 (CNIDARIA: HYDROZOA:

STYLASTERIDAE) FROM THE WATERS OF THE KURIL ISLANDS

¹Far Eastern Federal University, Institute of the World Ocean, FEFU

²A.V. Zhirmunsky National Scientific Center of Marine Biology, FEB RAS

³Far Eastern Federal University, Oriental Institute-School of Regional and International Studies, FEFU

Scientific advisor – T.N. Dautova²

Scientific consultant – O.K. Titova³

Styasteridae (commonly known as lace corals) is the most species-rich family of hydrocorals. It is widely distributed and of great importance to humans and marine ecosystems. Single colonies serve as a substrate for the attachment of various bottom inhabitants. Moreover, the very presence or absence of hydroids in a particular water area may indicate the degree of pollution. Despite its importance, it is still poorly known, especially in Russian waters [2, 3].

In this work we reviewed the material collected during the LV-86 expedition to the Kuril Islands in 2019.

THE 11th ANNUAL STUDENT SCIENTIFIC CONFERENCE IN ENGLISH
Vladivostok, May 2024

Samples were examined using binocular Zeiss Stemi 508. These 5 species of the genus *Errinopora* were found (Table 1). Images of the colony surface were obtained using a Zeiss Evo 40 scanning electron microscope.

Table 1. Locations of collected Kuril species

<i>Number of station</i>	<i>Date</i>	<i>The area of work</i>	<i>Coordinates</i>	<i>Depth (m)</i>	<i>Species</i>
4	27.06.19	Pacific ocean, Kuril Islands, Urup Island	45° 55.2 N 150° 15.8E	169-150	<i>Errinopora stylifera</i> <i>Errinopora sp. aff. dichotoma</i> <i>Errinopora sp.</i>
3	27.06.19	Pacific ocean, Kuril Islands, Urup Island	45°35.5 N 149°47.7 E	145-142	<i>Errinopora nanneca</i>
6	28.06.19	Okhotsk sea, Kuril Islands, Urup Island	46°16.8 N 150°14.9 E	174-128	<i>Errinopora sp. cf. porifera</i>

All of the described species were discovered by trawling the bottom at depths of 142-174 m. It is known, that in the area of the Kuril Islands, at a depth of about 100 m, there is a rocky bottom, to which the larvae of hydroids preferably attach. This may contribute to the distribution of representatives of the family Stylasteridae in the study area [1].

The main problem of identification is in the lack of research in Russian waters. The last work was written in 1960 by Naumov. Since the writing of his monograph, there have been no publications on the research of hydrocorals of the Far Eastern Seas. Since then, new research methods and a new terminology have been introduced for the family Stylasteridae. Also, the systematic position of some of the objects described in Naumov's monograph has been changed.

In this work, we described 2 more species of the genus *Errinopora*, which had not been previously observed around the Kuril Islands: *Errinopora nanneca*, previously described only for the Aleutian Islands [4], and *Errinopora sp. aff. dichotoma*. These species were already known in the Northern Pacific, the lack of their description in the Kuril Islands area can probably be explained by the insufficient number of studies of stylasterids in Russian waters.

The species described in Naumov's monograph were discovered: *E. stylifera* and *E. porifera*. The reason for the absence of their descriptions from other waters (including the Aleutian Islands) is not reliably known. This can probably also be attributed to the lack of research. Diagnosis of the species *E. porifera* is given for the first time (taking into account the data of Naumov, 1960). An expanded description of the morphology of representatives 60 years after the publication of D.V. Naumov is given. It is worth noting, that *E. porifera* is found only in the area of the Kuril Islands and in the future, it can be considered as an endemic of this area.

References

1. Antsulevich, A.E. Hydroids of the shelf of the Kuril Islands / A.E. Antsulevich // L.: Zoological institute of the USSR Academy of Sciences. – 1987. – 365 p.
2. Malyutin, A.N. Deep-sea (cold-water) coral communities of the Northern Pacific and problems of their conservation / A.N. Malyutin // Russian Journal of Marine Biology. – 2015. – vol. 41, №1. – P. 3-12
3. Naumov, D.V. Hydroids and hydromeduses of marine, brackish and freshwater basins of the USSR / D.V. Naumov // M.; Leningrad: Publishing House of the USSR Academy of Sciences, 1960. – 585 p.
4. Cairns, S.D. Global Diversity of the Stylasteridae (Cnidaria: Hydrozoa: Athecatae) / Stephen D. Cairns // — 2011. — July 22. — P.1-12

Burylova A.L.¹ Sabutsky Y.E.²

BIOLOGICAL ACTIVITY OF NEW THIOLYCOOSIDE DERIVATIVES OF 1,4-NAPHTHOQUINONE

¹Far Eastern Federal University, Institute of the World Ocean (School), FEFU

²G.B. Elyakov Pacific Institute of Bioorganic Chemistry PIBOC FEB RAS

³Institute of Oriental Studies - School of Regional and International Studies, FEFU

Scientific adviser - Menchinskaya E.S.²

Scientific consultant - G.L. Ardeeva³

One of the tasks of modern biochemistry is to establish the functional properties of biochemical compounds and their introduction into medicine as therapeutic drugs and tools for controlling biological systems.

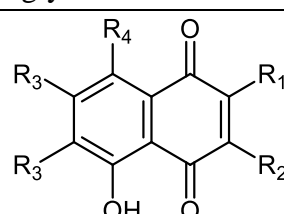
Natural 1,4-naphthoquinones (1,4-NQ) are secondary metabolites with a wide range of biological activities. Such properties as antimicrobial, anti-inflammatory and antifungal activity are characteristic of these compounds. Also 1,4-NQ possess pronounced cytotoxicity. Modification of natural compounds can lead to obtaining substances with enhanced or new biological activity.

All the above-mentioned indicates the relevance of the study of 1,4-NQ derivatives, as it can provide new knowledge about the mechanism of their action as natural bioregulators and the creation of drugs that will be necessary for humans in the future.

The aim of this work is to study the biological activity of 40 new thioglycoside derivatives of substituted 1,4-NQ obtained in the laboratory of organic synthesis of PIBOC FEB RAS with respect to different human tumor cell lines.

A comparative study of the effect of thioglycoside derivatives of 1,4-naphthoquinone on different human tumor cell lines: neuroblastoma SH-SY5Y, colon adenocarcinoma HCT-116, leukemia THP-1 and cervical adenocarcinoma Hela was carried out. The non-tumor cell line of human embryonic kidney HEK-293 was used for comparison. The table shows the structures of the most active thioglycoside derivatives (Table 1).

Table 1
Chemical structure of thioglycoside derivatives of 1,4-naphthoquinone



#	Code	R ₁	R ₂	R ₃	R ₄
5	U-697	OEt	AGSCH ₂	Cl	OH
12	U-704	AGSCH ₂	OMe	H	H
39	U-732	OMe	EAGSCH ₂	H	H
40	U-733	OMe	BAGSCH ₂	H	H

THE 11th ANNUAL STUDENT SCIENTIFIC CONFERENCE IN ENGLISH
Vladivostok, May 2024

The Hela cervical cancer cell line turned out to be the most sensitive to the action of 1,4-NQ compared to other tumor cells, so it was chosen for further study of the effect of thioglycoside derivatives of 1,4-NQ on migration and colony formation. The most active thioglycoside derivatives were selected: U-697 (5), U-704 (12), U-732 (39), U-733 (40), showing a pronounced cytotoxic effect in the micromolar concentration range, with $EC_{50} \leq 10 \mu\text{M}$ (Table 2, Fig. 1).

Table 2

Cytotoxic activity of thioglycoside derivatives of 1,4-naphthoquinone

Code	Cell lines, EC_{50} mM				
	Hela	HCT-116	THP-1	SH-SY5Y	HEK-293
U-697 (5)	3.84	4.72	5.75	6.67	3.87
U-704 (12)	3.77	3.49	8.18	8.44	5.99
U-732 (39)	3.95	5.09	4.74	4.3	4.41
U-733 (40)	3.54	4.39	4.88	3.71	4.47

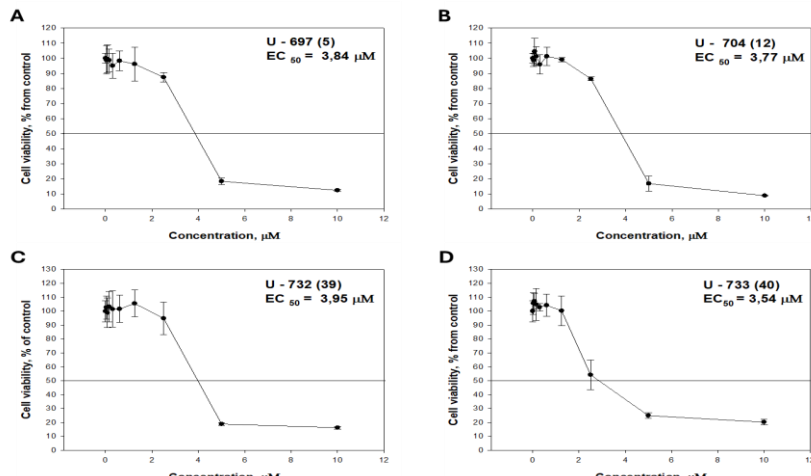


Fig. 1. Cytotoxic effect of thioglycoside derivatives of 1,4-naphthoquinone: (A)—U-697 (5); (B)—U-704 (12), (C)—U-732 (39), and (D)—U-733 (40) on Hela cells for 24 h. All experiments were carried out in triplicate. The data are presented as mean \pm SEM.

It was found that the studied thioglycoside derivatives statistically significantly block colony growth and inhibit migration of Hela tumor cells. Thus, U-697 (5), U-732 (39) and U-733 (40) at a concentration of 2 μM inhibit the growth of tumor cell colonies by 90% and more. It is also worth noting that U-732 (39) and U-733 (40) at a concentration of 1 μM inhibited the growth of tumor cell colonies by 55% and 80%, respectively (Fig. 2).

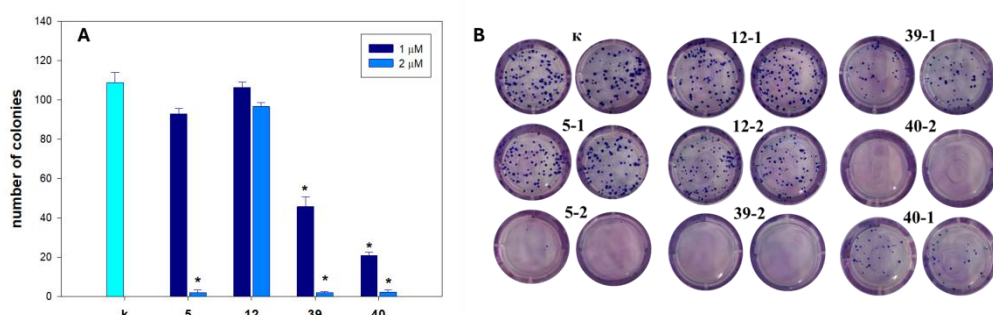


Fig. 2. The number of HeLa cell colonies when treated with different concentrations of thioglycoside derivatives of 1,4-NQ (A). Image J 1.52 software was used to count the cell colonies. Data are presented as means \pm SEM. * p value ≤ 0.05 considered significant. The colony of HeLa cells treated with different concentrations of thioglycoside derivatives of 1,4-NQ (B).

**THE 11th ANNUAL STUDENT SCIENTIFIC CONFERENCE IN ENGLISH
Vladivostok, May 2024**

When exposed to U-732 (39) and U-733 (40) at concentrations of 1 and 2 μM , the effect of inhibition and complete blocking of cell migration was observed. At the same time, compounds 5 and 12 at the same concentrations do not have the ability to inhibit the migration process. (Fig. 3).

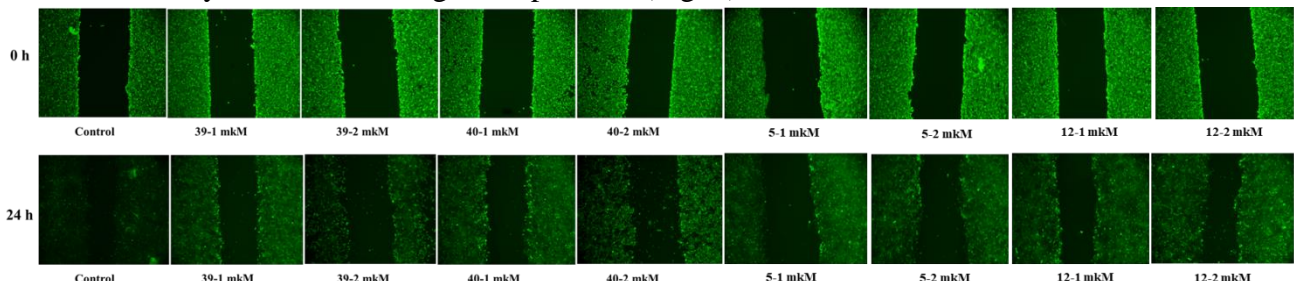


Fig. 3. Migration of HeLa cells into wound areas observed by using a tenfold fluorescence microscope MIB-2-FL.

Selected 1,4-NQ are able to reliably detect colony growth and tumor cell migration in the micromolar concentration range. Thus, they are promising compounds for studying the mechanisms of their antitumor action.

Variushina K.I.¹

COMMUNITY-FORMING ROLE OF BROWN ALGAE OF THE GENUS SACCHARINA IN MARINE ECOSYSTEMS OF THE BOREAL BELT

¹Far Eastern Federal University, Institute of the World Ocean, Department of Ecology, FEFU

²Far Eastern Federal University, Oriental Institute-School of Regional and International Studies, FEFU

Scientific adviser – Y.A. Galysheva¹

Scientific consultant - O.K. Titova²

Saccharina is a genus of large brown macroalgae, mostly distributed on the littoral and upper sublittoral in the temperate climate zone. The most abundant *Saccharina* thickets are located mainly in the horizon of 5-15 meters, where the most favorable conditions for its life are formed - the best lighting and active water movement. Within the boreal belt the most extensive areas of distribution are formed by species of *S. angustata*, *S. gurjanovae*, *S. latissima*, *S. japonica*, *S. cichorioides*. In addition, it is impossible not to mention the species *Hedophyllum bongardianum*, massively distributed in the Far Eastern region of the northern hemisphere, previously also referred to the genus *Saccharina*.

S. angustata is widespread both in the North Atlantic and the North Pacific, playing a huge role in the formation of primary production of coastal ecosystems, as well as the composition of benthic communities of this zone. In the Russian Far East, its thickets are distributed from the southern Kurils to the south of Primorsky Krai. *S. angustata* is one of the main commercial species. In the Kuril region there are significant stocks of this species, estimated at 200-281 thousand tons [1]. The biocenosis formed by *S. angustata* often includes the polychaetes *Chaetozone setosa*, *Capitella capitata*, *Nothria hyperborea*, the bivalves *Macoma nipponica*, *Liocyma fluctuosa*, *Spisula sachalinensis*, the amphipods *Eohaustorius cheliferu*, *Grandifoxus longirostris*, the ten-legged crayfish *Pagurus ochotensis*, *P. brachiomastus*, cumaceans *Alamprops quadriplicatus*, barnacles *Solidobalanus hesperius*, gastropods *Cryptonatica wakkaniensis* [8].

The stock of *S. gurjanovae* in the Bering Sea, in the very north - in Anadyr Bay, exceeds 200 thousand tons, in the Sea of Okhotsk near the Shantar Islands - 300-350 thousand tons. The total biomass of *S. gurjanovae* is almost commensurate with the biomass of *S. japonica* and amounts to about 600,000 tons. [1]. Together with *S. gurjanovae* other species of algae coexist - brown algae *Fucus evanescens*, *Alaria marginata*, *Pseudolessonia laminariooides*, *Stephanocystis crassipes*, red algae *Neoptilota asplenoides*, *Neohypophyllum middendorffii*, *Hymenena rutherica*, bivalves *Mytilus trossulus*, *Masoma calcarea*, *L. fluctuosa*, *Serripes fluctuosa*, *Serripes groenlandicus*, the sea

THE 11th ANNUAL STUDENT SCIENTIFIC CONFERENCE IN ENGLISH
Vladivostok, May 2024

urchin *Echinarachnius parma*, the multi-legged crayfish *Ampelisca eschrichti*, the cumacean crayfish *Diastylis bidentata*, sipunculids, polychaetes, and actinia [6]. *S. gurjanovae* is one of the main spawning substrates for Okhotsk herring [7].

S. latissima is one of the most widespread species of the genus *Saccharina*, forming underwater forests in the Atlantic Ocean, Arctic and northwestern Pacific, as well as in the Southern Hemisphere, including such regions as southern South America, South Africa and South Australia. In the northern hemisphere, *S. latissima* extends for the most part off the northwestern coasts of Europe, in the White and Barents Seas. The algae *F. vesiculosus* and *A. nodosum* are often found in association with *S. latissima*. In the zoocenosis, the most frequent species are the sea urchin *S. droebachiensis*, polychaetes *Spirorbis sp.* and *Nephtys paradoxa*, the coastal crab *C. pagurus*, barnacles *Balanus sp.*, and the bivalves *Astarte elliptica*, *A. borealis*, *Arctica islandica*, *Modiolus modiolus*, *Hiatella arctica*, the gastropods *Margarites helicinus*, *Onoba aculeus*, *Lacuna vincta*. The thickets of *S. latissima* are attracted by herring *Clupea harengus*, cod *Gadus morhua* and pollock *Pollachius virens* [5].

S. japonica and *S. cichorioides* inhabit mainly the sublittoral of the Sea of Japan and Sea of Okhotsk (mainly near the Kuril Islands and Sakhalin Island). In the Sea of Japan, *S. japonica* is the main commercial species of brown algae. According to modern estimates, the total stock of *S. japonica* is maximum in the coastal part of the Kuril Islands (426.1 thousand tons) [1] and minimum (65 thousand tons) off the coast of Primorye [4]. In addition to these areas, along the Asian coast *S. japonica* is known in the Bering Sea and off the Commander Islands. The stocks of *S. cichorioides* in the Far Eastern seas are not so significant. *S. japonica* and *S. cichorioides* are included in the diet of phytophagous animals such as gray and black sea urchins. Numerous invertebrates are found in the communities formed by these species: sea urchins *S. intermedius* and *Mezocentrotrotus intermedius* and *Mezocentrotus nudus*, sea stars *Leptasterias similispinis*, *Asterina pectinifera* and *Asterias amurensis*, holothurians *Apostichopus japonicus* and *Eupentacta fraudatrix*, gastropods *Littorina squalida*, *Niveotectura pallida*, *Nucella heyseana*, bivalves *Modiolus modiolus*, *Mytilus coruscus*, *H. arctica*, crustaceans, chitons and polychaetes.

H. bongardianum was previously defined as the species *Saccharina bongardiana*, but on the basis of molecular genetic studies it was transferred to the genus *Hadophyllum* and renamed [3]. However, despite the taxonomic rearrangement, the ecological role (function) of this species remained the same. Massive accumulations of *H. bongardianum* are the characteristic of the southeastern coast of Kamchatka - in Avacha Bay, as well as near the Commander and Kuril Islands [2]. Total stocks in the Russian waters of the Far East vary from 400 to 800 thousand tons. [1]. Together with *H. bongardianum*, red algae *Ptilota asplenoides*, *Phycodrys riggii* and *Odonthalia kamtschatica*, brown algae *Lomentaria articulata*, *A. nodosum* and *Chondrus crispus* are often found. The community includes in mass the barnacles *Chthamalus dalli*, *Balanus crenatus*, bivalves *M. trossulus*, gastropods *Littorina sitkana*, *L. squalida*, *Lottia cassis*, *Nucella freycinetii*, the equal-legged crustacean *Idotea ochotensis*, the hermit crabs *P. middendorffii* and *P. hirsutiusculus*, a large number of polychaetes *Nereis vexillosa* and nemertines.

Consequently, species of the genus *Saccharina* play a vital role in the formation of communities in marine ecosystems, concentrating high biological diversity and stock.

References

1. Aminina N.M. Comparative characterization of brown algae of the coastal zone of the Far East // Izvestiya TINRO No. 1(T182). 2015. C. 258-268.
2. Kusakin O.G., Ivanova M.B., Tarakanova T.F. Composition, Distribution and Quantitative Characterization of Macrofauna of the Littoral of South-Eastern Kamchatka // Izvestia TINRO No. 1(T130). 2002. C. 228-265.
3. Selivanova O.N., Zhigadlova G.G., Hansen G.I. Revision of the systematics of algae of the order Laminariales (Phaeophyta) from the Far Eastern seas of Russia on the basis of molecular phylogenetic studies // Marine Biology № 5(33). 2007. C. 329-340.

THE 11th ANNUAL STUDENT SCIENTIFIC CONFERENCE IN ENGLISH
Vladivostok, May 2024

4. Kulepanov V.N., Drobyazin E.N.. Species composition and quantitative distribution of macrophytes in the sublittoral and on the continental slope in the northwestern part of the Sea of Japan // Proceedings of TINRO No. 4 (T195). 2018. C. 151-160.
5. Kapkov V.I., Shoshina E.V. Macroalgae communities of the Arctic zone of the Barents Sea and climate change // Vestnik MSTU No. 2(T21). 2018. C. 185-198.
6. Dulenin, A.A. Distribution of sublittoral vegetation of the mainland coast of the Sea of Okhotsk (within the Khabarovsk Krai) // Izvestiya TINRO No.1(T180). 2015. C. 107-127.
7. Dulenin A.A., Didenko D.S. Quantitative regularities of distribution of common herring on natural spawning grounds of Okhotsk herring // Proceedings of VNIRO №4(T186). 2021. C. 5-20.
8. Labay V.S., Abramova E.V. and others Peculiarities of macrozoobenthos distribution of sublittoral macrozoobenthos in Malokurilskaya Bay (Shikotan Island) // Proceedings of VNIRO No.1. T182. 2020. C.104-120.

Gerasimova V.Yu.¹

CECINA TATARICA (GASTROPODA, POMATIOPSIDAE) – A NEW SPECIES OF MOLLUSKS FOR RUSSKY ISLAND (SEA OF JAPAN, PETER THE GREAT BAY)

¹Far Eastern Federal University, Institute of the World Ocean (School), FEFU

²Federal Scientific Center of the East Asia Terrestrial Biodiversity FEB RAS

³Far Eastern Federal University, Oriental Institute School of Regional and International Studies,

Scientific adviser – L.A. Prozorova²

Scientific consultant – G.L. Ardeeva³

Amphibious gastropods of the genus *Cecina* A. Adams, 1861 are widely distributed in Primorsky Krai along the sea shore in shallow waters. They prefer supralittoral zone of closed bays and polyhaline lagoons [1, 2]. Three species of the genus are known in Primorsky Krai: *C. manchurica* A. Adams, 1861, *C. tatarica* (Schrenck, 1867), *C. scarlattoi* (Prozorova, 1996), which also occur on Sakhalin, Kuril Islands and probably in Japan [1, 2, 3, 4].

The only species, *C. manchurica* was previously recorded in the supralittoral of Russky Island [5]. In May 2024 the second species *C. tatarica* was found in Novik Bay of Russky Island. This is a new species for malacofauna of the island.

Live specimens and empty shells of *C. tatarica*, as well as *C. manchurica*, were collected by hands in the apex of Novik Bay from wet muddy soil at about 30 cm from the water's edge. Natural conditions: salinity > 40 ‰, water temperature was +15.1 °C, air temperature was +18 °C.

Live mollusks and their shells were studied using a binocular microscope MBS-10 with a drawing device of the “camera lucida” type. Gastropods were compared with published pictures of the *Cecina* species [1, 2, 3] and diagrams of their shells of their shells (Fig. 1).

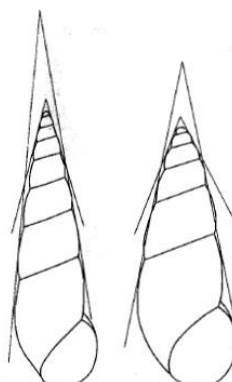


Fig.1. Schemes of shells of the species *Cecina manchurica* (left) and *C. tatarica* (right) with reconstructed upper whorls and constructions of apical angles [2]

THE 11th ANNUAL STUDENT SCIENTIFIC CONFERENCE IN ENGLISH
Vladivostok, May 2024

As a result of comparison, two species were identified in the samples: *C. manchurica* and *C. tatarica*. They differ in the shape of the shell, which is clearly visible when examining juveniles (figures 1, 2), but much worse in adults, who retain only the last 2–3 whorls [2, 3, 4].



Fig. 2. *Cecina tatarica* (left) and *C. manchurica* (right) from Novik Bay (Russky Island)

The shell of *C. tatarica* is wider, less elongated vertically and is therefore characterized by a larger apical angle than that of *C. manchurica* (figures 1, 2). Brief conchological diagnosis of *C. tatarica*: the shell is smooth, shiny, translucent, light brown, oval-conical, apical angle of the adult shell is 25°, apical angle of the embryonic shell is 50° [1, 2, 3].

References

1. Volova G.N., Golikov A.N., Kussakin O.G., Rakovinnye bruykhonogie mollyuski zaliva Petra Velikogo (Shell-bearing Gastropod Mollusks of Peter the Great Bay), Vladivostok: Dal. Vost. Kniz. Izd., 1979.
2. Prozorova L.A. 2003. Morphological features of supralittoral mollusks of the genus *Cecina* (Gastropoda, Pomatiopsidae) from Peter the Great Bay, Sea of Japan // Russian Journal of Marine Biology. Vol. 29. No 1. P. 49-52.
3. Prozorova L.A. 1996a. Specific content of the genus *Cecina* (Gastropoda, Pomatiopsidae) in the Russian Far East // Zoologicheskiy Zhurnal. Vol. 75. No. 5. P. 653-659.
4. Prozorova L.A. 1996b. A Some Data on the Exmonotypic Genus *Cecina* A. Adams // Western Society of Malacologists Annual Report. Vol. 28. P. 13.
5. Ivanova M.B., Belogurova L.S., Tsurpalo A.P. Composition and distribution of benthos in the intertidal zone of Russky Island (Peter the Great Bay, Sea of Japan) // Ecological Studies and State of the Ecosystem of Amursky Bay and Estuarine Zone of Razdolnaya River (Sea of Japan). Vladivostok: Dalnauka. 2009. V. 2. P. 87–146.

Dmitrenko G.D.¹ Zhankov G.V.¹ Ardeeva G.L.²

CONTENT OF AVAILABLE PHOSPHATES IN SOILS OF DIFFERENT MANUFACTURERS

¹Far Eastern Federal University, Institute of the World Ocean (School), FEFU

²Institute of Oriental Studies - School of Regional and International Studies, FEFU

Scientific adviser A.V. Brikman¹

Scientific consultant – G.L. Ardeeva²

Phosphorus is one of the most important agrochemical indicators of soil, included in the list of basic macronutrients. Phosphorus affects the availability of other macro- and micronutrients [3] as well as the formation of fruits in plants, for example, if there is too much phosphorus, the input of iron, iron and manganese is reduced. In addition, phosphorus is necessary at different stages of plant development, as well as nitrogen and potassium, because the deficiency or excess of these elements primarily affects the appearance of the plant, even in the early stages of its development [3]. Therefore, the aim of the study is to obtain data on the content of available phosphate in mixed soils and to compare this parameter with availability indicators for different types of crops (cereals, root crops, vegetable crops).

Objectives:

1. To obtain data on labile phosphorus content from selected soils.
2. To compare the content of available phosphates in soils with the indicators of availability for different types of crops (cereals, root crops, and vegetable crops).

The objects of the study were: Grunt Pal'ma Sad chudes (OOO "NORD PALP", Moscow), Grunt dlya dekorativno listvennykh rastenij Florizel (OOO Terra Master", Novosibirsk), Grunt BIUD Ovoshchnoj universal'nyj (OOO "BIUD", Moscow), Pitatel'nyj torfogrunt UNIVERSAL'NYJ Dobranya sila ((AO "GARDEN", Moscow), Grunt dlya tomatov i percev "Malyshok" (FASKO, Moscow), Grunt universal'nyj (FASKO, Moscow), Grunt dlya rassady Krepsh (FASKO, Moscow). Available phosphates were determined by Kirsanov's extract [1].

According to the above table, the availability of soils with available phosphates shows high phosphate supply in all categories relative to different plant crops (Table 1).

Table 1

P₂O₅ content in Kirsanov's extract [1]

Soil number	Name of soil	Experimental phosphorus values, mg/100g
1	Grunt Pal'ma Sad chudes (OOO "NORD PALP", Moscow)	185,00
2	Grunt dlya dekorativno listvennykh rastenij Florizel (OOO Terra Master", Novosibirsk)	105,42
3	Grunt BIUD Ovoshchnoj universal'nyj (OOO "BIUD", Moscow)	16,67
4	Pitatel'nyj torfogrunt UNIVERSAL'NYJ Dobranya sila (AO "GARDEN", Moscow)	86,67
5	Grunt dlya tomatov i percev "Malyshok" (FASKO, Moscow)	14,17
6	Grunt universal'nyj (FASKO, Moscow)	206,25
7	Grunt dlya rassady Krepsh (FASKO, Moscow)	220,83

The content of available phosphates in the studied soils is very high, except for: Grunt BIUD Ovoshchnoj universal'nyj (OOO "BIUD", Moscow) - high on a scale «for soils» and average on a scale «for peat», Grunt dlya tomatov i percev "Malyshok" (FASKO, Moscow) «for soils» - high, on a scale «for peat» - average. [2]

Of all the studied soils, two soils for plant cultivation were suitable according to indicators of labile phosphates (Table 2). Grunt dlya tomatov i percev "Malyshok" (FASKO, Moscow) according to the values of

THE 11th ANNUAL STUDENT SCIENTIFIC CONFERENCE IN ENGLISH
Vladivostok, May 2024

phosphates is suitable for growing only leguminous plants, Grunt BIUD Ovoshchnoj universal'nyj (OOO "BIUD", Moscow) is suitable for growing only root crops (Table 2).

Table 2

Availability of soils with available phosphates (P_2O_5 , in mg/100g of soil) in Kirsanov's extract [1]

Availability	Cereals, legumes	Root crops potatoes	vegetable crops
Very low	<3	<8	<15
Low	<8	<15	<20
Average	8-15	15-20	20-30
High	>15	>20	>30

Grunt Pal'ma Sad chudes (OOO "NORD PALP", Moscow), Grunt dlya dekorativno listvennykh rastenij Florizel (OOO Terra Master", Novosibirsk), Pitatel'nyj torfogrunt UNIVERSAL'NYJ Dobraya sila (AO "GARDEN", Moscow), Grunt universal'nyj (FASKO, Moscow), Grunt dlya rassady Krepysh (FASKO, Moscow), exceed the average value of labile phosphates by the content of available phosphates (Table 1).

The use of soils with high phosphate content for crop cultivation leads to suppressed state of plants or their possible death since excessive doses of phosphorus reduce the intake of copper, iron, manganese to plants. [3]. Soil mixtures with an excess of phosphorus are recommended to be mixed with other soils or sand to reduce phosphorus index.

Conclusions:

1. Data on the available phosphate content of the soil mixtures were obtained, their values showed that 5 samples were with high values and 2 - with average values.

2. According to phosphate values, the soil for tomatoes and peppers "Malyshok" (FASKO, Moscow) is suitable for growing only leguminous crops, Grunt BIUD Ovoshchnoj universal'nyj (OOO "BIUD", Moscow) is suitable for growing only root crops.

References:

1. Аринушкина, Е.В. Руководство по химическому анализу почв / Е.В. Аринушкина. – М.: Изд-во МГУ, 1970. - 478 с.
2. Дюрягин, И.В. Земледелие с основами почвоведения и агрохимии. / И.В. Дюрягин – Учебное пособие, Курган – 1997.
3. Ягодин, Б.А. Агрохимия / Б.А. Ягодин – М.: Агропромиздат, 1989. - 639 с.

Zhankov G.V.¹, Dmitrenko G.D.¹, Ardeeva G.L²

pH PROPERTIES OF SOILS FROM VARIOUS MANUFACTURERS

¹Far Eastern Federal University, Institute of the World Ocean (School), FEFU

²Institute of Oriental Studies - School of Regional and International Studies, FEFU

Scientific adviser - A.V. Brickmans¹

Scientific consultant - G.L. Ardeeva²

Ready-made soils are used not only for seedlings but also for full plant cultivation and in recent years the demand for them has increased significantly [4]. Each plant prefers its own pH condition for its most favorable growth [5], so each manufacturer of ready-made soils indicates a certain pH range on the package, which helps the consumer when choosing a substrate, since pH condition is important for all plants and affects the availability of mineral nutrients [5].

In this regard, the aim of the study is to determine the correspondence of actual and potential pH values with

THE 11th ANNUAL STUDENT SCIENTIFIC CONFERENCE IN ENGLISH
Vladivostok, May 2024

those stated by the manufacturers in different soils.

Objectives:

1. To select the commonly used universal soils from those available in the market.
2. To compare the pH values of soils as given by the manufacturers with the obtained data.

An analysis of the retail market of soil in Primorsky Krai was made, which allowed us to select the seven most common brands [3]. In this regard, the following soil mixtures were chosen as the object of the study: Grunt Pal'ma Sad chudes (OOO "NORD PALP", Moscow), Grunt dlya dekorativno listvennykh rastenij Florizel (OOO Terra Master", Novosibirsk), Grunt BIUD Ovoshchnoj universal'nyj (OOO "BIUD", Moscow), Pitatel'nyj torfogrunt UNIVERSAL'NYJ Dobranya sila (AO "GARDEN", Moscow), Grunt dlya tomatov i percev "Malyshok" (FASKO, Moscow), Grunt universal'nyj (FASKO, Moscow), Grunt dlya rassady Krepish (FASKO, Moscow).

The potentiometric method of determining the acid-alkaline properties of soils using a Mettler Toledo pH meter was chosen for the study of soil samples [1].

Based on the studies [2], all soils are categorized by their degree of acidity according to pHKCl. In accordance with the data obtained (table), BIUD Ovoshchnoj universal'nyj and Pitatel'nyj torfogrunt UNIVERSAL'NYJ Dobranya are strongly acidic, Grunt dlya tomatov i percev "Malyshok" has slightly acidic, grunt universal'nyj FASKO is close to neutral and Pal'ma Sad chudes, Florizel dlya dekorativno listvennykh rastenij and Grunt dlya rassady Krepish FASKO correspond to neutral acidity.

Only two values of acidity of soil mixtures comply with the manufacturers' data (table): Grunt Pal'ma Sad chudes, Grunt dlya rassady Krepish FASKO. The acidity values of Grunt BIUD Ovoshchnoj universal'nyj, Pitatel'nyj torfogrunt UNIVERSAL'NYJ Dobranya sila, Grunt dlya tomatov i percev "Malyshok" and Grunt universal'nyj FASKO is different by less than 1 from the manufacturers' data. In Grunt dlya dekorativno listvennykh rastenij Florizel the potential acidity value differs by more than 1.

Table

Results of actual and potential pH measurements and manufacturer's data

№	Object of study	pH H ₂ O		pH KCl	
		measured	manufacturer	measured	manufacturer
1	Grunt Pal'ma Sad chudes	6,67	-	6,34	6-6,5
2	Grunt dlya dekorativno listvennykh rastenij Florizel	6,62	5-5,5	6,04	-
3	Grunt BIUD Ovoshchnoj universal'nyj	5,33	5,7-6,4	4,04	-
4	Pitatel'nyj torfogrunt UNIVERSAL'NYJ Dobranya sila	5,28	-	4,51	5,4-6,6
5	Grunt dlya tomatov i percev "Malyshok"	5,58	6-7	5,13	-
6	Grunt universal'nyj FASKO	5,85	6-7	5,71	-
7	Grunt dlya rassady Krepish FASKO	6,69	6-7	6,53	-

Thus, studies have shown that seven soils are the most widespread in the market, but only two of them comply with the pH values of the manufacturer's stated data, such as: Grunt Pal'ma Sad chudes and Grunt dlya

THE 11th ANNUAL STUDENT SCIENTIFIC CONFERENCE IN ENGLISH
Vladivostok, May 2024

rassady Krepish FASKO. Also, although in the Grunt dlya dekorativno listvennykh rastenij Florizel (pH2O - 6,62) values do not comply with the stated 5,0-5,5, nevertheless this soil will be effective for most crops preferring nearly neutral pH condition.

References:

1. GOST 26423-85: methods for determining the specific electrical conductivity, pH and dense residue of aqueous extract: approved and put into effect by the USSR State Committee for Standards of February 8, 1985 N 283: date of introduction 01.01.1986.
2. Mineev V.G. Practicum on agrochemistry / V.G.Mineev. - Moscow: MGU Publishing House, 2001. - 689 c.
3. Farpost online store: website. – URL:
<https://www.farpost.ru/dir?query=%D0%B3%D1%80%D1%83%D0%BD%D1%82+%D0%B4%D0%BB%D1%8F+%D1%80%D0%B0%D1%81%D1%82%D0%B5%D0%BD%D0%B8%D0%B9> (Date of reference: 5.03.2024).
4. Wholesale online store from the manufacturer Buisky Chemical Plant: official site. – URL:
<https://bhzshop.ru/information/news/buyskie-grunty-rost-obemov-umenshenie-zatrat/> (Date of reference: 3.04.2024).
5. Yagodin, B.A. Agrochemistry / B.A. Yagodin - M.: Agropromizdat, 1989. - 639 c.

Zamurueva V. V.¹

THE FIRST STAGES OF OVERGROWTH OF GAPS IN THE CANOPY OF A STAND IN BLACK FIR-CEDAR-DECIDUOUS FORESTS

¹Far Eastern Federal University, Institute of the World Ocean, FEFU

²Botanical Garden-Institute of the Far Eastern Branch of the Russian Academy of Sciences

³Far Eastern Federal University, Oriental Institute-School of Regional and International Studies, FEFU

Scientific adviser – T. Ya.Petrenko²

Scientific consultant – O. K. Titova³

The impact of various endogenous factors on forest phytocenoses contributes to the formation of a spatial mosaic structure and is a natural and unchangeable component of the dynamics of forest communities. The partial disintegration of the canopy of the stand and the formation of gaps in it contribute to the formation of multi-age and polydominant forest communities [1]. Black fir-cedar-broadleaf forests are the indigenous and most complex in spatial structure forests in the Primorsky Territory and throughout the Far East [2]. The formation of small natural fallouts consisting of one or two trees is one of the main reasons for the formation of a complex spatial structure of cedar-broadleaf communities. The gaps formed at the sites of such falls create the conditions necessary for the renewal of various tree species. Studying the process of renewal of these species will allow to have a broader understanding of the formation of complex spatial structures of black fir-cedar-broadleaf forests. In this regard, the purpose of this work is to investigate the first stages of overgrowth of gaps in the black fir-cedar-deciduous forests in the south of the Primorsky Territory.

Based on the results of the work done, we can draw the following conclusions:

1. All windows are small-scale; the area does not exceed 185 m². The gaps are formed by trees in the amount from 1 to 5. Among the deadwood, both broken trees and trees with the formation of a wind-soil complex are observed.
2. In total, we found 2304 individuals belonging to 28 species in the renewal. In comparison with the stand,

THE 11th ANNUAL STUDENT SCIENTIFIC CONFERENCE IN ENGLISH
Vladivostok, May 2024

there was no flat-leaved birch, Manchurian linden (*Tilia mandshurica* Rupr. & Maxim.) and the pointed yew (*Tilia mandshurica* Rupr. & Maxim.).

3. The most numerous species in the renewal are 2 species – Amur lilac and Manchurian ash (40 and 34% of all individuals, respectively). Among the other species, the most common are mono maple, Amur maakia, bearded maple, Mongolian oak, Amur linden, hornbeam. Among conifers, 3 species are found – Korean cedar, whole-leaved fir and white fir, their share does not exceed 3%. For all species, there is a strong thinning with increasing height.

4. The main limiting factors affecting the resumption turned out to be among the abiotic ones: the position relative to the center of the gap, which affects the illumination and the microrelief of the terrain, which determines the amount of free substrate. Biotic ones include competition of the undergrowth for substrate and light, shading by herbaceous plants, shrubs, and lianas, as well as damage of the undergrowth by herbivores (biting). There was no correlation between the size of the gap and the number of species or individuals found in it.

References

1. Eastern European forests: history in the Holocene and modernity: in 2 books. / Ed. by O. V. Smirnov. – M. : Nauka. - 2004. – 479 p.
2. Kolesnikov B.P. Cedar forests of the Far East / B.P. Kolesnikov // Tr. DVF SB AN USSR. Ser. botan.- 1956.- No. 2, vol. 4.- 262 p.

Katugina L.O.¹

PHYLOGENETIC RELATIONSHIPS OF THE MOLLUSCS *KOREOLEPTOXIS AMURENSIS* (SEMISULCOSPIRIDAE) BASED ON MOLECULAR MARKERS

¹Far Eastern Federal University, Institute of the World Ocean (School), FEFU

²Federal Scientific Center of the East Asia Terrestrial Biodiversity FEB RAS

³Far Eastern Federal University, Oriental Institute School of Regional and International Studies

Scientific adviser – V.A. Tatonova^{1,2}

Scientific consultant – G L. Ardeeva³

Freshwater molluscs are important benthic animals that are dominant in many rivers and lakes in terms of abundance and biomass [1]. They play a role of aquatic biofilters, take part in decomposition of organic matter and are a food source for many birds and mammals. Freshwater molluscs are also the first intermediate hosts for various parasites such as *Nanophyetus salmincola* and *Metagonimus suifunensis*.

In 2009, based on molecular analysis, Strong and Köhler indicated that *Parajuga* is not a valid taxon [2]. Later, Köhler [3], based on molecular data for one specimen of *Parajuga amurensis*, suggested that it belongs to *Koreoleptoxis amurensis*. However, the systematic position of other members of the genus *Parajuga* is not clear due to the lack of molecular, anatomical, and morphological criteria.

In this study, the nucleotide sequences of the *cox1* and 16S rRNA genes of mitochondrial DNA are analyzed to clarify the phylogenetic position of representatives of the genus *Parajuga* inhabiting different water bodies in the south of the Russian Far East. P-distances obtained for partial sequences of both genes for all specimens indicated on the basis of morphological data as *Koreoleptoxis amurensis*, *Parajuga nodosa*, *P. czerski*, *P. heukelomiana* and *P. amurensis* have intraspecific level. Thus, all mollusks in this study are members of a single species, *Koreoleptoxis amurensis*.

References

1. Prozorova, L.A. Freshwater mollusks of the Lower Amur and Primorye basins. Species diversity, keys

THE 11th ANNUAL STUDENT SCIENTIFIC CONFERENCE IN ENGLISH
Vladivostok, May 2024

of genera and families, rare species – Germany: Palmarium Academic Publishing, 2013. – 552-560p.

2. Strong, E.E. Morphological and molecular analysis of “Melania” jacqueti Dautzenberg and Fischer, 1906: from anonymous orphan to critical basal offshoot of the Semisulcospiridae (Gastropoda: Cerithioidea) / E.E. Strong, F.Köhler – *Zoologica Scripta*, 2009. – 483-487p.

3. Köhler, F. Rampant taxonomic incongruence in a mitochondrial phylogeny of Semisulcospira freshwater snails from Japan (Cerithioidea, Semisulcospiridae) / F. Köhler – *Journal of Molluscan Studies*, 2016. – 268-281p.

Kashina A.A.¹, Zavalnaia E.G.^{1,2}

IDENTIFICATION OF PIWI PROTEIN AS A STEM CELL MARKER IN SOMATIC TISSUES OF SEA CUCUMBER *APOSTICHOPUS JAPONICUS*

¹Far Eastern Federal University, Institute of the World Ocean, FEFU

²A.V. Zhirmunsky National Scientific Center of Marine Biology, FEB RAS

³Far Eastern Federal University, Oriental Institute-School of Regional and International Studies, FEFU

Scientific supervisor – E.G. Zavalnaia^{1,2}

Scientific consultant – O.K. Titova³

Echinoderms are well known for their regenerative abilities. Due to this fact they are often used as model objects for science explorations in the field of tissue regeneration [3]. In particular, sea cucumber *Apostichopus japonicus* belongs to this phylum and is characterized by its capacity for evisceration – a protective mechanism induced by the changes of environmental conditions and involves throwing out a part of the internal organs with their subsequent regeneration [2]. Along with the internal organs, a significant volume of cells of the coelomic fluid (CF), an important component of echinoderms immune system, is lost. The mechanisms of coelomocytes fast reparation after evisceration have not been studied yet. The main role in this process may belong to stem cells, circulating in coelomic fluid or migrating from tissues [4]. Molecular markers of "stemness" should be used for approving this hypothesis. Genes or products of their expression that are activated only in stem cells can be used for this purpose. In the present work we used the protein Piwi as a molecular marker of "stemness", which is expressed in germ line stem cells of different animals. Moreover, it is found in somatic stem cells of many invertebrates [1]. The aim of the current work is the search of the Piwi protein in *A. japonicus* tissues.

Applying the method of immunocytochemistry and antibodies against Piwi protein, was shown, that among the coelomocytes of sea cucumber there are cells of a small size (3-5 micrometers) characterized by a high nuclear-cytoplasmic ratio and containing Piwi protein in the cytoplasm (Figure 1).

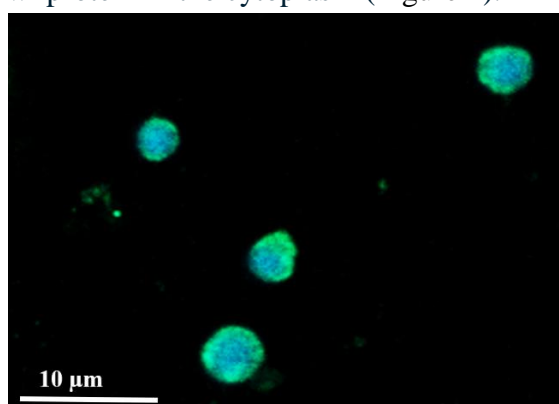


Figure 1 – Piwi-positive cells in the coelomic fluid of sea cucumber *A. japonicus*

Blue fluorescence marks nuclear DNA stained with DAPI, green fluorescence – components stained with antibodies to Piwi

Analysis of Piwi-positive cells dynamics across the process of CF cells regeneration after evisceration demonstrated the following. In intact animals labeled cells in the coelomic fluid were very rare. At 1 h after evisceration the number of Piwi-positive cells increases dramatically against the general decrease in the number of CF cells. Finally, the number of labeled cells returns to the values close to the "normal" state in 24 h after evisceration (Figure 2). The obtained data indicate the participation of Piwi-positive cells in the early stages of sea cucumber *A. japonicus* coelomocytes regeneration after evisceration.

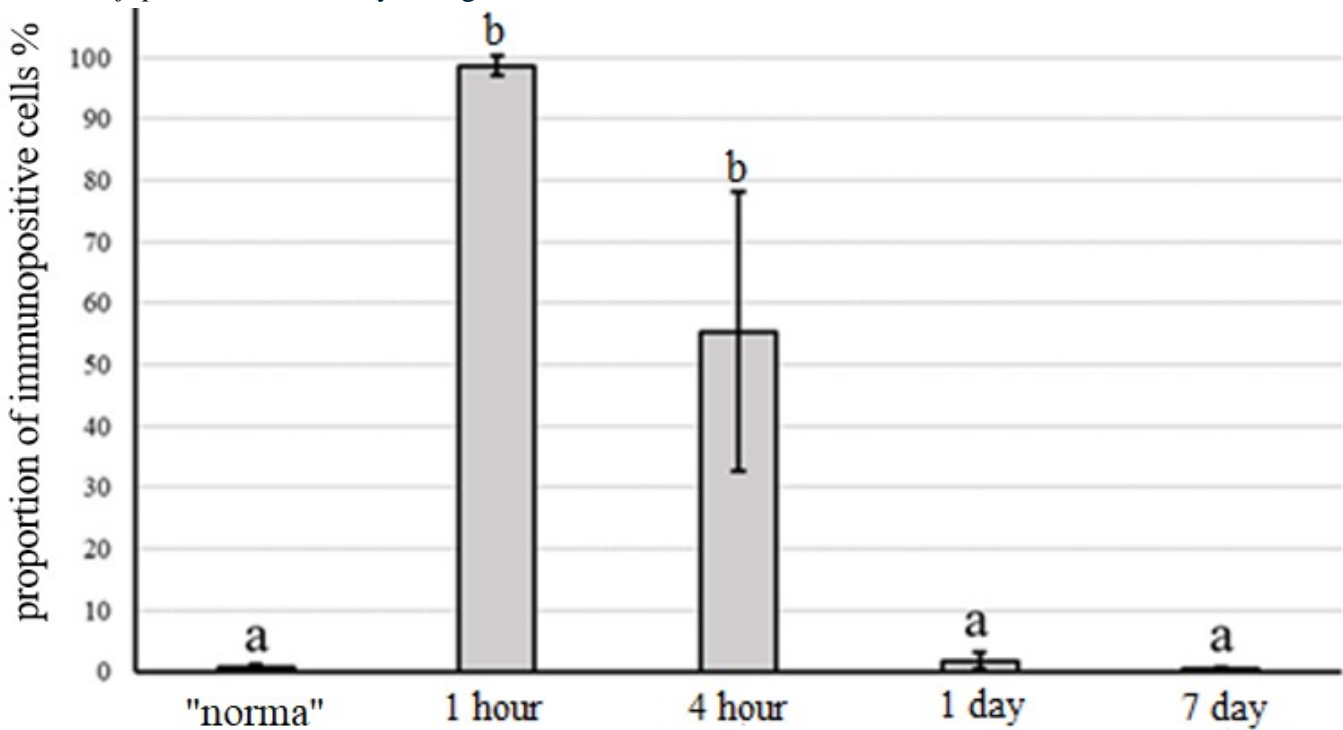


Figure 2 – The change in the content of Piwi-positive cells in the coelomic fluid of *Apostichopus japonicus* in "normal" state and after evisceration

On the axis OX is the time after evisceration, on the axis OY is the proportion of immunopositive cells, expressed as a percentage; the same letter indexes show the absence of statistically significant differences between the values, at $p<0.05$ and $n=3$

Identification of Piwi protein in intact *A. japonicus* somatic tissues using antibodies made it possible to detect antibody-labeled cells inhabiting different levels of the body wall coelomic epithelium. Thus, the coelomic epithelium can serve as a source of new coelomocytes that restores the CF cellular composition during regeneration.

References:

1. Bak, C. W. Functions of PIWI proteins in spermatogenesis / C. W. Bak, T. K. Yoon, Y. Choi // Clinical and Experimental Reproductive Medicine. – 2011. – Vol. 38. – № 2. – P. 61-67.
2. Dolmatov, I.Y. Regeneration in echinoderms / I.Y. Dolmatov // Russian Journal of Marine Biology. – 1999. – Vol. 25. – № 3. – P. 225-233.
3. Gahn, F. J. Evolutionary history of regeneration in Crinoids (Echinodermata) / F. J. Gahn, T. K. Baumiller // Integrative and Comparative Biology. – 2010. – Vol. 50. – № 4. – P. 514.
4. Petukhova, O. Small undifferentiated cells from starfish *Asterias rubens* L.: candidates to the role of progenitor cells / O. Petukhova, N. Sharlaimova, S. Shabelnikov, D. Bobkov, M. Martynova, O. Bystrova // Invertebrate Survival Journal. – 2018. – Vol. 15. – P. 111-112.

Nagornaya O.A.¹

EFFICIENCY OF CARBON FOOTPRINT ABSORPTION IN VLADIVOSTOK DUE TO MARINE SUBMERGENT VEGETATION OF PETER THE GREAT BAY

¹Far Eastern Federal University, Institute of the World Ocean (School), FEFU

²Far Eastern Federal University, Oriental Institute School of Regional and International Studies

Scientific adviser – T.V. Boichenko¹

Scientific consultant – G.L. Ardeeva²

Carbon footprint is one of the main environmental problems today. One of the solutions is its capture and accumulation in marine ecosystems [5]. Seagrass beds are an ecosystem that can capture, deposit in the soil and retain carbon for a long time in the process of feeding due to the root system [4]. In Peter the Great Bay, seagrass is represented by the Zosteraceae family [3]. Vladivostok is the largest source of emissions of carbon-containing inorganic compounds located in this area. From the environmental report for Primorsky Krai for 2022, it is possible to calculate approximate values of carbon emissions [2]. According to the article “ORGANIC MATTER DIAGENESIS IN SEDIMENTS COVERED WITH ZOSTERA MARINA L. THICKETS” by P. Y. Tishchenko the rate of carbon uptake by Zostera marina is 1.6 (gC/m² day) [3]. Due to the lack of current data on the area of Zostera marina growth, data for 1984 [1] were used. According to approximate calculations, sea grass beds in Peter the Great Bay absorb 33% of Vladivostok's carbon emissions.

References

1. Paimeeva L.G. Biology of *Zostera marina* L. and *Zostera asiatica* Miki of Primorye -Vladivostok, 1984
2. Government of Primorsky Krai. REPORT on the ecological situation in Primorsky Krai in 2022, pp. 159-160
3. Tishchenko P.Ya. DIAGENESIS OF ORGANIC Matter IN ISLANDS COVERED BY ZOSTERA MARINA (ZOSTERA MARINA L.) - Oceanology, 2020, T. 60, no. 3, pp. 393-406
- 4 Tishchenko P.Ya. ORGANIC CURBON AND CARBONATE SYSTEM IN BORN DEPOSITS OF SHALLOW WATER BOOKS OF PETRA GREAT GULF (JAPAN SEA) - GEOCHEMIA, 2020, Vol. 65, No. 6, pp. 583-59.
5. Scott M, Lindsey R. Understanding blue carbon - September 29, 2022

Oskerko S.E.¹

THE ROLE OF EELGRASS (ZOSTERA MARINA L.) IN MARINE COMMUNITIES AND ITS POTENTIAL FOR CLIMATE CHANGE MITIGATION

¹Far Eastern Federal University, Institute of the World Ocean, Department of Ecology, FEFU

²Far Eastern Federal University, Oriental Institute-School of Regional and International Studies, FEFU

Scientific adviser – Y.A. Galysheva¹

Scientific consultant - O.K. Titova²

An eelgrass (*Zostera marina* L.) is a marine angiosperm species which forms extensive meadows. Eelgrass grows in sublittoral zone in waters less than 4 m deep, where sunlight can penetrate the seafloor. It is the most abundant and a foundational seagrass species in coastal zones of the northern hemisphere. These plants host rich biodiversity. Eelgrass meadows serve as a shelter for various marine species, particularly to juvenile fish, crabs, gastropods, and bivalves. A perfect example of this is a species known as rock cod (*Gaud ogac* R.). As juveniles, they hide inside eelgrass from predators because structurally complex habitats impair the visual capabilities of

THE 11th ANNUAL STUDENT SCIENTIFIC CONFERENCE IN ENGLISH
Vladivostok, May 2024

predators, thereby reducing the risk of predation. Eelgrass meadows have been found to be densely populated by rock cods, suggesting it is a preferred nursery habitat [1]. Rock cod are harvested commercially, underscoring the significance of conserving eelgrass meadows [2]. The presence of eelgrass meadows in shallow waters indicates good ecosystem health [1]. One study showed that *Z. marina* is a euryhaline species, meaning it can tolerate a wide range of salinity in the water [3]. The benthic infauna of *Z. marina* meadows is very diverse; a study found a total of 117 macroinvertebrate taxa in *Z. marina* beds [4].

Carbon sequestration potential of marine ecosystems exceeds that of terrestrial ecosystems. Carbon is stored in the sediments of eelgrass beds. Thus, coastal ecosystems play a crucial role for climate change mitigation, increasing the protection of these meadows can help compensate for increasing carbon dioxide emissions in the atmosphere [5]. In one study, researchers collected sediments from eelgrass meadows spanning the west coast from Vancouver (Canada) to Oregon (USA). Their findings suggest that the carbon within these meadows is predominantly allochthonous, meaning it originates from sources outside the eelgrass beds, highlighting the significance of eelgrass communities in sequestering carbon and their impact on climate regulation. Hence, they are important carbon sinks [6].

Swedish scientists found that hydrodynamic exposure is directly proportional to absolute organic carbon stocks in sediments. Waves and currents compact sediment, increasing its density and accumulation of carbon within the sediment. This higher density in turn increases erosion threshold of an eelgrass bed. As storms will get more extreme due to climate change, hydrodynamically exposed meadows can be more resilient toward the storms than nonexposed eelgrass meadows [7].

Human activity is known to disrupt natural environments. Coastal marine ecosystems are no exception. Research conducted in Spain revealed that *Z. marina* meadows become fragmented due to the practice of bottom raking, a method used to harvest shellfish that grow in these habitats. This harvesting technique results in the destruction of seagrass, ultimately leading to the fragmentation of meadows into smaller patches. Not only the meadow fragmentations harm the ecosystem, but they also result in economic losses, as the reduced area hinders shellfish cultivation [8]. Despite the areal reduction of *Z. marina* meadows, they can be restored. American scientists conducted a study that spanned approximately 20 years. 74.5 million seeds were broadcast into 536 individual restoration plots totaling 213 ha. So far this has resulted in a total 3612 ha of vegetated bottom from virtually no coverage before the restoration efforts took place. These previously barren habitats now house very rich biodiversity. Well-developed meadows now foster productive and diverse animal communities, sequester substantial stocks of carbon and nitrogen, and have prompted a parallel restoration for bay scallops (*Argopecten irradians*). This study demonstrates that the restoration of one species' habitat can lead to the restoration of other species, as eelgrass meadows are vital for survival and reproduction of various other species. This unparalleled study underscores the significance of restoration efforts and showcases the feasibility of such restoration projects [9].

References:

1. Labrador Shelf Offshore Area Strategic Environmental Assessment Update. // C-NLOPB : site. – URL: <https://www.cnlopbc.ca/wp-content/uploads/sealab/lsp5.pdf> (accessed on: 30.04.2024)
2. Lilley, R. Atlantic Cod (*Gadus morhua*) benefits from the availability of seagrass (*Zostera marina*) nursery habitat / R. Lilley, R. Unsworth // Global Ecology and Conservation. – 2014. – Т. 2, № 11. – Р. 367-377.
3. Мосеев, Д. С. Структура растительного покрова юго-восточного побережья Белого моря (залив Сухое море) / Д. С. Мосеев, Л. А. Сергиенко // Hortus botanicus. – 2016. – Т. 11, № 3. – Р. 19-33.
4. Orth, R. J. Benthic infauna of eelgrass, *Zostera marina*, beds. / R. J. Orth // Chesapeake Science. – 1973. – Т. 14, № 4. – Р. 258-269.
5. Factors Influencing Carbon Stocks and Accumulation Rates in Eelgrass Meadows Across New England,

THE 11th ANNUAL STUDENT SCIENTIFIC CONFERENCE IN ENGLISH
Vladivostok, May 2024

USA / A. B. Novak, M. C. Pelletier, P. Colarusso [et al.] // *Estuaries and Coasts.* – 2020. – T. 43, № 2. – P. 2076-2091.

6. A Synthesis of Blue Carbon Stocks, Sources, and Accumulation Rates in Eelgrass (*Zostera marina*) Meadows in the Northeast Pacific / C. Prentice, K. L. Poppe, M. Lutz [et al.] // *Global Biogeochemical Cycles.* – 2020. – T. 34, № 2. – P. 1-16.

7. The influence of hydrodynamic exposure on carbon storage and nutrient retention in eelgrass (*Zostera marina* L.) meadows on the Swedish Skagerrak coast / D. Martin, A. Maria, B. Mats [et al.] // *Scientific Reports.* – 2020. – T. 10, № 1. – P. 1-13.

8. Population dynamics of a fragmented subtidal *Zostera marina* population affected by shell fishing / C. Barañano, E. Fernández, P. Morán [et al.] // *Estuarine, Coastal and Shelf Science.* – 2022. – T. 269, № 1. – P. 107818.

9. Restoration of seagrass habitat leads to rapid recovery of coastal ecosystem services / R. J. Orth, J. S. Lefcheck, K. S. McGlathery [et al.] // *Science Advances.* – 2020. – T. 6, № 41. – P. eabc6434.

Rostovtceva M.O.¹

**DESCRIPTION OF RHODYMENICHTHYS DOLICHOGASTER LARVAE
FROM PETER THE GREAT BAY**

¹Far Eastern Federal University, Institute of the World Ocean (School), FEFU

²A.V. Zhirmunsky National Scientific Center of Marine Biology FEB RAS

³Far Eastern Federal University, Oriental Institute School of Regional and International Studies, FEFU

Scientific advisor – A.A. Balanov²

Scientific consultant – G.L. Ardeeva³

The family Pholidae includes three genera: *Pholis*, *Rhodymenichthys* and *Apodichthys*. The genus *Rhodymenichthys* includes only one species – *Rhodymenichthys dolichogaster* [1]. Adult fish are characterized by a monophonic coloration with small black dots and a silver stripe extending from the posterior edge of the eye to the pectoral fin base [1]. Despite the sufficient study of adult fish, there are very few papers on the larvae description of this species.

The aim of the work is to characterize the larval stages of *Rhodymenichthys dolichogaster* of Peter the Great Bay.

The material used was larvae (TL 12.0–36.1 mm, n = 21 specimens) collected at light stations with a landing net. To describe larval development, larvae were divided into stages depending on the degree of notochord bent [2]: *preflexion* – the stage of strait notochord; *flexion* – the stage of bending notochord; *postflexion* – the stage after the completion of the notochord bent. To describe the internal pigment and the degree of skeleton development, larvae were simultaneously stained with alizarin red and cleared in 1.5% KOH. Stereo Discovery V 12 dissecting microscope ("K.Zeiss", Germany) was used to take photographs before and after staining and clearing.

The *preflexion* stage was found at a length of TL 12.0 – 18.0 mm (n = 14 specimens). Throughout the stage, the notochord was straight. Jaw, *arcusbranchialis*, *cleithrum*, pectoral and caudal fin rays, vertebrates (except 5 pre-caudal centra) were stained with alizarin red. By the end of the stage, 7 principle rays in caudal fin were stained with alizarin red. Caudal fin is symmetrical. On the head, melanophores were found in the *otic capsule*, along the *cleithrum*, and on the *isthmus*. One oval melanophore was located above *cor saculum*. There were 1–2 large (sometimes small) melanophores on the nape. External abdominal lateral row lined below the midline of the body. Melanophores were stellate or round. As a rule, in this row fist melanophores were stellate and larger. A row of paired rounded melanophores extended on dorsal side of the gut, separated by the same distance from each other.

THE 11th ANNUAL STUDENT SCIENTIFIC CONFERENCE IN ENGLISH
Vladivostok, May 2024

There was an aggregation of melanophores at the end of the gut. In the caudal section, melanophores were at the base of the anal fin rays and on the caudal fin.

The *flextion* stage was found at a length of *TL* 19.0 – 25.0 mm (*n* = 6 specimens). The notochord was slightly bent. The bones of the skull, anal and pectoral fin rays, dorsal fin spines, all vertebrates (including first pre-ural centra), *spinous process*, *hypaxial* and two *epaxial hypuralia* were stained with alizarin red. In more developed larvae, *epuralia* have begun to stain. During *flextion* 12 principle rays, 2–5 upper and 1–2 lower edge rays were stained. Caudal fin is unsymmetrical. At this stage, melanophores appeared at the junction of *dentale* and *articulare*. A melanophore on *cor saculum* was small, in some individuals it was noticeable only after clearing.

Only one larva of the *postflextion* stage was caught, with a *TL* length of 36.1 mm. At this length the notochord was bent. First pre-ural centra wasn't shortened yet. Due to the bending of the notochord, the hypurals moved upwards. Caudal fin is symmetrical. Fry coloration was formed: a silvery stripe appeared on the head, extending from the edge of the snout through the middle of the eye to the pectoral fin.

References:

1. Yatsu A. A revision of the gunnel family Pholididae // Bull. Natn. Sci. Mus. 1981. P. 165–190.
2. Kendall A.W. Jr., Ahlstrom E.H., Moser H.G. 1984. Early life history stages of fishes and their characters // Ontogeny and systematics of fishes / Eds. Moser H.G. et al. Amer. Soc. Ichthyol. Herpetol. Spec. Publ. № 1. P. 499–510.
3. Yakubovsky M. Methods of detecting and coloring the lateral line canal system and bone formations of fish // Zool Zhurnal. 1970. Vol. XLIX. №. 9. P. 1398–1402.

Rudenko D.A.¹, Shkryl Y.N.²

THE INFLUENCE OF THE *ROLB* AND *ROLC* GENES ON THE COMPOSITION OF SECONDARY METABOLITES OF *ARISTOLOCHIA MANSHURIENSIS* AND STUDY OF THEIR ANTICANCER ACTIVITY

¹Far Eastern Federal University, Institute of the World Ocean (School), FEFU

²Federal Scientific Center of the East Asia Terrestrial Biodiversity FEB RAS

³Far Eastern Federal University, Oriental Institute School of Regional and International Studies,
Scientific advisor – Y.A. Yugay²

Scientific consultant – G.L. Ardeeva³

Relict plant *Aristolochia manshuriensis* Kom. is an endemicto Korea, China and the southeastern part of Russia. The substances contained in this plant have antitumor and anti-inflammatory effects. Magnoflorin is of particular interest owing to its large spectrum of pharmacological properties, namely antioxidant and cytotoxic activity against human glioblastoma, cervical and colorectal carcinoma cancer cells. But *A. manshuriensis* also contains phenanthrene derivatives of aristolochic acids (AA) with nephrotoxicity, mutagenic and carcinogenic effects in chronic use, so the use of this plant in pharmacology was prohibited. [1].

Traditional propagation of *A. manshuriensis* is a long and arduous process, so an important task was to create an alternative source of biomass with an increased yield of useful substances and minimization of toxic ones. It was necessary to study the effect of different cultivation methods on the metabolomic profile of *A. manshuriensis* extracts. A promising approach was the production of hairy roots that had a high growth rate and productivity [2] compared to cell cultures and which had not yet been studied for *Aristolochia*.

Leaf, petiole, and stem explants were infected with *A. tumefaciens* carrying *rolA*, *rolB*, and *rolC* genes. Over time, primary tumors developed on the explants, then *rolC*- and *rolB*-infected stem and petiole explants developed

THE 11th ANNUAL STUDENT SCIENTIFIC CONFERENCE IN ENGLISH
Vladivostok, May 2024

adventitious roots. In *rolA* explants root growth was not observed as well as induction effects were not observed in leaves. Biomass growth increased several times compared to the control callus (36.6 and 7.4 g/l - fresh and dry), *rolC* - 111.4 and 22.5 g/l, *rolB* - 219.0 and 57.5 g/l [3]. The data emphasize the importance of selecting the appropriate explant and *rol* gene for the induction of hairy root syndrome in *A. manshuriensis*. It was found that the content of magnoflorin in *rolC*- and *rolB*- transformed hairy roots exceeds its values in the control callus line by 5.8 and 2.8 times, respectively. The magnoflorin content in the *rolC* line reached 5.72 ± 0.686 mg/g. The total content of aristolochic acids (AA) in transgenic hairy roots lines was 7–8 times higher than in control callus, but 1.5–1.6 times lower than in *A. manshuriensis* stems, and the accumulation of AA-I and AA-II was greatly decreased, while the content of AA-IIIa, AA-IVa/b and AA-IIIa-G increased up to 40 times compared to the control callus. Extracts of hairy roots of *A. manshuriensis* showed obvious cytotoxic effects against human glioblastoma cells U-87 MG, cervical cancer cells HeLa CCL-2 and colon carcinoma cells RKO [4].

Aqueous extracts obtained from callus cultures of *A. manshuriensis* and hairy root lines transformed with the *rolC* and *rolB* genes demonstrated high efficiency in the formation of silver nanoparticles that had a cytotoxic effect against pathogenic microorganisms and fibroblasts [5]. These properties make the particles promising for biotechnology and biomedicine.

Thus, the successful use of the *rolB* and *rolC* genes to alter the qualitative composition of secondary metabolites in *A. manshurensis* has been demonstrated. However, it is necessary to carry out a thorough study of gene expression of this metabolic pathway for a deep understanding and targeted regulation of the biosynthesis of phenanthrene derivatives.

References

1. Martena M.J., van der Wielen J.C.A., van de Laak L.F.J., Konings E.J.M., de Groot H.N., Rietjens I.M.C.M. Enforcement of the ban on aristolochic acids in Chinese traditional herbal preparations on the Dutch market // *Anal. Bioanal. Chem.* 2007, 389, 263–275.
2. Gutierrez-Valdes N., Häkkinen S.T., Lemasson C., Guillet M., Oksman-Caldentey K.-M., Ritala A., Cardon F. Hairy root cultures – A versatile tool with multiple applications // *Front. Plant Sci.* 2020, 11, 33.
3. Bulgakov V.P., Zhuravlev Y.N. Generation of *Aristolochia manshuriensis* Kom. callus tissue cultures // *Rastitel'nye Resur.* 1989, 25, 266–270.
4. Shkryl Y.N., Tchernoded G.K., Yugay Y.A., Grigorchuk V.P., Sorokina M.R., Gorpenchenko T.Y., Kudinova O.D., Degtyarenko A.I., Onishchenko M.S., Shved N.A., Kumeiko V.V., Bulgakov V.P. Enhanced production of nitrogenated metabolites with anticancer potential in *Aristolochia manshuriensis* hairy root cultures // *International Journal of Molecular Sciences*, 2023, 24, 11240.
5. Yugay Y.A., Sorokina M.R., Grigorchuk V.P., Rusapetova T.V., Silant'ev V.E., Egorova A.E., Adedibu P.A., Kudinova O.D., Vasyutkina E.A., Ivanov V.V., Karabtsov A.A., Mashtalyar D.V., Degtyarenko A.I., Grishchenko O.V., Kumeiko V.V., Bulgakov V.P., Shkryl Y.N. Biosynthesis of functional silver nanoparticles using callus and hairy root cultures of *Aristolochia manshuriensis* // *Journal of Functional Biomaterials*, 2023, 14, P. 451.

Ryabtseva S.D.¹

SACHALINOCETUS CHOLMICUS (ODONTOCETI: SQUALODONTIDAE): SKULL MORPHOMETRY AND CRANIAL RECONSTRUCTION

¹Far Eastern Federal University, Institute of the World Ocean, FEFU

²The Borissiak Paleontological Institute of the Russian Academy of Sciences, Moscow

³Far Eastern Federal University, Oriental Institute-School of Regional and International Studies, FEFU

Scientific advisor - K.K.Tarasenko²

Scientific consultant – O.K. Titova³

Cetaceans, like Sirenia, among other secondary aquatic mammals, have fully adapted to life in the aquatic environment during their evolution, and, as a rule, their fossils are associated with marine and coastal marine sediments. On the territory of the Russian Federation, fossils are known from the Paleogene [4, 7] up to the Late Miocene [6, 8]. However, the finds of the Russian Far East are not as numerous as those in the European part of the country. The first representative finding of a Miocene whale skeleton in the Far East was made on the right bank of the Sova River, 2 km from the Grebenskaya station in the Makarovsky district of Sakhalin Island [2]. The skeleton belonged to a representative of a new genus of toothed whales (*Odontoceti*) of an extinct family *Squalodontidae*, which are characterized by an elongated stature, the position of the nasal openings between the orbits, the proliferation of the mandibul backward and the supraoccipital forward, an archaic triangular configuration and double-rooted teeth [1] and is described as *Sachalinocetus chomlicus* [5].

Sachalinocetus possessed a large raster, which was almost twice as long as the cerebral part of the skull, a short symphysis of the lower jaw and small notches on the back edges of the cheek teeth. Its body, judging by the skeleton, was torpedo-shaped and, most likely, this whale inhabited in the open seas [2]. This is the only representative of the family *Squalodontidae*, found in the Russian Far East, and therefore it is of scientific value.

The morphometric study of the *Sachalinocetus* skull conducted by the author was necessary for the reconstruction of individual sections of the skull, which will help expand morphological information, supplementing the initial description, and it is important, especially in the context of the application of new technologies and techniques. Such research can lead to new discoveries and an in-depth understanding of the structure of extinct cetaceans.

The measurement of the *Sachalinocetus* skull was carried out with a mechanical caliper. The material is a holotype PIN RAS, № 2798/1, skull, Sova River, Grebenskaya station in the Makarovsky district, Miocene. In the course of the work, the morphometric parameters of the skull were calculated. It is established that the specimen under study is an adult animal with a special rostrum structure – its anterior third is bent upwards with respect to the longitudinal axis of the skull at a slight angle, and the teeth are differentiated into two-rooted and single-rooted, and two single-rooted teeth are located in front of the rostrum, which are absent in beluga whales and bottlenose dolphins, but were present in propoises.

The morphological characteristics of the *Sachalinocetus* skill were analyzed and correlated with other specimens. The skulls of modern representatives of cetaceans were considered: beluga whales (*Delphinapterus leucas*), bottlenose dolphins (*Tursiops truncatus*), porpoises (*Phocoena phocoena*), as well as extinct whales *Microcetus charkovi*, *Leptodelphius stavropolitanus* и *Waipatia maerewhenua*. The similarity of some morphological characteristics of the *Squalodontidae* family with the whale *Waipatia maerewhenua* served as the choice of the main object for the reconstruction of some sutures of the *Sachalinocetus* skull based on *Waipatia* [3].

Thus, as a result of the conducted research, a diagram of the sutures of the *Sachalinocetus chomlicus* skull was compiled, as well as the lost sections of the skull of this whale were reconstructed.

THE 11th ANNUAL STUDENT SCIENTIFIC CONFERENCE IN ENGLISH
Vladivostok, May 2024

References

1. Carroll, R. L. Vertebrate Paleontology and Evolution. Volume 3 / R. L. Carroll, - Journal of Vertebrate Paleontology, 1993. – 310 p.
2. Dubrovo, I. A. A new genus of cetaceans (*Sachalinocetus cholmicus* gen. et sp. nov.) from the Miocene of the island of Sakhalin / I. A. Dubrovo – Proceedings of the Paleontological Institute of the USSR Academy of Sciences, 1971. – V. 130. – p. 87-103.
3. Forduce, R. E. *Waipatia maerewhenua*, New Genus and New Species (*Waipatiidae*, New Family), an Archaic Late Oligocene Dolphin (*Cetacea: Odontoceti: Platanistoidea*) from New Zealand / R. Ewan Fordyce – Department of Geology, University of Otago, 1994.
4. Gingerich, P. D. Skull and partial skepeton of a new pachycetine genus (*Cetacea, Basilosauridae*) from the Aridal Formation, Bartonian middle Eocene, of southwestern Morocco / Philip D. Gingerich, Ayoub Amene, Samir Zouhri – Museum of Paleontology, Department of Geology and Health and Environment Laboratory, 2022.
5. Siryk, I. M. Fossil whale in the Miocene sediments of southern Sakhalin / I. M. Siryk, I. A. Dubrovo – Geologiya I Geofizika, 1970(9). – 123-129 p.
6. Tarasenko, K. K. New baleen whale genera (*Cetacea, Mammalia*) from the Miocene of the Northern Caucasus and Ciscaucasia: 2. *Vampalus* gen. nov. from the Middle-Late Miocene of Chechnya and Krasnodar Region / K. K. Tarasenko, A. V. Lopatin – Paleontological Journal, 2012. – V. 46 #6. – p. 620-629.
7. Tarasenko, K. K. The first record of *Basilosauridae* (MAMMALIA, CETACEA) in the Eocene of the Krasnodar region (Apsheron district, Gorny Luch) / K. K. Tarasenko – Doklady Biological Sciences, 2022. – V. 502. – p. 66-69.
8. Zelenkov, N. V. Southeastern Europe as the Arena of Vertebrate Evolution in the Late Miocene / N. V. Zelenkov, E. V. Syromyatnikova, K. K. Tarasenko – Paleontological Journal, 2022. – V. 56 #2. – p. 213-226.

Teshchina Z.V.¹, Panova A.S.², Kameneva L.A.², Berdasova K.S.²

INTRODUCTION OF ASTRAGALUS ULIGINOSUS L. (FABACEAE) INTO IN VITRO CULTURE

¹Far Eastern Federal University, Institute of the World Ocean, FEFU

² Botanical Garden-Institute Far Eastern Branch of the Russian Academy of Sciences (FEB RAS)

³ Far Eastern Federal University, Oriental Institute School of Regional and International Studies,

Scientific advisers – A.S. Panova², L.A. Kameneva²

Scientific consultant - G.L. Ardeeva³

Legumes of the genus *Astragalus* have been used by humans for various purposes for more than 1000 years [1]. *Astragalus uliginosus* L. is no exception. This species is a perennial herbaceous plant with upright shoots, compound pinnate leaves, and a leguminous fruit. It is widespread in the North Asian region: Kazakhstan, Mongolia, Siberia, northern China, and the Korean Peninsula [2]. Currently, *A. uliginosus* is of interest to the pharmaceutical industry [3] due to the potential use of bioactive compounds found in its aerial parts: flavonoids and coumarins [2]. The use of extracts of this species for treating cardiovascular diseases has also long been known [1]. Despite its wide distribution, *A. uliginosus* does not form large thickets, thus making it difficult for use as a raw material for the pharmaceutical industry. Therefore, the aim of this work is to study the feasibility of introducing *A. uliginosus* into culture in vitro.

Seeds of *A. uliginosus* (156 seeds) were collected their natural habitats on the sandy shores of Lake Khanka (Khankaisky District, Primorsky Krai) in the fall of 2023 (obtained by Index Seminum - VLA). The seeds, ranging from 1 to 1.8 mm in width, were predominantly kidney-shaped or occasionally kidney-elongated with colors varying from yellow-green to brownish. Morphological examination [4] and seed quality assessment were carried out using

THE 11th ANNUAL STUDENT SCIENTIFIC CONFERENCE IN ENGLISH
Vladivostok, May 2024

a Stemi DV4 stereomicroscope (Carl Zeiss, Germany). It was found that 66 seeds were severely damaged and incapable of germination (42.3%).

The germination experiment was carried out in triplicate (30 seeds each). Based on previous findings [7,8], the seeds were scarified for 20 minutes with concentrated H₂SO₄ before sterilization. Then, after rinsing with distilled water, they were sterilized with a 1% solution of AgNO₃ for 15 minutes followed by rinsing with a 1% solution of NaCl. The seeds were then rinsed three times with sterile distilled water and planted on hormone-free Murashige and Skoog medium [6]. Cultivation was carried out under 3000 lux illumination and a light regime of 16/8 hours light/dark with a constant temperature of 24 ± 2 °C.

The seeds swelled after 24 hours, and the first sprouts appeared after 4 days: 8 sprouts (26.6%) in Replicate I, 6 (20%) in Replicate II, and 5 (16.6%) in Replicate III. Sprouting was considered successful if the length of the root exceeded the seed width by 2 times [5]. The first dicotyledonous leaves began to appear on day 6, and true leaves appeared on day 11. Branching of the shoot and continued germination of the remaining seeds were noticeable by day 20. During the experiment, fungal growth was observed on days 4–11, affecting 10% of the total seeds (Table).

Table

Germination of *Astragalus uliginosus L.* seeds

	Germination on Day 20, %	Seed Loss on Day 20, %	Development of True Leaves on Day 20, %
Replicate I	50	30	33,3
Replicate II	46,6	0	43,3
Replicate III	36,6	0	30
Average	44,4	10	35,5

By day 20, 44.4% of seeds had germinated and the remaining seeds were still swelling. Some sprouts from Replicates I, II and III were transferred to a medium containing the growth regulator 6-benzylaminopurine for further study of mass propagation of *A. uliginosus*.

Thus, the possibility of obtaining viable aseptic *Astragalus uliginosus* sprouts has been demonstrated. Further research will contribute to the development of actively proliferating culture of this species in vitro.

This study was conducted at the "In Vitro Plant Collection" of the Botanical Garden-Institute FEB RAS Vladivostok, Russia under the state assignment "Introduction into culture, study, and conservation of genetic resources of economically valuable plants of East Asia." Registration number: 122040800086-1

References

1. Bajaj, Y. P. S. (1995). [Biotechnology in Agriculture and Forestry] Medicinal and Aromatic Plants VIII Volume 33 // *Astragalus Species (Milk Vetch): In Vitro Culture and the Production of Saponins, Astragalin, and Other Biologically Active Compounds.*, 10.1007/978-3-662-08612-4(Chapter 6), 97–138.
2. Kotsupii O.V., Vysochina G.I. Composition and Content of Flavonoids in Plant Species from Sections Eudmus Bunge and Melilotopsis Gontsch. of the Genus *Astragalus L.* in Siberia // Scientific Notes of ZabGU. Series: Biological Sciences. 2016. No. 1.
3. Lysiuk R., Darmohray R. Pharmacology and Ethnomedicine of the Genus *Astragalus* // International Journal of Pharmacology Phytochemistry and Ethnomedicine 3:46-53 (2016).
4. Shemetova T.; Erst A.; Wang W.; Xiang K.; Vural C.; Aytaç, Zeki (2018) "Seed morphology of the genus *Astragalus L.* from North Asia," *Turkish Journal of Botany*: Vol. 42: No. 6, Article 4.
5. Firsova, M.K. Seed Control / M.K. Firsova. – Moscow: Kolos, 1969. – 295 pages.
6. Murashige T., Skoog F. (1962) A revised medium for rapid growth and bioassays with tobacco tissue cultures. *Physiol. Plant.* 15: 13, 473 – 497.
7. Berdasova K.S., Pianova A.S. & Kameneva L.A. The effect of abiotic factors on *in vitro* seed germination

THE 11th ANNUAL STUDENT SCIENTIFIC CONFERENCE IN ENGLISH
Vladivostok, May 2024

in *Oxytropis chankaensis* Jurtz., a rare endemic species of the Russian Far East // *Botanica Pacifica. A journal of plant science and conservation* 2023. 12(2): 168-171.

8. Thai H.N., Nesterova S.V., Gorobets K.V., Tsarenko N.A. Germination and Dynamics of Seed Sprouting in *Astragalus uliginosus* L. and *Lespedeza cytobotrya* Miq. (Fam. Fabaceae Lindl.) at Different Storage Times // Proceedings of the Regional Scientific and Practical Conference on Natural Sciences for Students, Postgraduates, and Young Scientists, Vladivostok, April 15 – May 10, 2023 / Ministry of Science and Higher Education of the Russian Federation Far Eastern Federal University. – Vladivostok: FEFU, 2023. – pp. 18-21.

Thai H.N.¹, Tsarenko N.A.¹, Zorina E.V.²

THE POLLEN GRAIN VIABILITY OF THE GARDEN ROSE COLLECTION OF THE BOTANICAL GARDEN-INSTITUTE FEB RAS

¹Far Eastern Federal University, Institute of the World Ocean (School), FEFU

²Botanical Garden-Institute Far Eastern Branch of the Russian Academy of Sciences (BGI FEB RAS)

³Far Eastern Federal University, Oriental Institute School of Regional and International Studies,

Scientific adviser - N.A. Tsarenko¹

Scientific consultant – G.L. Ardeeva³

The rose collection in the Botanical Garden of the Far Eastern Branch of the Russian Academy of Sciences (BGI FEB RAS) is the largest in the Russian Far East. However, the monsoon climate and the resistance of the varieties to unfavorable environmental conditions have a limiting effect on the hybridization of roses. For successful rose hybridization, it is necessary to know the viability of their pollen so as not to waste time on pollination with varieties whose pollen is sterile or have a low percentage of viability.

The purpose of this research is to study the pollen grain viability in garden roses from the collection of the BGI FEB RAS.

Pollen grains from 17 different *Rosa* L. varieties were used as the work's source material. Pollen of each variety was germinated in glucose solution on slides placed in Petri dishes, the bottom and lid of which were lined with moist filter paper. Pollen grains of each variety were germinated in three concentrations of glucose solution (10%, 12% and 15%) in triplicates of each concentration. The germinated pollen grains were evaluated after 24 hours by determining the germinated pollen grains under a Zeiss Primo Star microscope. Viewing was carried out in 3-5 fields of view, 1000 pollen grains were calculated for each concentration of glucose solution (Basina, 1980).

Table

The germination of pollen grains of garden roses from the collection of BGI FEB RAS.

Variety	3 days			5 days			7 days		
	10%	12%	15%	10%	12%	15%	10%	12%	15%
<i>Aloha</i>	10.60	16.53	23.47	10.93	10.90	12.80	0.77	0.33	0.83
<i>Anabell</i>	0	0	0	0	0	0	0	0	0
<i>Frau Karl Druchski</i>	0.67	0.83	1.47	0,03	0	0,03	0	0	0
<i>Poulsen's Pink</i>	11.31	12.09	16.73	4.71	5.24	6.73	0.42	0.42	0.62
<i>Satchmo</i>	4.87	5.93	12.70	2	2.07	4.43	0	0.03	0.07
<i>Sonnenwelt</i>	0.17	0.63	3	0.07	0.07	0.27	0	0	0
<i>Utro Moskvy</i>	2.87	4.36	7.36	2.07	3.16	5.22	0.02	0.02	0.07

THE 11th ANNUAL STUDENT SCIENTIFIC CONFERENCE IN ENGLISH
Vladivostok, May 2024

The study of pollen grain viability showed that

1. The pollen grains of garden roses lose germination rapidly, retaining the ability to germinate to a maximum of seven days (Table).
2. The germination percentage of pollen grains is proportional to the concentration of glucose solution. Pollen grains showed the best germination in 15% glucose solution. The highest germination of pollen grains was in Aloha variety (23.47%).
3. There are 6 varieties of garden roses from the collection of BGI FEB RAS whose pollen grains did not germinate at all: '*Allure Winter Jewel*', '*Annabelle*', '*Jubile du Prince de Monaco*', '*Kent*', '*Martin Frobisher*', and '*Rhapsody in Blue*'.

References

1. Basina, I.G. Determination of pollen quality // The program and methodology of fruit, berry and nut crop selection / I.G. Basina. – Michurinsk, 1980. – P. 426-428. (in Russian).

Yachmen L.P.¹, Biklibayeva A.R.¹, Gilyov A.M.^{1,2}, Sukhin D.V.¹, Sotskaya A.A.¹, Lapshina N.V.¹, Ardeeva G.L³

DYNAMICS OF SWEET BASIL (OCIMUM BASILICUM) DEVELOPMENT ON VARIOUS SUBSTRATES WITH THE APPLICATION OF MINERAL FERTILIZER IN A HYDROPONIC SETUP

¹Far Eastern Federal University, Institute of the World Ocean (School), FEFU

²RUBISCO LLC Company

³Far Eastern Federal University, Oriental Institute School of Regional and International Studies,
Scientific adviser - A.M. Gilyov¹

In recent years, it has become popular to grow leafy crops using hydroponic technologies. Hydroponics is the cultivation of various crops without using soil, in various substrates such as mineral wool, expanded clay, etc. [1] by using a nutrient solution which is the basis of the whole growing process. It should be noted that inorganic substrates, such as mineral wool and expanded clay, do not contain nutrients, so the application of mineral fertilizers is necessary for successful plant cultivation in hydroponics. However, products grown using exclusively mineral fertilizers may differ from those traditionally grown in soil due to a lack of organic compounds such as amino acids, vitamins, etc. [2]. To improve the quality of hydroponic products, it is possible to introduce the use of an organic substrate such as *Ahnfeltia*.

The aim of the study was to investigate the effect of organic substrate (*Ahnfeltia tobuchiensis*) and a synthetic substrate (foam rubber) on stem height, leaf length and width of sweet basil (*Ocimum basilicum*) with the application of mineral fertilizer when grown in a hydroponic setup.

Objectives:

- measure substrate parameters (humidity, temperature);
- measure nutrient solution parameters (ppm, pH);
- measure plant growth parameters (number of leaves, internodes, leaf width, leaf length).

The object of the study as an organic substrate was the *Ahnfeltia* (a red alga from the *Ahnfeltiaceae* family). Seeds of sweet basil from the GAVRISH company were used as plants.

The treatment and preparation of *Ahnfeltia* for further cultivation was carried out in several stages: rinsing with distilled water and soaking in KMnO₄ (potassium permanganate), then rinsing and pouring with a 15% hydrogen peroxide solution, followed by rinsing with distilled water and drying. Before transferring to hydroponics, the *Ahnfeltia* was placed in mesh cups, and then sweet basil seeds were placed in it for germination. After the plants germinated and rooted in the *Ahnfeltia*, they were placed in a hydroponic setup. There were 10 plants in total

THE 11th ANNUAL STUDENT SCIENTIFIC CONFERENCE IN ENGLISH
Vladivostok, May 2024

During the thirty-three-day study, regular measurements of substrate parameters (moisture, temperature) and nutrient solution (pH, electrical conductivity), as well as plant growth, were carried out. For this purpose, special measuring instruments were used, such as a moisture meter to determine substrate humidity, a thermometer to measure temperature, a conductivity meter to assess the electrical conductivity of the nutrient solution and a pH meter to control the pH level. Plant growth dynamics was also measured using a ruler. The obtained data are presented in the table as average values, which were obtained as a result of analysis and processing using Microsoft Excel.

Indicators of plants, nutrient solution and substrates during the vegetation experiment

Indicators Experimental stage	Average plant height (cm)		Nutrient solution		Substrate indicators			
	Polyurethane foam	Anfelta Tobuchinsky	pH environment	Conductivity, ppm	Humidity, %		Table Temperature, °C	
Beginning of the experiment	2,32	1,82	6,1	62	Polyurethane foam	Anfelta Tobuchinsky	Polyurethane foam	Anfelta Tobuchinsky
Middle of the experiment	10,84	7,2	6,4	98			23	22,3
End of the experiment	22,35	14,6	6,6	109				

Substrate humidity and temperature data were obtained: during the experiment the moisture content of the foam rubber increased from 20% to 30-35%, which is twice less than the moisture content of *Ahnfeltia*, which ranged from 60 to 65%, indicating a higher moisture-retaining ability of *Ahnfeltia*. The substrate temperature remained stable throughout the experiment and ranged from 20 to 25°C.

The actual acidity and electrical conductivity of the working solutions were measured: in the control solution the reaction of the medium changed from neutral to slightly alkaline (from 7 to 7.5), and the salt content changed insignificantly (from 62 to 109 ppm); in the solution with mineral fertilizer, the acidity slightly decreased during the experiment (from 6.1 to 6.6), and the salt content increased almost 2 times as a result of increasing fertilizer concentration. The most favorable parameters of nutrient medium for basil growth were observed in the solution with mineral fertilizer.

The growth of basil in foam rubber, both in the control solution and in the mineral fertilizer, exceeded the growth of plants in *Ahnfeltia* by 2 times: in the control solution, the growth of basil in *Ahnfeltia* was 2.9 cm, while in foam rubber it was 3.62 cm; in the mineral fertilizer the growth of basil in foam rubber was 21.6 cm, while in *Ahnfeltia* it was 14.4 cm. In the control solution, the leaf width of basil grown on *Ahnfeltia* reached 2 cm by the end of the experiment, which is half a centimeter less than the leaf width in foam rubber. In the mineral fertilizer, the leaf width in foam rubber reached 9 cm, while in *Ahnfeltia* it was 8 cm. The difference in leaf width was only 1 cm. The length of basil leaf on different substrates also had a difference of about one centimeter in both solutions. Basil growth in foam rubber exceeded basil growth in *Ahnfeltia* by an average of 1.5 times, which indicates a more effective plant development in synthetic substrate and the need to improve the technique of *Ahnfeltia* treatment for using in hydroponics.

**THE 11th ANNUAL STUDENT SCIENTIFIC CONFERENCE IN ENGLISH
Vladivostok, May 2024**

References:

1. Bogoslovsky V.N. Agrotechnology of the future / V.N. Bogoslovsky, B.V. Levinskiy, V.G. Sychev. - Moscow: Izd-vo RIF “Antikva”, 2004. - 163 c.
2. Oliva T.V. Ecologization of greenhouse production of lettuce on soil-less substrate using drip irrigation system // Oliva T.V., Panin S. I., Shevel N.M., Kulikova M.A. // Modern Problems of Science and Education. - 2014. - № 6. C. 1644

Section II

CHEMISTRY AND CHEMICAL TECHNOLOGY

Artemov P.M.¹, Frolov K.R.^{1,2}

PHYSICOCHEMICAL MODELING OF DALNRGORSK DISTRICT ACID MINE DRAINAGE

¹FEFU, Department of Nuclear Technologies, Institute of High Technology and Advanced Materials

²FEFU, Polytechnic institute, Department of Oil and Gas Technologies and Petrochemicals

Scientific adviser – K.R. Frolov^{1,2}

The key aspect of the negative impact of mining technogenic systems on the hydrosphere is the occurrence of hypergenic and technogenic processes as a result of interaction of sulfide ores with weathering agents. As a result of these processes in the mining areas, the quality of surface water deteriorates [1], which increases the risks to public health [2].

In previous works [3-5] the pollution of natural waters of the Dalnegorsk district by technogenic discharges and water treatment were considered. The purpose of this work is to evaluate the possibility of modeling the processes of mine water formation by computer physicochemical modeling.

Modeling was carried out using the software package Selektor-Windows (developed at the Institute of Geochemistry SB RAS). It implements a convex programming approach to calculating equilibrium in heterogeneous systems by minimizing thermodynamic potentials [6].

For consideration of processes in the program complex Selektor two-reservoir models on type of flow reactor were formed. Phase composition included chemical composition (kg): 10 - atmosphere, 1 – mine water, 0.1 – sulfide ores. The modelling was performed for temperature range from -25 to +50 °C degrees in 5 °C increments and a constant pressure of 1 Bar. A total of 336 variants of the mine water formation process were considered.

Modeling showed that the interaction of mine water with sulfide minerals produced highly concentrated aqueous solutions with pH ranging from 0.31 to 3.53. At that, the highest mineralization is noted in case of negative temperatures (more than 300 g/L); at positive temperatures it decreases several times - up to 68.5 mg/L.

The obtained results were verified by their comparison of the mineral composition of the models with hypergene and technogenic minerals found in the Dalnegorsk area, as well as with the results of monitoring works [5].

Thus, the conducted work showed the possibility of computer physicochemical modeling of mine water formation processes and formulate the methodology of this experiment.

References:

1. Frolov, K. Assessment of the Rudnaya River geochemical barriers water composition using physico-chemical modeling method (Dalnegorsk Ore District, Russia) / K. R. Frolov. 10.1007/978-3-030-45263-6_17 // Sustainable Development of Water and Environment: Proceedings of the ICSDWE2020. – Springer International Publishing, 2020. – P. 177-189. https://link.springer.com/chapter/10.1007/978-3-030-45263-6_17
2. Risk Assessment on Human Health: the Case of Primorsky Krai Abandoned SulfideRich Tailings Dump / K. R. Frolov, Artemova, M. I., O. A. Ponomarev. 10.1088/1755- 1315/666/3/032017 // Science and technology conference «Earth science»: proceedings. - 2021. - Vol. 666, N. 7. - P. 1-6. <https://iopscience.iop.org/article/10.1088/1755-1315/666/3/032017>
3. Artemova, M. I. Mining-chemical and mining plants wastewater treatment using artificial geochemical barriers / M. I. Artemova, P. M. Artemov, K.R. Frolov // The 10th annual student scientific conference in English - Vladivostok: FEFU, 2023. – P. 39-41. – URL: <https://www.elibrary.ru/item.asp?id=50326431>
4. Artemov, P. M. Pollution of natural waters by technogenic discharges from mining systems in

THE 11th ANNUAL STUDENT SCIENTIFIC CONFERENCE IN ENGLISH
Vladivostok, May 2024

Primorsky krai / P. M. Artemov, K.R. Frolov // The 10th annual student scientific conference in english - Vladivostok: FEFU, 2023. – P. 74-75. – URL: <https://www.elibrary.ru/item.asp?id=54321373>

5. "Environmental monitoring of natural waters in the zone of Primorsky krai mining technogenic systems impact / K.R. Frolov, M.I. Artemova, A.E. Cheshkin, P.M. Artemov. - Vladivostok : Vladivostok State University of Economic Development, 2023 - P. 191-201. <https://www.elibrary.ru/item.asp?id=53931845>

6. Minimization of gibbs free energy in geochemical systems by convex programming / Karpov I.K., Chudnenko K.V., Bychinskii V.A., Kulik D.A., Avchenko O.V // Geochemistry International. – 2001. – Vol. 39, N. 11. – P. 1108-1119. <https://repository.geologyscience.ru/handle/123456789/24918>

Vashchenko M.V.¹

THE STUDY OF METABOLITES OF 2,3,6,-TRIHYDROXY-7-METHYLNAPHTHAZARIN, A FUNCIONAL ANALOGUE OF ECHINOCHROME USING A DEUTERIUM LABEL

¹Far Eastern Federal University, Institute of High Technologies and Advanced Materials

²G.B. Elyakov Pacific Institute of Bioorganic Chemistry FEB RAS

³Far Eastern Federal University, Oriental Institute School of Regional and International Studies, FEFU

Scientific adviser – V. Ph. Anufriev²

Scientific consultant - V.B. Kolycheva³

The problem of coronary heart disease is among the most important medical problems. One of the causes of the disease is the formation of reactive oxygen species; therefore, antioxidant therapy is used. The basis of the antioxidant therapy drug Histochrome (registered trademark) is echinochrome (Figure.1). In vivo studies have shown that a structural analogue of echinochrome (2) using a methyl substituent instead of ethyl has higher activity [1]. The drug activity is known to be provided by its metabolites. To date, the metabolism of echinochrome has been studied in very few studies [2, 3], and there have been no reports about the metabolism of the methyl analogue.

The purpose is to identify the structure of metabolites formed with the substrate 2 by high-resolution chromatography-mass spectrometry using a deuterium label. For this purpose, synthetic 2,3,6-trihydroxy-7-(methyl-d₃)naphthazarin (3) was used.

Deuterated functional analogue 3 was injected into BALB/c mice and renal excretions were analyzed by high-resolution chromatography-mass spectrometry. First, the introduced compound itself was detected (Figure 2), monomethyl esters at the 2(4) and 3(5) positions, 6 monomethyl ether glucuronides (6-11) (which being a new observation compared to echinochrome, there were only 4 isomers), dimethyl ether glucuronides (12-14) and one quinonylurea derivative 15.

Thus, after the introduction of the methyl analogue of echinochrome by high-resolution chromatography-mass spectrometry using a deuterium label, thirteen metabolites were detected in the excreta of BALB/c mice, among which 1-((1,4,6,7-tetrahydroxy-3-methyl-1,4 naphthoquinone-2-yl)-

-oxy)urea, the probable substance responsible for the biological activity.

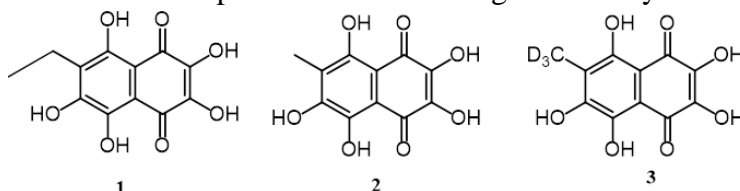


Fig. 1 – Structural formulas of echinochrome (1), its functional analogue (2) and d₃-methyl derivative (3)

THE 11th ANNUAL STUDENT SCIENTIFIC CONFERENCE IN ENGLISH
Vladivostok, May 2024

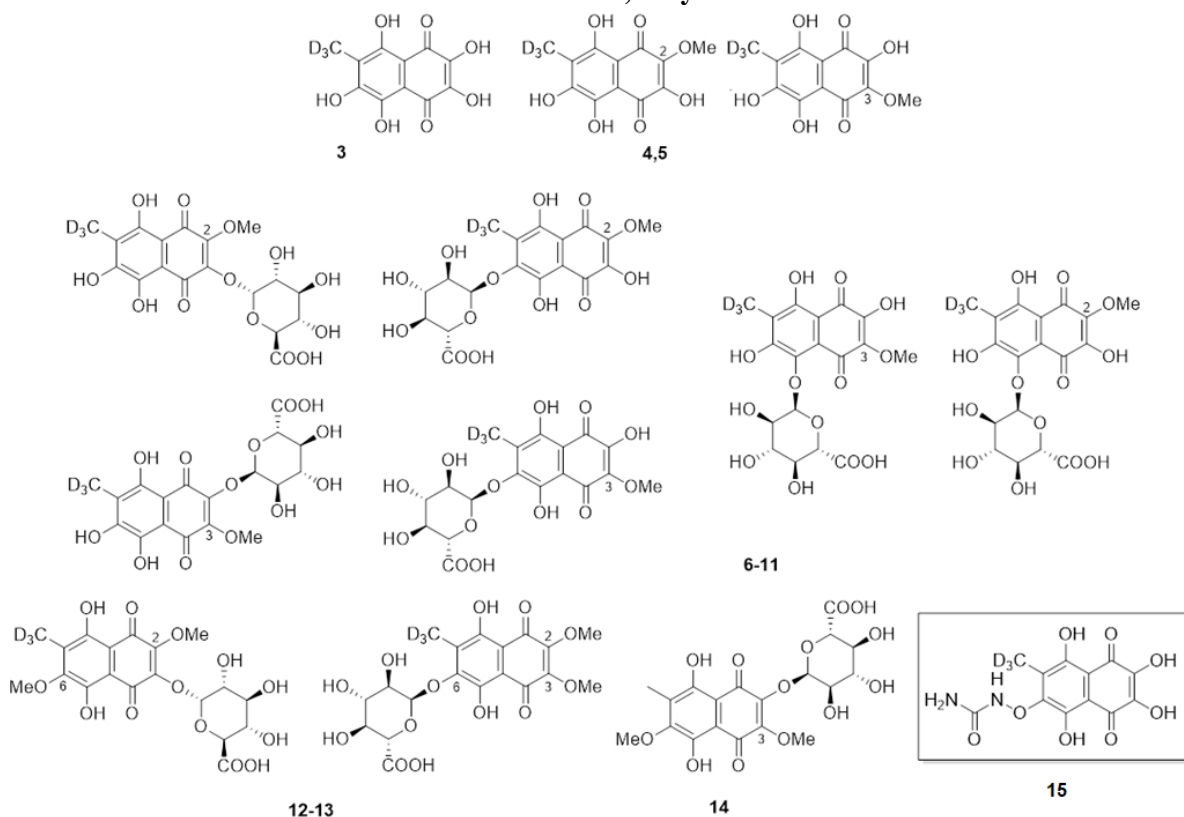


Fig. 2 – The supposed structures of 2,3,6-trihydroxy-7-methylnaphthazarin metabolites detected in renal excretions using a deuterium label

References:

1. Synthesis of some hydroxynaphthazarins and their cardioprotective effects under ischemia-reperfusion in vivo / V. Ph. Anufriev, V. L. Novikov, O. B. Maximov [et al]. – DOI: 10.1016/s0960-894x(98)00075-4 // Bioorg Med Chem Lett – 1998. – Vol.8, P. 587-592
2. Structures of renal excretions of Histochrome using a deuterated label / A.E. Zakirova, R.S. Popov, V.V. Makhan'kov, B.P. Mashnev, V.F. Anufriev. – DOI 10.1007/s10600-023-03909-9 // Chem. Nat. Comp. – 2023. – Vol. 59, P. 21.
3. Derivatives of (tetrahydroxyethyl-1,4-naphthoquinonyl)-hydroxyurea – metabolites of Histochrome preparation / A.E. Zakirova, R.S. Popov, V.V. Makhan'kov, V.Ph. Anufriev. – DOI 10.1007/s10600-023-04147-9 // Chem. Nat. Comp. – 2023. – Vol. 59, P. 906.

Gavrik A.E.¹, Kovshun A.A.¹

COMPARISON OF SCHEMES FOR UTILIZATION OF ALKALINE HYDROLYSATES OF RICE HULLS TO OBTAIN SOLID PRODUCTS

¹Far Eastern Federal University, School of Engineering, FEFU

²Far Eastern Federal University, Oriental Institute School of Regional and International Studies,
 Scientific adviser – A.A. Kovshun¹
 Scientific consultant - V.B. Kolycheva²

Rice husk is multi-tonnage by-product of rice production, the main components of which are cellulose, lignin and mineral ash consisting of amorphous silica. Rice husk utilization is an important environmental issue. One method of utilization is the production of cellulose by the sodic method. The main by-product of such production is

THE 11th ANNUAL STUDENT SCIENTIFIC CONFERENCE IN ENGLISH
Vladivostok, May 2024

alkaline hydrolysate, which can serve as a source of biogenic silicon dioxide due to the high silica content in rice hulls.

In [1], the authors studied the alkaline hydrolysate and proposed a scheme of utilization with the separation of amorphous silicon dioxide. A promising scheme of utilization is presented in [2], on its basis a new scheme with reduced water consumption rates and a high degree of purity of the target product was developed and proposed.

Rice husk of mixed varieties with predominance of "Doliny" variety was used as a raw material. Hydrolysis was carried out in accordance with the scheme proposed in [1].

The obtained hydrolysates were utilized by different methods. According to the first scheme, the hydrolysate was evaporated, the obtained dry residue was calcined in a muffle furnace at 650 °C for 180 minutes, the calcined sample was dissolved in distilled water and filtered. By addition of concentrated hydrochloric acid solution, the silicon-containing substance was precipitated from the filtrate as silicic acid. The resulting samples were washed to remove chlorides and dried in air. According to the second scheme, the hydrolysate was utilized. by adding a concentrated hydrochloric acid solution to extract the precipitated silica. The yield of silica obtained by the first scheme of utilization was 10-21 %; the yield of silica obtained by the second scheme of utilization was 9-11 %.

Reference:

1. Zemnukhova L.A. Composition and purification of waste water from the alkaline hydrolysis of rice shuck / L.A. Zemnukhova, O.D. Arefieva, A.A. Kovshun // Chemistry for sustainable development. – 2011. – Vol. 19. – P. 509-514. [Electronic resource] / Scientific digital library E-library.ru – URL: <https://www.fao.org/faostat/ru/#data>.
2. Zhang W. A comprehensive green utilization strategy of lignocellulose from rice husk for the fabrication of high-rate electrochemical zinc ion capacitors / W. Zhang, W. Jian, J. Yin [et al.] // Journal of Cleaner Production. – 2021. – Vol. 327. – P. 1-8. [Electronic resource] / Scientific digital library E-library.ru – URL: <https://elibrary.ru/item.asp?id=47734338>.

Emelianova V. G.^{1,2} Shchitovskaya E. V.,^{1,2} Kolzunova L. G.²

ELECTROCHEMICAL SYNTHESIS OF POLYMER COMPOSITES WITH INCLUSION OF NOBLE METAL NANOPARTICLES

¹Department of Chemistry and Materials IHTAM, FEFU

²Institute of Chemistry FEB RAS

³Academic Dep. of English Language, Oriental Institute School of Regional and International Studies, FEFU

¹Scientific advisers – E. V. Shchitovskaya¹, L. G. Kolzunova²

²Scientific consultant – V. B. Kolycheva³

Currently, composite materials with the inclusion of metal nanoparticles in a polymer matrix are of particular interest. The peculiarity of such materials is that the active component in the form of nanoparticles is distributed in the volume of the polymer matrix, which stabilizes and holds them firmly, while maintaining the high activity of metal particles and remaining a highly elastic carrier [1]. Such materials have a wide range of applications and can be used as catalysts, chemical and biological sensors, various optical materials, light filters, and biocidal coatings [2-3].

The purpose of the work was to develop a one-stage method for the formation of composites based on polymethylolacrylamide (PMAA) with the inclusion of gold (AuNPs) and platinum (PtNPs) nanoparticles, as well as to study their electrochemical properties.

Composite films were formed on an AISI304 stainless steel cathode in a potentiostatic mode from an aqueous solution of a base electrolyte containing acrylamide, formaldehyde, N, N'-methylene bisacrylamide and

THE 11th ANNUAL STUDENT SCIENTIFIC CONFERENCE IN ENGLISH
Vladivostok, May 2024

zinc chloride, the composition of which is given in [3], with the addition of chlorauric acid (1 mM) and chloroplatinic acid (1 mM). The symbols of the composites are as follows: PMAA/AuNPs – composite with the addition of gold nanoparticles; PMAA/PtNPs – composite with the addition of platinum nanoparticles; PMAA/PtNPs-AuNPs – composite with the addition of platinum and gold nanoparticles.

The initial PMAA matrix film was colorless and transparent whereas the composite films PMAA/PtNPs, PMAA/AuNPs and PMAA/PtNPs-AuNPs had respectively gray, pink-lilac and gray with a pink tinge.

A study of the swelling of the formed polymer composites was carried out (Fig. 1). The inclusion of metal nanoparticles AuNPs and PtNPs was found to lead to an increase in the swelling of composite films compared with unmodified PMAA. The greatest effect on swelling was exerted by the combined addition of AuNPs and PtNPs nanoparticles, in the presence of which the value of the degree of swelling was maximum. This effect might be due to the inclusion of metal nanoparticles leading to pore loosening in the polymer matrix.

Cyclic voltammograms (CVA) of 0.5 M K₄[Fe(CN)₆]/0.1 M LiClO₄ were taken to study the permeability of composite polymer films. As follows from Fig. 2, when the potential was expanded with each new cycle, the value of the current density corresponding to the concentration of the depolarizer increased. This effect indicates that on electrodes modified with a polymethylolacrylamide film the limiting stage of the redox process was the diffusion of matter through the film. It was found that a similar dependence was observed not only on the matrix PMAA film but also on all samples of composites with the addition of gold and platinum nanoparticles.

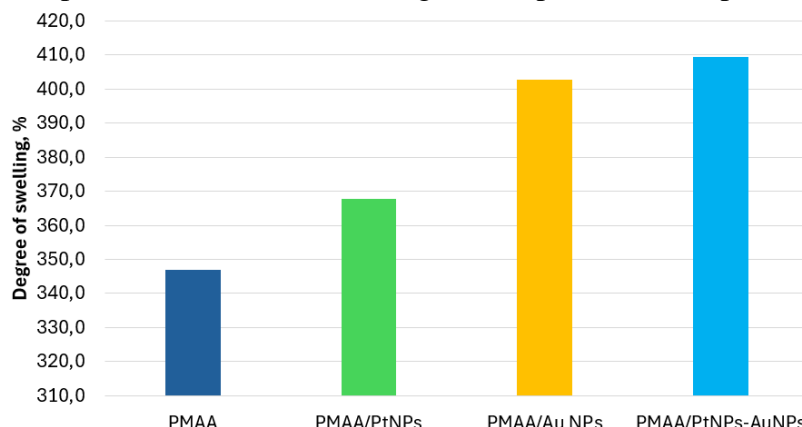


Figure 1 – Dependence of the degree of swelling on the composition of the composite

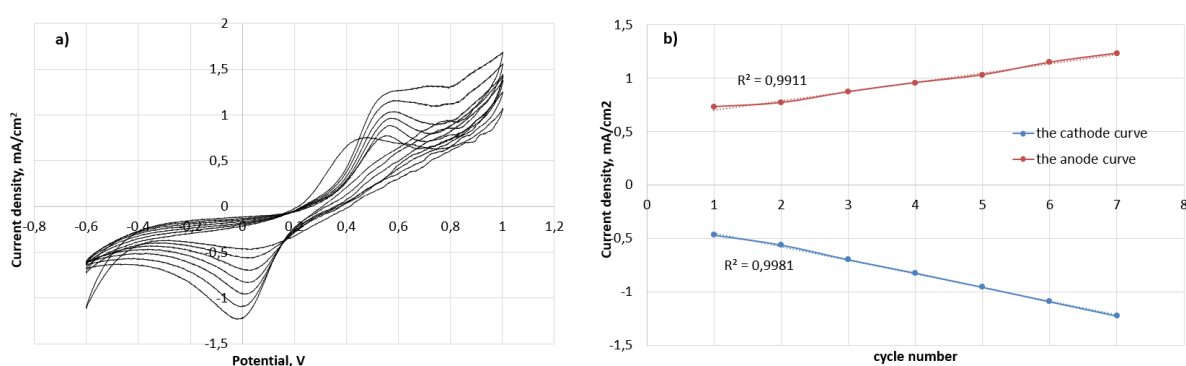


Figure 2 – a) Cyclic voltammogram (for PMAA) obtained in 0.5 M K₄[Fe(CN)₆]/0.1 M LiClO₄.

The potential sweep rate is 50 mV/s; b) the dependence of the current density on the cycle number

Further research was aimed at studying the sensory characteristics of electrodes modified with polymer/metal nanoparticle composite films. For this purpose, cyclic voltammograms were taken in a phosphate buffer with the addition of 1.28*10⁻³ M H₂O₂ (Fig. 3). As can be seen from the CVA curves, with each addition of a new portion of hydrogen peroxide, an increase in current density was observed, indicating an increase in the concentration of the injected substance (Table 1). The most effective catalyst was found to be composite with the inclusion of PtNPs. The combined presence of PtNPs and AuNPs in the composite had virtually no effect on the

THE 11th ANNUAL STUDENT SCIENTIFIC CONFERENCE IN ENGLISH
Vladivostok, May 2024

efficiency of the catalyst compared to PMAA/PtNPs.

Thus, the conducted studies have shown that electrodes modified with composite films based on PMMA with the inclusion of platinum and gold nanoparticles can be used as sensors for the determination of hydrogen peroxide.

Table 1

Maximum values of current densities depending on the content of hydrogen peroxide.

Concentration of H ₂ O ₂ , mM	Current density, mA/cm ²			
	PMAA	PMAA/AuNPs	PMAA/PtNPs	PMAA/AuNPs-PtNPs
0.128	-0.305	-0.294	-0.314	-0.339
0.256	-0.348	-0.343	-0.401	-0.399
0.383	-0.386	-0.399	-0.469	-0.467
0.512	-0.418	-0.458	-0.537	-0.546

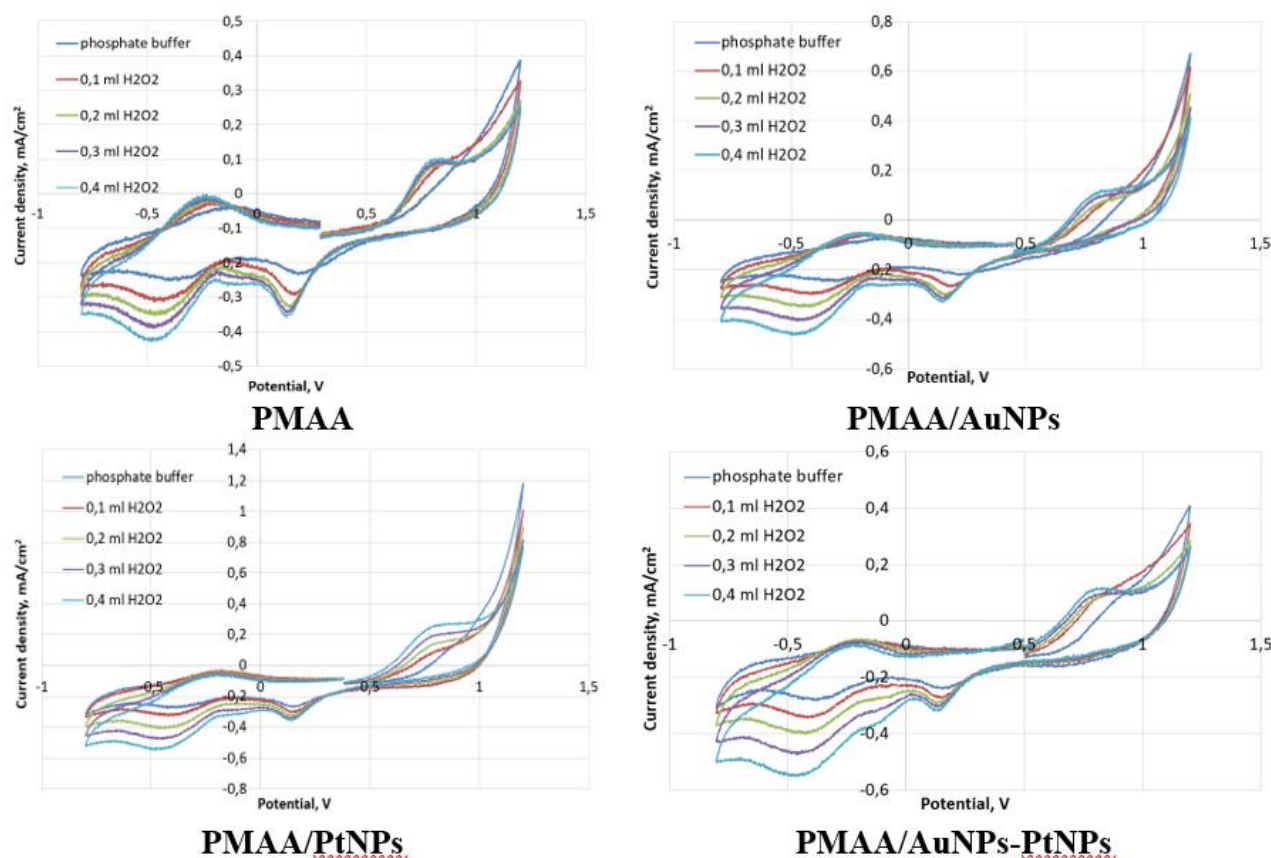


Figure 3 – Cyclic voltammograms obtained in a phosphate buffer with the addition of 1.28×10^{-3} M H₂O₂. The potential sweep rate is 50 mV/s

The work was performed in accordance with the Russian Federation State Order of the Institute of Chemistry FEBRAS, project No. 3 FWFN-0205-2022-0001.

References:

1. Electrochemical formation and properties of polymethylolacrylamide film with inclusion of platinum particles / E. V. Shchitovskaya, L. G. Kolzunova, V. G. Kuryavy, A. B. Slobodyuk. – DOI 10.7868/S0424857015110158 // Encyclopedia, 2015. – Vol. 51. – №. 12. – P. 1235-1246.
2. Xuea, K. One-step synthesis of 3D dendritic gold@polypyrrole nanocomposites via a simple self-assembly method and their electrocatalysis for H₂O₂ / K. Xuea, Y. Xub, W. Songa. – DOI 10.1016/j.electacta.2011.11.003 // Electrochimica Acta, 2012. – Vol. 60 – P. 71-77.

**THE 11th ANNUAL STUDENT SCIENTIFIC CONFERENCE IN ENGLISH
Vladivostok, May 2024**

3. Kolzunova, L. Polymethylolacrylamide / AuNPs Nanocomposites: Electrochemical Synthesis and Functional Characteristics / L. Kolzunova, E. Shchitovskaya, M. Karpenko. – DOI 10.3390/polym13142382 // Polymers, 2021. – Vol. 13. – P. 2382.

Ivanov N.P.¹, Rastorguev V.L.¹, Marmaza P.A.¹, Seroshtan A.I.¹, Dran'kov A.N.¹, Shichalin O.O.²

HYDROPHOBIZATION OF MAGNETIC SORPTION MATERIALS BASED ON LAYERED DOUBLE HYDROXIDES FOR SELECTIVE OIL REMOVAL

¹Far Eastern Federal University, Institute of High Technologies and Advanced Materials, FEFU

² Sakhalin State University, Yuzhno-Sakhalinsk

Scientific advisor– O.O. Shichalin²

As a result of marine ecosystems pollution by oil and its components, a serious environmental threat to the safety of present and future generations is created. To effectively eliminate emergency oil spills from the surface of water, there is a need to develop new sorption materials with the properties of selectivity, hydrophobicity, high oil capacity, as well as magnetic susceptibility to enable rapid extraction of saturated material.

Porous polymer materials (in particular, melanin-formaldehyde resin) have a huge absorption capacity for oil and petroleum products due to the possibility of a multiple increase in the volume of the polymer network because of swelling. However, to impart hydrophobicity to such materials (providing selectivity in the separation of oil-water mixtures), as well as magnetic susceptibility, their surface must be modified. This work examines a new method for modifying the surface of a porous melanin-formaldehyde sponge by coating it in-situ with a nanocomposite suspension of layered double hydroxide Zn-Al-LDH and iron oxide Fe₃O₄. To impart hydrophobicity to a composite porous magnetic material, various methods of hydrophobization are considered: (a) using sodium stearate, (b) using sodium oleate, (c) using sodium dodecyl sulfate.

Therefore, the purpose of this work is to study the influence of the modification method on the hydrophobicity/hydrophilicity of the surface of the composite material, on the sorption properties in relation to oil, as well as on its structural and disperse characteristics. The scientific novelty of the work lies in the fact that the method of modifying the surface of a porous melanin-formaldehyde matrix using the Fe₃O₄/Zn-Al-LDH nanocomposite was considered for the first time. Besides, the influence of the type and concentration of the modifier (stearate, oleate, sodium dodecyl sulfate) on structural and disperse characteristics of the material was studied.

Prior to surface modification, the spongy melanin-formaldehyde resin was cut into rectangular pieces with a volume of 1 cm³ and placed for 24 hours in a freshly deposited suspension of the Fe₃O₄/Zn-Al-LDH magnetic nanocomposite, after which the modified material was dried for 24 hours at a temperature of 60 °C. The composites were then washed to remove crystallized salt and dried again for 24 hours. After this, the sponge magnetic material was hydrophobized by keeping it for 24 hours at a temperature of 50 °C and constantly stirring in an alcohol solution of a water repellent: 0.01 and 0.05 M sodium stearate, sodium oleate and sodium dodecyl sulfate.

The phase composition of the consolidated materials was studied by X-ray phase analysis (XPD) using a Bruker D8 Advance instrument (Germany). The surface morphology of the materials and their elemental composition were studied using a scanning electron microscope ULTRA 55+ ZEISS (Germany). To determine the specific surface area and study the pore size distribution, the method of low-temperature nitrogen adsorption at a temperature of 77 °K was used on an Autosorb IQ instrument (Quantachrome Instruments, USA). The specific surface area was calculated using the Brunauer–Emmett–Teller (BET) method and the pore size distribution in the samples was calculated using the density functional theory (DFT) method. The values of sorption capacity in relation to VSTO grade crude oil, motor oil and water were determined by weighing samples after sorption saturation.

Fig. 1 shows diffraction patterns of modified sorbents. Organic modifiers that crystallize on the surface of

THE 11th ANNUAL STUDENT SCIENTIFIC CONFERENCE IN ENGLISH
Vladivostok, May 2024

LDH are amorphous and therefore do not change the diffraction pattern. According to XRD data, the phase composition after modification is represented by the phases of layered double hydroxide $Zn_{0.7}Al_{0.5}(OH)_2(CO_3)_{0.15}$ and zinc oxide ZnO . A slight shift of the first diffraction maximum to the region of large angles 2θ is observed, which indicates a narrowing of the interlayer space of the LDH. Thus, intercalation of these modifiers into the interlayer space of the LDH is not observed.

In Fig. 2 the values of the specific surface area of composite materials modified with various molecules are presented. Modification with sodium stearate and oleate leads to the most significant decrease in the specific surface area (by 70.87 and 76.46%). Modification with sodium dodecyl sulfate leads to a decrease in the specific surface area by 50.49%. As the salt concentration increases, the specific surface area decreases proportionally. The dimensions of mesopores (5 nm for the starting material) increase when modified with sodium sterate and oleate, but do not change for dodecyl sulfate. The observed picture of changes in the porous structure confirms the crystallization of salts on the outer surface and in the pores of the starting material due to adsorption, leading to an increase in the hydrophobicity of the composite.

Figure 3a shows the contact angles of a water drop and the surface of a consolidated disk of powdery material. In this case, only materials modified with sodium stearate at a concentration of 0.05 M meet the hydrophobicity criterion. However, when modifying melanin sponge composites, a significant excess of the contact angle of 90° is also observed when sodium stearate with a concentration of 0.01 M is used as a modifier. Thus, based on the results of measuring contact angles, the optimal processing method is modification with sodium stearate.

In Fig. 4 shows the adsorption values of oil, water and motor oil on both powdered materials and sponge composites. As can be seen from Fig. 4, melanin sponge composites have high capacity values with respect to petroleum and motor oil. At the same time, in the case of using 0.01 M sodium stearate as a modifier, the optimal degree of hydrophobization is achieved.

In the course of the work, the optimal method for hydrophobizing the surface of a magnetic sponge composite melanin resin/ Fe_3O_4 -Zn-Al-LDG was determined: treatment with a 0.01 M solution of sodium stearate. Hydrophobized materials are characterized by high capacity values relative to VSTO grade oil of 22.70 g/g, which indicates prospects for their use as oil sorbents.

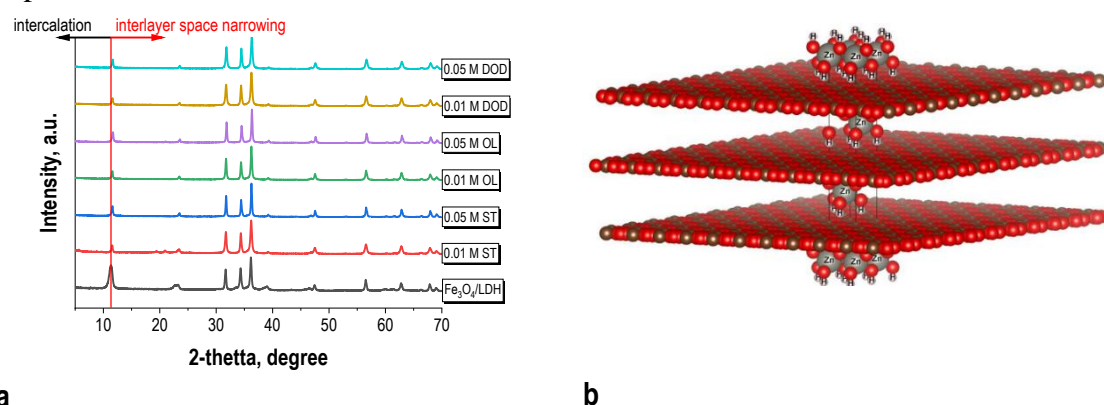
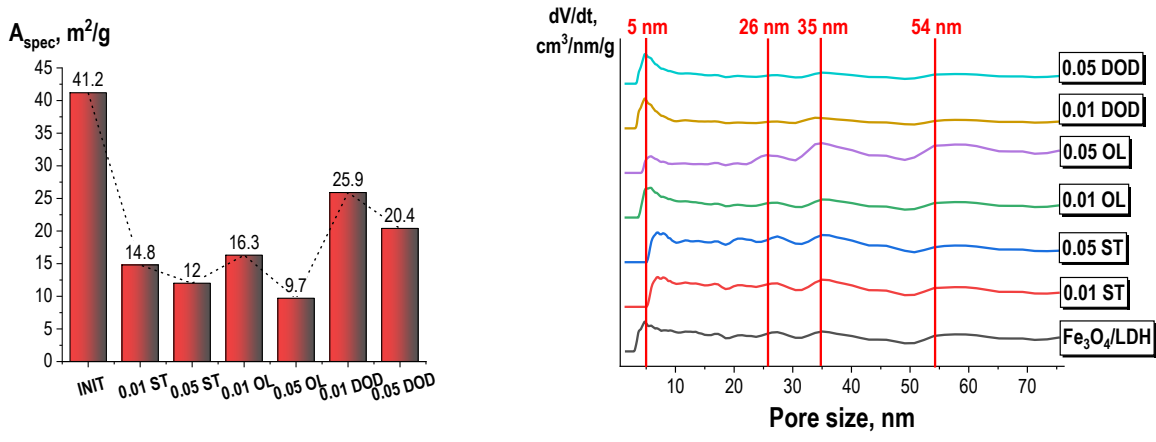


Fig. 1. (a) XRD patterns of modified materials and (b) model image of initial LDH unit cell

THE 11th ANNUAL STUDENT SCIENTIFIC CONFERENCE IN ENGLISH
Vladivostok, May 2024



a

b

Fig. 2. (a) Specific surface area and (b) DFT pore size distributions of modified materials

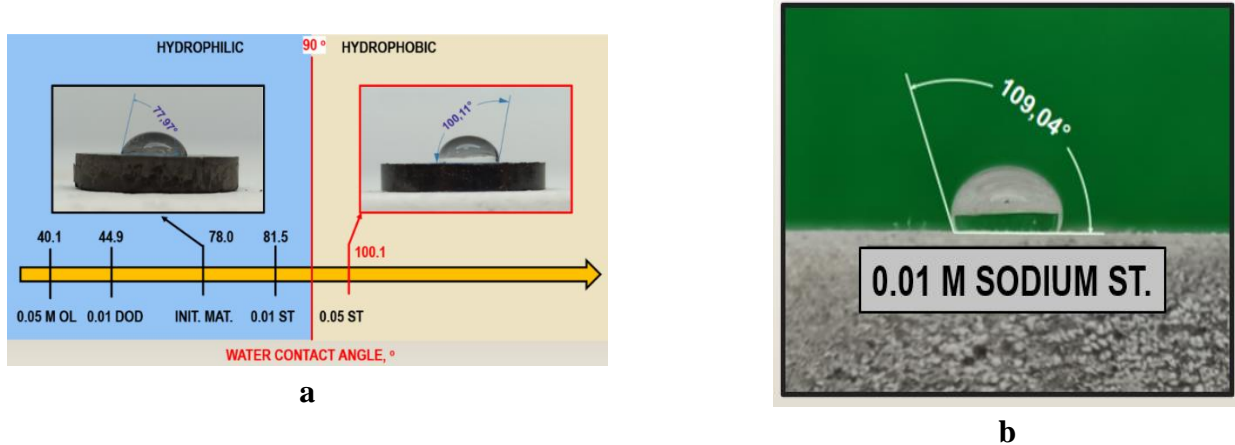


Fig. 3. Water contact angles on (a) modified powdered materials and
(b) modified melanin sponge-like composites

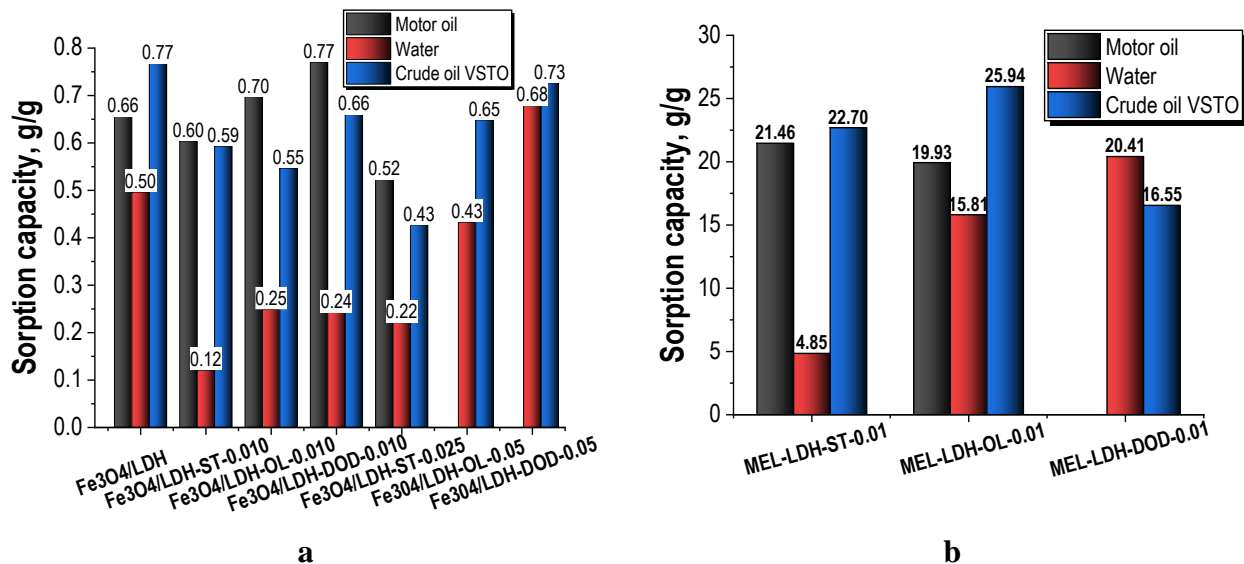


Fig. 4. Sorption capacity of granulated materials (a) and modified melanin sponges (b) towards water, motor oil and VSTO crude oil

ELECTROCHEMICAL ACTIVITY OF Ti₂AlC/TiC MAX-PHASE COMPOSITE CERAMICS OBTAINED BY SPARK PLASMA SINTERING

¹Far Eastern Federal University, Institute of High Technologies and Advanced Materials, FEFU

² Sakhalin State University, Yuzhno-Sakhalinsk

Scientific adviser – O.O. Shichalin ²

In the last decade, there has been increasing interest in a new family of 2D materials containing transition metal carbides, nitrides and carbonitrides (MX-enes). Representatives of this family were successfully obtained by selective etching of metal “A” from the corresponding MAX phases. The general formula of these compounds is $M_{n+1}AX_n$, where M is a transition metal, A is an A-group element, X is C and/or N, and n = 1, 2 or 3. Up to date, more than thirty types of MX-enes have been synthesized, including $Ti_3C_2T_x$, Ti_2CT_x , $Ta_4C_3T_x$, V_2CT_x , Nb_2CT_x and so on, where T_x denotes terminal functional groups of a different nature. Due to their unique layered structure, MX-enes are used in the field of catalytic energy conversion, as electrode materials and supercapacitors. However, due to the novel nature of this class of functional nanomaterials, efficient methods for the synthesis of MX-enes and MAX phases from available raw materials have not been explored. Also, the use of spark plasma sintering (SPS) technology to obtain functional ceramic materials based on MX-enes and MAX phases is of scientific interest.

In this regard, the goal of this study is to obtain functional ceramic materials based on MAX phase Ti_2AlC from precursors such as Al_4C_3 , Ti and TiC using SPS technology, which was first proposed to the global scientific community. To prepare a mixture of powdered MAX-phase precursors, methods of dry mechanochemical synthesis were used utilizing a high-energy planetary mill, which made it possible to achieve complete homogenization of the reaction mixture. Spark plasma sintering of a homogenized mixture of precursors was carried out on an SPS-515S installation from Dr. Sinter LABTM (Japan) at temperatures of 1200, 1300, 1400 °C. The phase composition of the consolidated materials was studied by X-ray phase analysis (XRD) using a Bruker D8 Advance device, (Germany). The elemental composition of the materials was studied using a Shimadzu EDX-7000 spectrometer (Japan). The morphology of ceramic materials was studied using a scanning electron microscope ULTRA 55+ ZEISS (Germany). The microhardness of the samples was measured using a Shimadzu HMV-G-FA-D tester (Japan). The electrochemical characteristics of ceramic materials were studied by cyclovoltamperometry (CV) using an Autolab PGSTAT302 N Potentiostat/Galvanostat EcoChemie electrochemical workstation (Netherlands).

Figure 1 shows the diffraction patterns of the obtained samples of functional ceramic materials. As can be seen from the given diffraction patterns, the phase composition of the samples is represented by Ti_2AlC and TiC, which indicates the formation of the target MAX phase Ti_2AlC under spark plasma sintering conditions.

Figure 2 shows SEM images of the surface of consolidated materials, as well as the distribution of elemental composition on a ceramic section. The uniform distribution of the main structural elements Ti, Al and C over the surface of the ceramic compound indicates the uniformity of the phase composition. As the sintering temperature increases, a decrease in the number of defects is observed, caused by the final consolidation of the material.

Mechanical properties of obtained ceramic composites are presented on the Figure 3. Materials, obtained by SPS at 1200 °C are characterized by relatively low absolute density of 94.42 % and microhardness of 580.8 HV due to the incomplete consolidation and presence of apparent porosity.

CV curves in 0.1 M Na_2SO_4 solution are presented on the Figure 4. Ceramic composites, obtained by SPS at 1200 °C demonstrate relatively high capacitance of $\approx 70 \mu F/g$ due to incomplete consolidation and abundance of micro- and microdefects. Subsequent consolidation leads to degradation of electrochemically active area.

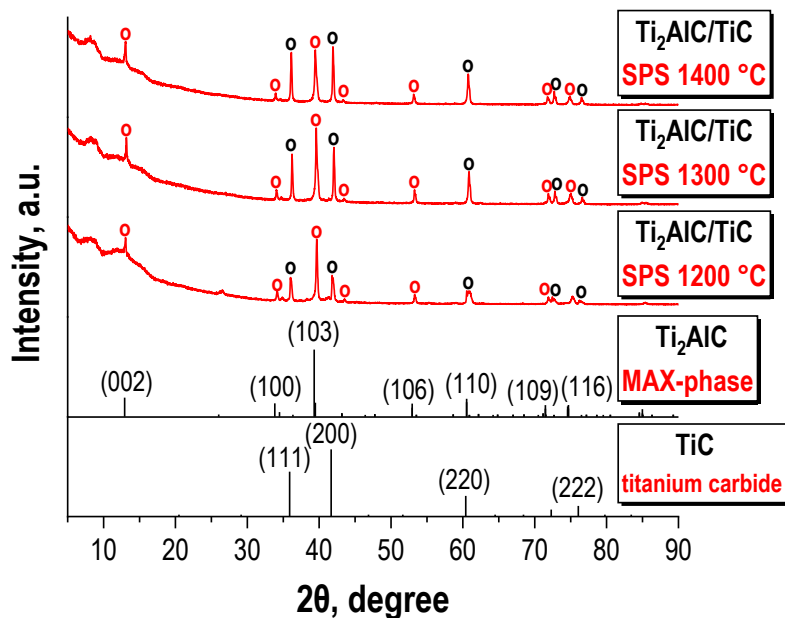


Fig. 1. XRD patterns of obtained Ti₂AlC/TiC ceramic composites

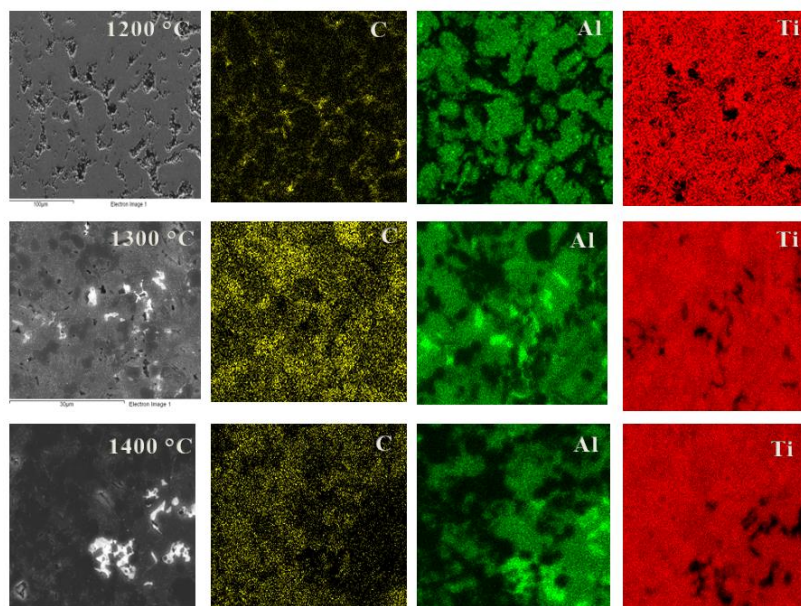


Fig. 2. SEM images of obtained Ti₂AlC/TiC ceramic composites

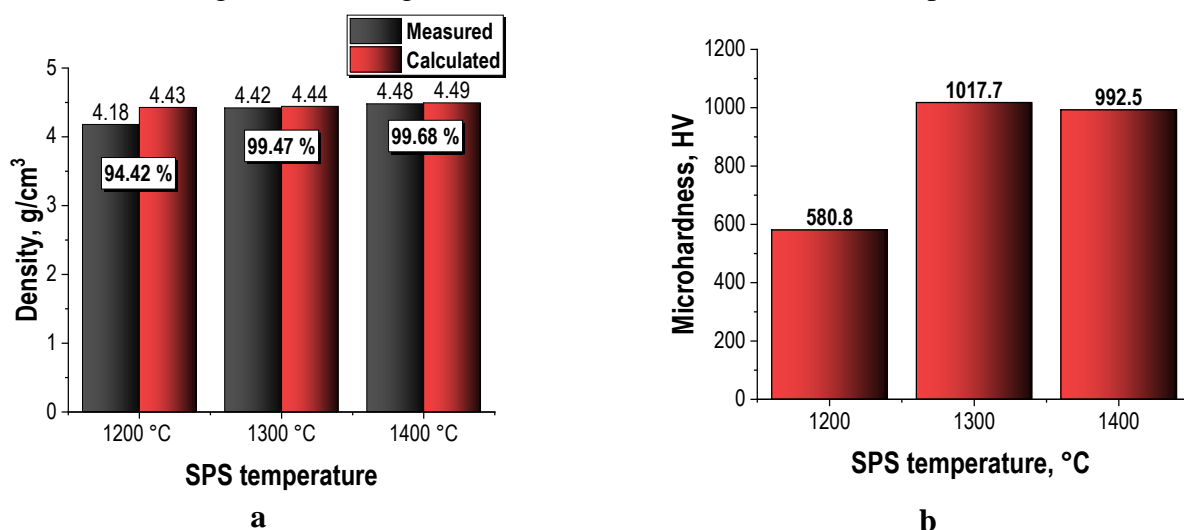


Fig. 3. Absolute density of obtained materials (a) and microhardness average values (b)

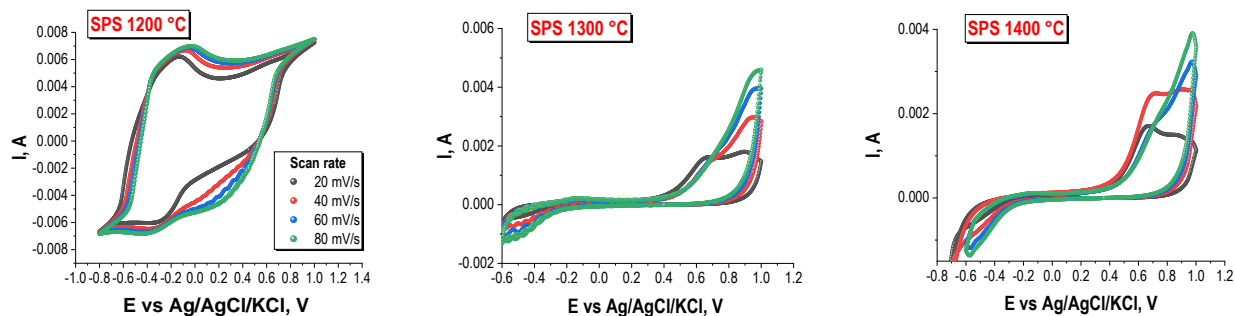


Fig. 4. CV curves of obtained materials in 0.1 M Na₂SO₄ solution.

The results obtained demonstrate the prospects of using ceramic composites consolidated at an optimal SPS temperature of 1200 °C as a material for capacitors due to the relatively high capacitance of $\approx 70 \mu\text{F/g}$. In addition, due to the presence of clearly defined oxidation-reduction peaks on the CV curves related to hydrogen and oxygen release reactions, the materials have prospects of being used as electrodes for hydrogen energy generation.

The electrochemical properties of the samples were studied with the support of the State Assignment of Sakhalin State University No. FEFF-2024-0001.

O. V. Kapustina¹, Ya. G. Zernov¹, S. M. Pisarev¹

COMPONENT RATIO EFFECT ON THE BIOPOLYMER PROPERTIES FOR BONE REGENERATION

¹Department of Nuclear Technologies Institute of High-Tech Technologies and Advanced Materials, FEFU

²Far Eastern Federal University, Oriental Institute School of Regional and International Studies, FEFU

Scientific supervisor – O. O. Shichalin¹

Scientific consultant – V. B. Kolycheva²

Injuries and bone diseases such as osteosarcoma, osteoporosis, infections, functional atrophy, congenital diseases can result in bone defects. [1]. Currently, the main method of repairing bone defects is the installation of a biocompatible implant capable of osteoregeneration.

Silicate, hydroxyapatite (HAP) and calcium phosphate are elective materials for the regeneration of bone tissue due to their compositional mimicry with bone [2].

Bioceramics for the regeneration of bone tissue bind to living bone through hydroxyapatite layer forming on the surface of the material. In addition, the ratio of the rates of biomaterial dissolution and bone tissue growth is of key importance.

The present study investigates in vitro efficacy for a series of biocomposites containing a different ratio of calcium silicate and HAP, previously obtained by wet deposition followed by hydrothermal treatment at 150°C.

The surface morphology of the obtained samples is different. A clear difference is noticeable for samples containing pure wollastonite (Fig. 1, № 1) and HAP (Fig. 1, № 11).

Wollastonite has a layered structure with visible needle-like formations. The structure of hydroxyapatite consists of interconnected cylinders with rounded edges. It is noteworthy that the transition from the wollastonite structure to the HAP structure occurs gradually i.e. the flakes forming the layers gradually begin to decrease and aggregate more strongly, then the formation of aggregated ellipsoids occurs and finally cylinders are formed (Fig. 1, № 3).

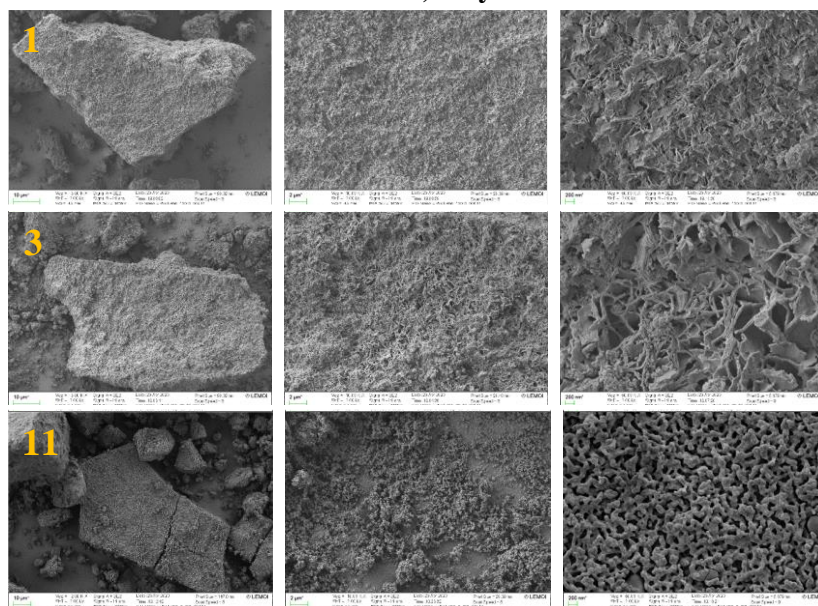


Figure 1 – SEM images of the sample surface

The change in the mass of the samples after exposure to simulated body fluid (SBF) solution and drying is determined by the ratio of the dissolution rates of the matrix and the formation of calcium hydroxyapatite on the sample surface. With the predominance of the dissolution process, the mass of the sample decreases sequentially, and the formation of hydroxyapatite increases.

According to the graph of the mass change depending on the exposure in the simulative body fluid solution, with an increase in the mass of HAP in the composite, the rate of formation of HAP on the surface increases, the rate of dissolution of the matrix decreases (Fig. 2).

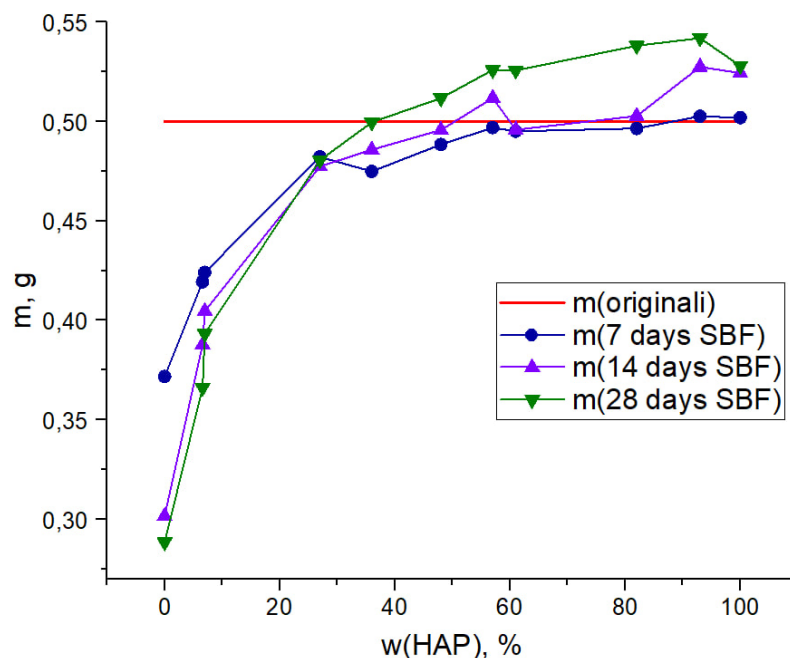


Figure 2 – Dependence of the change in the mass of samples on the holding time in SBF solution

References

- Pan P. et al. // Advanced Science. – 2001. V. 8. – P. 126.
- Oliveiraa J. M. Osteochondral Tissue Engineering Nanotechnology, Scaffolding-Related / J. M. Oliveira et al.// Developments and Translation: Nanotechnology, Scaffolding-Related Developments and Translation. Luxembourg : Springer Link. 2018. 470 p.

Marmaza P.A.¹, Ivanov N.P.¹, Kaptakov V.O.²

**HYDROTHERMAL SYNTHESIS OF DUAL-CATION GRACE TITANOSILICATE FOR EFFICIENT
¹³⁷Cs REMOVAL FROM LIQUID WASTE WITH HIGH SALINITY**

¹Far Eastern Federal University, Institute of High Technologies and Advanced Materials, FEFU

²Frumkin Institute of Physical Chemistry and Electrochemistry, Moscow

³Sakhalin State University, Yuzhno-Sakhalinsk

⁴Far Eastern Federal University, Oriental Institute School of Regional and International Studies, FEFU

Scientific supervisor – O. O. Shichalin³

Scientific consultant - V. B. Kolycheva⁴

Liquid radioactive wastes (LRW) are generated by nuclear industry enterprises at all stages of the nuclear fuel cycle and during the operation of power reactors. In addition to the nuclear power industry, LRW are generated in medical and scientific institutions, in the military-industrial complex and other industries. Cesium radionuclides (Cs-137, Cs-134) are uranium fission products and one of the main sources of radioactive contamination. They are very dangerous because of their long half-life (30 years for Cs-137 and 2 years for Cs-134), high specific activity and tendency to be included in food chains and accumulate in soft tissues of living organisms. Crystalline titanosilicates, promising sorption materials, are successfully used to effectively extract Cs+ cations from liquid media.

Crystalline titanosilicates are natural or synthetic crystalline frame materials, the structural components of which are titanium-oxygen octahedra and silicon-oxygen tetrahedrons. Titanosilicates are widely used for effective treatment of liquid radioactive wastes(LRW); the main advantage of titanosilicates is their high selectivity for Cs(I) in the presence of interfering cations. The main advantage of titanosilicates is their high selectivity for Cs(I) in the presence of interfering cations being widely used for effective purification of LRW. Titanosilicates are widely used for effective purification of LRW, the main advantage of titanosilicates being their high selectivity for Cs(I) in the presence of interfering cations

In the research, samples of dual-cation (sodium-potassium) incorporated pharmacosiderite type titanosilicate were synthesized by directed hydrothermal synthesis with varying conditions of synthesis duration from 24 hours to 7 days at 180 °C, as well as in atmospheric synthesis at 25 °C for 4 days.

The crystalline phases of the samples were identified by X-ray diffraction (XRD) analysis. Scanning electron microscopy (SEM) with Carl Zeiss ULTRA 55 Plus device (Germany) was used to determine the surface morphology. The energy dispersive spectroscopy (EDS) with Oxford X Max 80 device (UK) was used to determine the elemental composition of the samples. The texture characteristics of obtained material were studied by the low-temperature N₂ adsorption–desorption method using Quantachrome Autosorb IQ (USA). The values of the specific surface area ABET (m²/g) were calculated by isotherms of low-temperature N₂ adsorption single-point BET method. The pore size distributions in the studied materials were determined applying the DFT method.

The sorption characteristics of the samples toward ¹³⁷Cs were studied in batch sorption mode. The concentration of stable cesium isotope in the solution before and after adsorption was determined by atomic adsorption spectroscopy. The specific activity of ¹³⁷Cs in the filtrate was determined by the direct radiometric method using the spectrometric complex SKS-50M (Green Star Technologies, Moscow).

Figure 1 shows the diffraction patterns of the obtained samples of dual-cation (sodium-potassium) incorporated pharmacosiderite type titanosilicates. The obtained samples have well-defined Bragg diffraction peaks being characteristic of crystalline titanosilicate of the pharmacosiderite type- corresponding to reference patterns from the PDF-2 crystal structure database. GTS-4 synthesized in air is X-ray amorphous. The phase composition of the samples GTS-1 and GTS-2 is represented by crystalline titanosilicate of the pharmacosiderite type PDF #86-665. On the 7th day of hydrothermal synthesis the phase composition undergoes changes: the material recrystallizes

into titanosilicate with a structure similar to natisite (PDF #85-512).

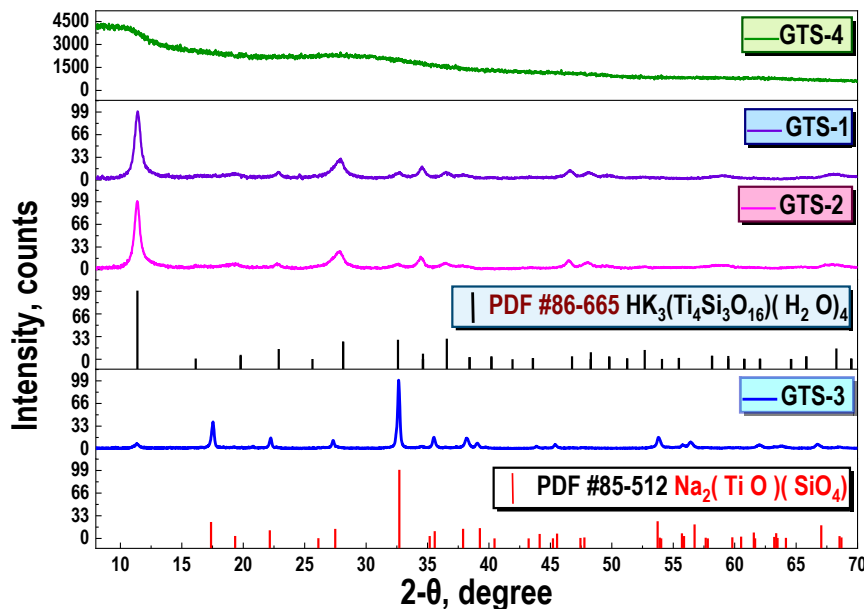


Fig. 1. XRD patterns of obtained materials.

The obtained samples of crystalline titanosilicates demonstrate high sorption-selective properties toward ^{137}Cs in microconcentration. The distribution coefficients in model solutions of low and medium salinity (0.1 M and 1 M NaNO_3) exceed 10^5 mL/g indicating a high degree of selectivity of the obtained materials. The distribution coefficients in low salinity (0.1 M NaNO_3) model solutions of LRW: GTS-1 — $5.83 \times 10^4 \text{ mL/g}$; GTS-2 — $1.83 \times 10^5 \text{ mL/g}$; GTS-3 — $5.34 \times 10^5 \text{ mL/g}$; GTS-4 — $2.34 \times 10^3 \text{ mL/g}$. In medium salinity model solutions (1 M NaNO_3): GTS-2 — $1.25 \times 10^5 \text{ mL/g}$; GTS-3 — $2.01 \times 10^5 \text{ mL/g}$; GTS-4 — $3.51 \times 10^2 \text{ mL/g}$.

A correlation between the hydrothermal synthesis time and the values of sorption-selective characteristics towards ^{137}Cs was found according to analysis report. With increasing the hydrothermal synthesis time there is an increase in the values of distribution coefficient. In general, the obtained values of sorption exchange capacity and distribution coefficients are quite high. Thus, the obtained results allow us to conclude that the synthesized samples can be used as effective sorbents for the extraction of Cs^+ from liquid media.

The study was performed within the framework of the government assignment of the Ministry of Science and Higher Education of the Russian Federation no. FZNS-2023-0003, theme: Fundamental Principles of Chemical Designing of Novel Functional Materials Adaptive to Nuclear and Radiation Technologies.

Marchenko A.V.^{1,3}

EXPLORATION OF THE ACTIVE SPECIES IN THE PHOTOCATALYTIC DEGRADATION OF METHYL ORANGE UNDER UV LIGHT IRRADIATION

¹Far Eastern Federal University, School of Engineering, FEFU

² Far Eastern Federal University, Oriental Institute School of Regional and International Studies, FEFU

³ Institute of Chemistry Far Eastern Branch of the Russian Academy of Sciences, Institute of Chemistry FEB RAS
Scientific adviser – O.D. Arefieva^{1,3}
Scientific consultant – V.B. Kolycheva²

Photocatalysis is considered one of the most promising and innovative types of advanced oxidation processes, which has the advantage of not requiring additional methods for wastewater treatment. Currently, there is active development of photocatalysts based on semiconductor materials, such as ZnO/SiO_2 . However, the

THE 11th ANNUAL STUDENT SCIENTIFIC CONFERENCE IN ENGLISH
Vladivostok, May 2024

mechanism of photocatalytic activity in the presence of these materials is not fully understood. In particular, the role of active species ($\cdot\text{HO}$, O_2^\cdot , h^+ , e^-) involved in the degradation of organic pollutants is still being studied.

The aim of this research is to investigate the mechanism of methyl orange degradation using active particle scavengers in the presence of a ZnO/SiO_2 photocatalyst. For this purpose, a photocatalyst with a composition of 40 % ZnO and 60 % SiO_2 was synthesized using the sol-gel method. The starting materials were silicon dioxide xerogel and zinc acetate dihydrate. The xerogel was obtained from rice husk, which was treated with 0.1 M hydrochloric acid [1]. The photocatalyst was then calcined at 350 °C for 30 minutes. The synthesized photocatalyst was characterized using IR spectroscopy, SEM, XRD, EDS, and XRF.

To study the active particles involved in the photocatalytic degradation of methyl orange (MO) in the presence of Zn-Si-0.4-350 when exposed to UV light, p-benzoquinone (BQ), sodium oxalate ($\text{Na}_2\text{C}_2\text{O}_4$), hydrogen peroxide (H_2O_2) and tert-butyl alcohol (t-BuOH) were used as scavengers of superoxide radicals (O_2^\cdot), holes (h^+), electrons (e^-) and hydroxyl radicals ($\cdot\text{OH}$), respectively.

According to the results of X-ray fluorescence analysis, the sample contains zinc oxide (28 %) and silicon dioxide (72 %). The infrared spectrum contains absorption bands at 783 and 1043 cm^{-1} , corresponding to valence vibrations of siloxane bonds in silicon-oxygen silicates. The band at 1427 cm^{-1} corresponds to valence vibrations of the carbonate ion, and the bands in the 420–432 cm^{-1} region correspond to zinc oxide bonds. According to the results of X-ray phase analysis, the samples were found to be in an amorphous-crystalline state. Hexagonal photoactive ZnO was identified in the crystalline phase. A study of the surface morphology revealed that the samples had a developed surface with a floral structure. Zinc oxide was unevenly distributed on the surface.

A study of the mechanism of photocatalytic degradation of a dye under UV light irradiation conditions showed that the greatest reduction in χ was observed when BQ, t-butOH, and H_2O_2 were used. The degree of degradation of methyl orange (MO) when using sodium oxalate ($\text{Na}_2\text{C}_2\text{O}_4$) did not statistically differ. Based on these results, it can be concluded that $\cdot\text{OH}$, O_2^\cdot , and e^- are involved in the degradation process.

In this work, photoactive materials based on ZnO/SiO_2 were produced. The mechanism of photocatalytic decomposition of methyl orange dye in the presence of ZnO/SiO_2 under ultraviolet radiation was studied. It was found that superoxide and hydroxyl radicals play a major role in the decomposition process.

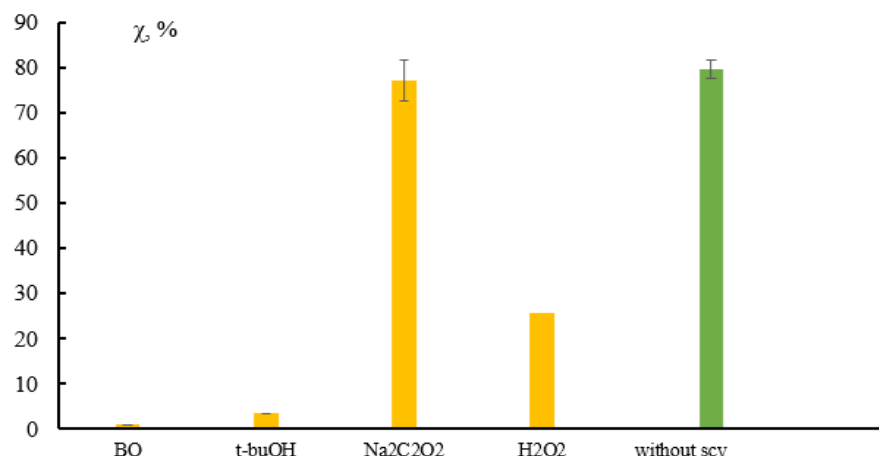


Fig.1. The degree of decomposition of methyl orange in the presence of active particle absorbents

References:

1. Zemnukhova L.A. Properties of amorphous silica obtained from rice and rice processing waste / L.A. Zemnukhova, A. G. Egorov, G. A. Fedorishcheva [et al.] // Inorganic materials. - 2006 – Vol. 42, №1 –P. 24-29.

Orinicheva P.D.¹, Kharchenko V.G.¹, Tsyganok V.S.¹, Frolov K.R.^{1,2}

TAILING DUMPS OF DALNEGORSK MINING AND PROCESSING PLANT: WASTE CHARACTERIZATION, IMPACT ON THE HYDROSPHERE

¹FEFU, Polytechnic institute, Department of Oil and Gas Technologies and Petrochemicals

²Far Eastern Federal University, Department of Nuclear Technologies

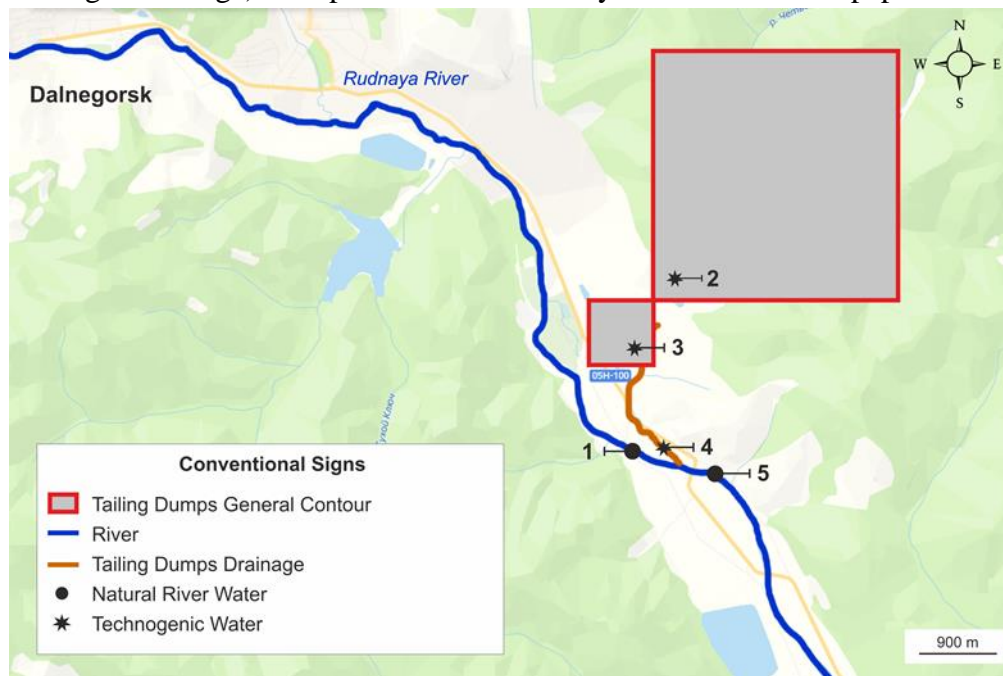
³Far Eastern Federal University, Oriental Institute School of Regional and International Studies

Scientific adviser – K.R. Frolov^{1,2}

Scientific consultant – V.B. Kolycheva³

Dalnegorsk Mining and Processing Plant (MPP) is an enterprise developing a deposit of borosilicate skarns in the Russian Far East. When producing boric acid and boric anhydride, tailings are placed in a cascade of tailing dumps. As a result of interaction of tailings with weathering agents (precipitation and air, temperature gradient) technogenic solutions are formed: slurry and drainage water of tailings. The purpose of the work is to characterize the waste and the impact of waste from the tailing dumps complex of Dalnegorsk Chemical Plant (DCP) on the hydrosphere.

At the first stage the borohypsum waste hazard class was calculated in accordance with the Order of the Ministry of Natural Resources and Environment of the Russian Federation 2014 № 536 [1]. The calculation was based on the composition of borohypsum determined by X-ray fluorescence and chemical analysis; the components of the waste include silicon oxide, aluminum oxide, iron (III) oxide, manganese (II) oxide, magnesium oxide, calcium oxide, boron oxide, sulfate anion [2]. At the second stage of the work the chemical analyses of hydrochemical samples was carried out in FEGI FEB RAS by ICP-AES and ICP-MS methods. The samples were technogenic discharge of tailing dumps (slurry and drainage) and natural waters of the Rudnaya River (before and after technogenic drainage discharge). Samples were collected by the authors of the paper in 2018-2023 (Figure 1).



1 – Rudnaya River natural waters, tailing dumps upstream; 2 – slurry waters of the operating tailing dumps; 3 – slurry waters of the closed tailing dumps; 4 – tailing dumps drainage waters; 5 – Rudnaya River natural waters, tailing dumps downstream

Figure 1. Sampling scheme

According to the calculations, the degree for the environment for borohypsum hazard is 64.49. In accordance with the calculations carried out, the environmental hazard level of borogypsum to the environment is 64.49. This value belongs to IV class by the criteria for assigning waste to hazard classes I-V. By the regulatory legal acts of the Russian Federation the DCP tailings are low-hazardous wastes and have a low negative impact on the

THE 11th ANNUAL STUDENT SCIENTIFIC CONFERENCE IN ENGLISH
Vladivostok, May 2024

environment degree.

The analysis of hydrochemical water samples showed that the maximum permissible concentrations for fisheries were many times exceeded in the technogenic waters of the tailings complex of the Dalnegorsk Mining and Processing Plant [3]: B (up to 20 times), Ni (6.5), Cu (4), Zn (15), As (1.2), Mn (92) and Ca (1.9). At the point after the drainage was discharged in the Rudnaya River, excesses of the maximum permissible concentration for fisheries were observed: B – up to 4.4, Cu – 14.5, Zn – 6.7, Al – 17.8 and Mn – 2.1.

References:

1. Ministry of Natural Resources and Environment of the Russian Federation. Order of December 04, 2014 No. 536 On Approval of the Criteria for Attributing Waste to Hazard Classes I-V by Degree of Negative Environmental Impact. – Moscow : Ministry of Natural Resources, 2014. – 17 p.
2. Yarusova S. B. Synthesis of calcium silicates in multicomponent systems and their physicochemical properties : dissertation abstract for the degree of candidate of chemical sciences / S. B. Yarusova. – Institute of Chemistry FEB RAS, Vladivostok, 2010. – 31 p.
3. Ministry of Agriculture of the Russian Federation. Order of December 13, 2016 No. 552: On approval of water quality standards of water bodies of fishery significance, including standards of maximum permissible concentrations of harmful substances in the waters of water bodies of fishery significance. – Moscow : Ministry of Agriculture of Russia, 2016. – 78 p.

Pisarev S.M.¹, Lembikov A.O.,¹ Kolodeznikov E.S.¹, Marmaza P.A.¹

**STRENGTHENING OF TITANIUM COMPOSITE BY MICRO- AND NANO-ENTROPIC SYSTEMS
OBTAINED BY SPARK PLASMA SINTERING METHOD**

¹ Far Eastern Federal University, Institute of High Technologies and Advanced Materials

²Far Eastern Federal University, Oriental Institute School of Regional and International Studies FEFU

Scientific adviser – A. N. Dran'kov¹

Scientific consultant – V. B. Kolycheva²

The key task of materials science is considered to be the development of methods for improving and regulating the properties of functional materials. Entropic materials are of interest due to their outstanding properties like hardness, strength and corrosion resistance. The concept of strengthening materials by adding entropic systems to them is a completely new approach. A completely new approach is the concept of strengthening materials by adding entropic systems, in particular entropic ceramics.

The purpose is to present a method of obtaining a titanium-based composite material by a combination of mechanical activation (MA) and electric pulse plasma sintering (EPS) methods with a hardening additive based on fine powder of high-solid equimolar medium entropic ceramics (SEC) (W,Ti,Ta)C.

Table

Physical characteristics of obtained composites

Atomic content MEC, %	Density, g/cm ³	Microhardness, μHV	Average grain size, μm
0.2	4.5760	409	9
0.5	4.5734	450	9
1	4.5713	417	5

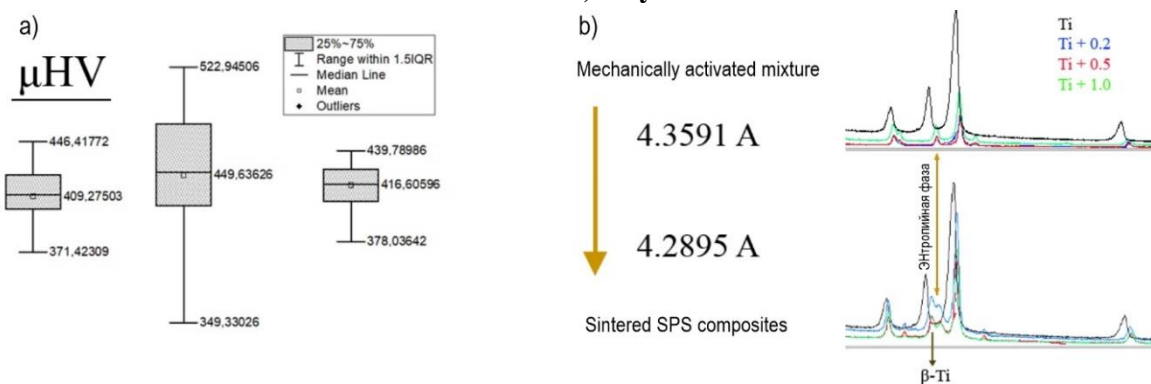


Figure 1. (a) Dispersion of hardness values. (b) Phase changes during the SPS process

This work was financially supported by the State Assignment of the Ministry of Science and Higher Education of the Russian Federation, № FZNS-2024-0014.

Savelyeva N.Yu., Balybina V.A., Kuular J.S., Kokorina N.G.

SYNTHESIS AND STUDY OF FERROCYANIDE-BASED COMPOSITE MATERIALS FOR CESIUM RECOVERY FROM LIQUID MEDI

¹ Far Eastern Federal University, School of Natural Sciences, FEFU

² Far Eastern Federal University, Oriental Institute School of Regional and International Studies, FEFU

Scientific adviser – Dran’kov A.N.¹

Scientific consultant – Kolycheva V.B.²

Synthesis of composite materials based on mixed ferrocyanides (FC) K-Co and K-Cu with a siloxane-acrylate emulsion and polyethylene in composition was carried out. The phase composition of the materials was found to be characterized by a highly organized crystal structure.

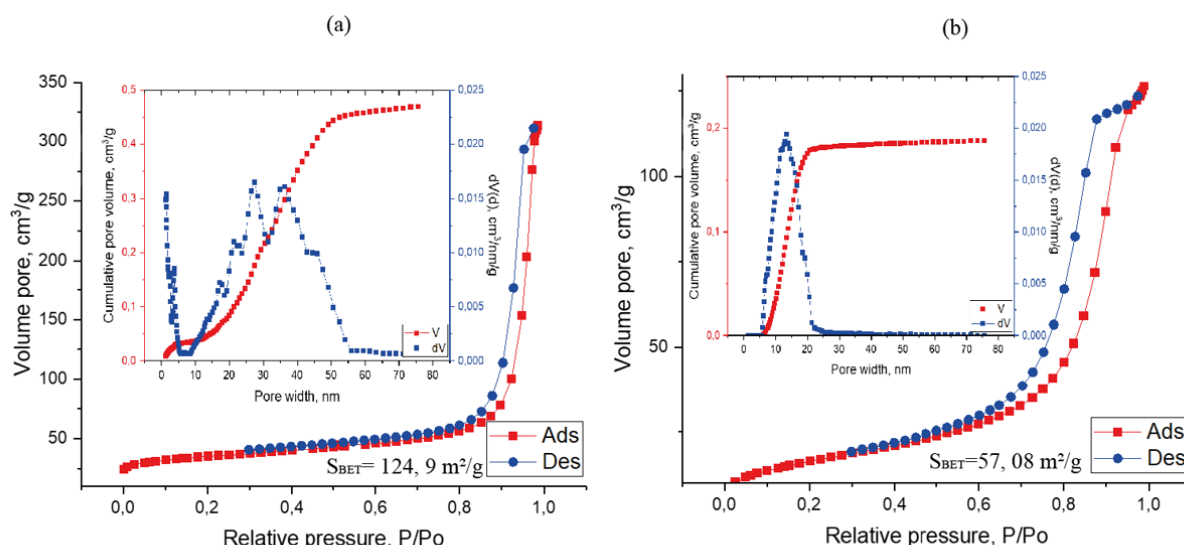


Fig.1. Low-temperature sorption-desorption isotherms of nitrogen and histograms of pore size distribution calculated by the DFT method: (a) - FC K-Cu + PE; (b) – FC K- Co + PE

Complete filling of the pores occurring at very low relative pressures and confirmed by an identical range of micropore size was determined using the density functional method (Fig. 1a). An obvious difference has the

THE 11th ANNUAL STUDENT SCIENTIFIC CONFERENCE IN ENGLISH
Vladivostok, May 2024

sample (FC K-Cu-PE) with the value of S_{BET} increases to 124.9 m²/g, and the transition of the hysteresis loop shape of the adsorption-desorption isotherm of nitrogen from H1 to H2 indicating the formation of mesopores in the composition of the sample (Fig. 1a). The pore size distribution shows that mesopores with sizes in the range of 10-60 nm are formed in the volume of the sample, that is confirmed by DFT calculation.

Sorption properties of the sorbents produced with respect to ¹³⁷Cs extracted from model solutions have been studied. The distribution coefficients (Kd) of ¹³⁷Cs for different sorbent specimens in sodium nitrate solutions with a concentration of 0.1 and 1.0 mol/dm³ and 5 times diluted seawater (SW/5) are shown in the table.

Table 1

Values of distribution coefficients (Kd) of ¹³⁷Cs on different sorbents during sorption from model solutions

Sorbent	Values of Kd ¹³⁷ Cs, cm ³ /g for sorption from solution		
	0.1 mol/dm ³ NaNO ₃	1 mol/dm ³ NaNO ₃	SW/5
FC K-Cu-PE	22600	21800	38000
FC K- Co-PE	21800	11200	20800
WS	19000±400	2400±100	-
Clinoptilolite	1800±100	64± 3	1500
NaA	680±20	20± 2	200
FNS	84000±2500	60000±2000	11000

The results of the study show that the highest sorption characteristics in relation to ¹³⁷Cs possess the sample of FC K-Cu-PE, the value of Kd for which exceeds the values for industrially used sorbents by two orders of magnitude (Table 1). The developed sorption materials are promising for the synthesis of effective and practically demanded selective sorbents that can be obtained by a simple and cheap method.

This work was financially supported by the State Assignment of the Ministry of Science and Higher Education of the Russian Federation, № FZNS-2024-0014.

Section III

EARTH SCIENCE

Grebennik P.V.¹

THE COMPARISON OF THE HYDROLOGICAL CHARACTERISTICS OF THE SOUTHEASTERN AND SOUTHWESTERN COASTAL WATERS OF THE KAMCHATKA PENINSULA OBTAINED DURING CTD-SENSING ON CRUISE 23/4 OF THE RV "PROFESSOR MULTANOVSKY"

¹Far Eastern Federal University, Institute of the World Ocean, Department of Earth Sciences, FEFU

²A. V. Zhirmunsky National Scientific Center of Marine Biology, FEB RAS

³Far Eastern Federal University, Oriental Institute-School of Regional and International Studies, FEFU

Scientific adviser – T.Y. Orlova²

Scientific consultant – O.K. Titova³

Comprehensive marine research is an integral part of the system for assessing the impact of climate change on ecosystems. Currently, there are global trends of more frequent occurrence of red tides – harmful blooms of toxic algae [1]. This phenomenon also affected the Far East of the Russian Federation in autumn 2020 [3].

The expedition of the Pacific Floating University was conducted from August 10 to September 20, 2023. As a part of this task, an extensive range of work was carried out at 93 oceanographic stations [4].

The purpose of this study was to process and analyze the hydrological parameters of conductivity-temperature-depth (CTD) measurements of all expedition stations.

In the course of the work, data processing and formulation of the characteristic features of the hydrological conditions of the Sea of Okhotsk and the Pacific Ocean in the coastal part of the Kamchatka Peninsula were carried out. The primary hydrological information on the stations was obtained during the processing of data from the Sea-Bird SBE 9 plus probe in the SBE Data Processing program. Further analysis was carried out using the Ocean Data View program and the Jupiter Notebook environment using the pandas, matplotlib, seaborn modules.

The main types of water masses in the waters of the Pacific Ocean and the Sea of Okhotsk in the area of the southeastern and southwestern coasts of the Kamchatka Peninsula were determined.

During the cruise, observations were carried out at 49 oceanological stations off the Pacific water area. The salinity in the study area ranged from 23.02 PSU to 34.13 PSU. The temperature ranged from 1.0°C to 16.19 °C. Also, observations were carried out at 44 oceanological stations in the waters of the Sea of Okhotsk. The salinity in the study area ranged from 30.51 PSU to 34.04 PSU. The temperature ranged from 1.1 °C to 13.93 °C. The observations showed that the waters of the Sea of Okhotsk are colder than the waters of the Pacific Ocean. The difference was approximately 2 degrees Celsius at the appropriate depth.

At the most marine and deep-water stations in the Pacific Ocean and the Sea of Okhotsk, a cold intermediate layer was recorded in the depth range of 75-350 meters with a temperature less than 2.0 °C [2]. At the same time, the Sea of Okhotsk is characterized by a depth of 150 to 350 m, and the Pacific Ocean from 75 to 300 m.

The research was performed within the framework of the scientific and educational program Floating University (research project № 075-01593-23-06).

References:

1. Dai, Y. et al. Coastal phytoplankton blooms expand and intensify in the 21st century // Nature. - 2023. – Art. 615. - P. 280–284. - DOI: <https://doi.org/10.1038/s41586-023-05760-y>
2. Moroz I.F. Seasonal changes of the cold subsurface layer in the Okhotsk Sea // Izv. TINRO. – 2009. – Vol. 156. – P. 192-202.
3. Orlova T. Y., et al. A massive bloom of Karenia species (Dinophyceae) off the Kamchatka coast, Russia, in the fall of 2020 // Harmful Algae. – 2022. – Vol. 120. – DOI: <https://doi.org/10.1016/j.hal.2022.102337>

Denga V.S.^{1,2}

FEATURES OF THE QUATERNARY GLACIATION OF THE EASTERN FLANK OF THE BUREINSKOYE HIGHLANDS (SOUTH OF THE FAR EAST)

¹Far Federal University, Institute of the World Ocean, FEFU

²Pacific Geographical Institute, Far-Eastern Branch, Russian Academy of Sciences, PGI FEB RAS, Russia

³Far Eastern Federal University, Oriental Institute-School of Regional and International Studies, FEFU

Scientific adviser – A.M. Sazykin¹

Scientific consultant – O.K. Titova³

The specifics of the quaternary glaciation on the Mevandzha and Etkil-Yankansky ridges, which are located on the eastern flank of the Bureinskoye Highlands, are associated with an unusually low position of cirques at altitudes between 1100 and 1400 meters, which is 300–400 meters lower than in other areas of the highland [1, 3–4]. The Late Pleistocene glaciation is characterized by a snowline that reaches a height of 110 km². It was formed in the upper part of the ridges, with absolute heights between 1600 and 1800 m. A clear meridional orientation of the cirques (fig.1) is evident, with 64% of the Mevandzha ridge and 75% of the Etkil-Yankansky ridge exhibiting a northern aspect, and only 16% and 25% respectively displaying a southern aspect [1]. This geomorphological anomaly can be explained by the significant influence of cold and humid air masses from the Okhotsk Sea, which penetrate meridionally along the «Amur-Tugur corridor» to the margins of the highlands [3].

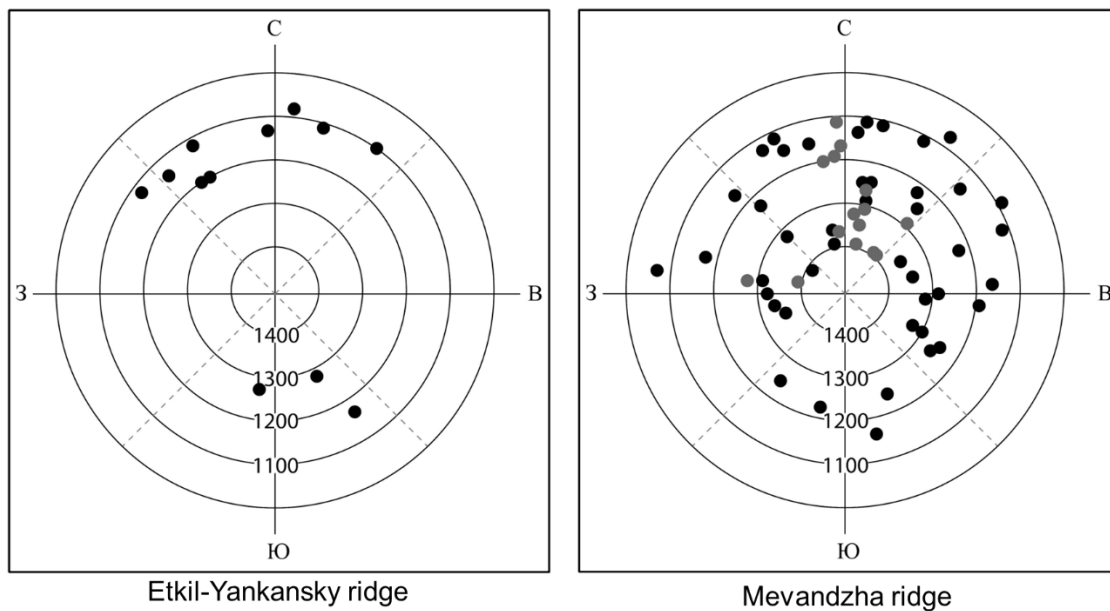


Fig. 1 – Polar diagrams of the altitude position and orientation of the cars in relation to the cardinal directions

The exaration (72 cirques) and accumulative glacial relief (30 km²) of the Mevandzha and Etkil-Yankansky ridges have been deciphered and analyzed from satellite imagery for the first time. Most of the glacial valleys (1.0-3.6 km) are represented by «pseudo troughs»: there are no trough-like valleys, the slopes are gentle, the flat bottom is filled with a convex moraine. The diagnosis of glacial forms and deposits is complicated by the poor study of the area and the presence of pseudo-glacial forms. The formations are represented by hillslopes and rock glaciers, some of the moraines have been transformed by rock movement. The «fluid pattern» of the surface of rock glaciers (Fig. 2) and transformed moraines differs significantly from the hilly-moraine form of the ground moraine.

THE 11th ANNUAL STUDENT SCIENTIFIC CONFERENCE IN ENGLISH
Vladivostok, May 2024

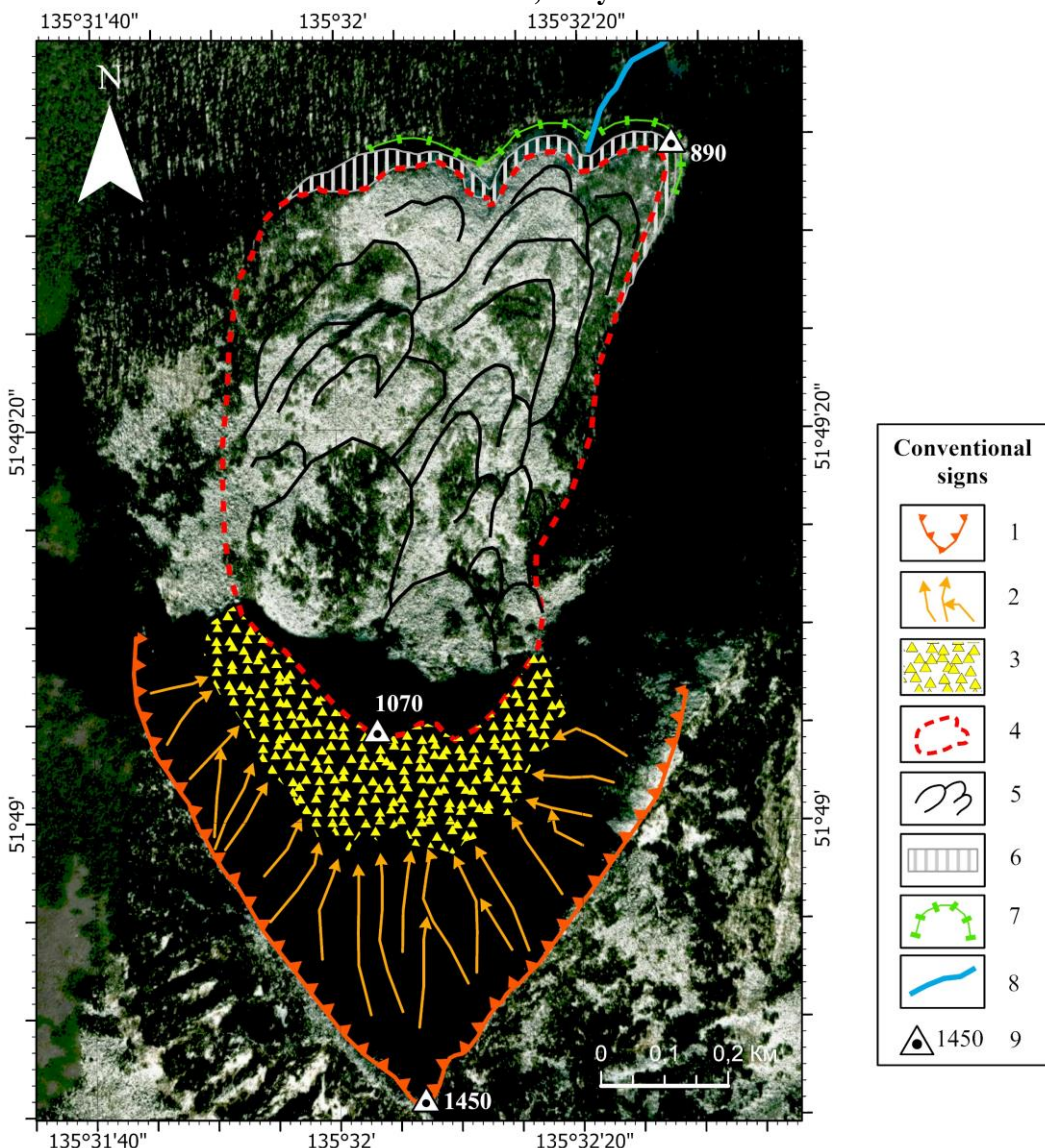


Fig. 2 – Singular valley tongue-shaped rock glacier on the the Etkil-Yankansky ridge: 1 – glacier cirque; 2 – scree troughs; 3 – colluvium; 4 – surface of active rock glacier; 5 – «fluid structures»; 6 – front scarp; 7 – pressure rollers; 8 – tributary Berendya; 9 – altitude marks.

The northern position and high altitudes of the Mevandzha ridge have led to the presence of a wider range of cryogenic and glacial morphosculpture. Of the two ridges, it is here that stepped staircase cirques, amphitheater cirques and «twisting cirques» are developed. The surfaces of the char planation with a width of up to 1.1 km, upland terraces and a wide distribution of structural soils are common features of the area. These are less common on the Etkil-Yankan ridge [1]. An interbasin river interception has been identified on the Mevandzha ridge, expressed in the relief by the Otun-Nimnyagun pass with a chain of residual lakes. The largest lake, Perevalnoe, was formed as a result of spring loading by a sloping lobate rock glacier.

In contrast to other territories, only one Late Pleistocene glaciation with two stages has been recorded. The glacial maximum is observed during the early stage of glaciation development and corresponds to the American [5] or Lazovsky time (Q^2_{III}) [2]. Traces of this stage are marked for both ridges. The latter, corresponding to the Selitkan [5] or partisan time (Q^4_{III}) [2], was identified only on the Mevandzha ridge.

The outcomes of this study can be employed by the Far Eastern PGO during geological survey work to identify potential mineral deposits (e.g., tin, gold, etc.) and create a comprehensive set of geological maps (e.g., quaternary deposits, geomorphological, etc.) for this area.

THE 11th ANNUAL STUDENT SCIENTIFIC CONFERENCE IN ENGLISH

Vladivostok, May 2024

References:

1. Denga, V.S. Quaternary glaciation of the Etkil-Yankansky Ridge / V.S. Denga // Geographical and geoecological studies in the Far East. - Vladivostok: Pacific Institute of Geography FEB RAS, 2022. - P. 8-19.
2. Korotkiy, A.M. et al. Quaternary sediments of Primorye. Stratigraphy and Palaeogeography // A.M. Korotkiy, L.P. Karaulova, T.S. Troitskaya. - Novosibirsk: Nauka, 1980. - 234 p.
3. Sazykin, A.M. Glacial geomorphology of the Bureya Plateau / A.M. Sazykin. Autoref. diss. ... candidate of geogr. sciences. - Vladivostok. 1994. - 24 p.
4. Sazykin, A.M., Denga V.S. Stone glaciers of the Bureinsky Plateau / A.M. Sazykin, V.S. Denga // Notes of the Society for the Study of the Amur Region. - VOL. XLVIII. - P. 109-117.
5. Chemekov, Yu.F. Western Priokhotee / Yu.F. Chemekov. - Moscow: Nauka, 1975. - 123 p.

Kuzmina N.A.¹

THE INFLUENCE OF COMFORT INDICATORS ON THE COST OF RENTING A ONE-ROOM APARTMENT ON THE EXAMPLE OF SOVETSKY DISTRICT, VLADIVOSTOK

¹Far Eastern Federal University, Institute of the World Ocean, FEFU

²Far Eastern Federal University, Oriental Institute-School of Regional and International Studies, FEFU

Scientific adviser – L.I. Ryabinina¹

Scientific consultant – O.K. Titova²

Purpose of the study is to find the relationship between comfort indicators and the cost of renting a one-room apartment or to prove that there is no such connection.

The relevance of the study lies in the need to assess the cost of renting an apartment in Sovetsky district, Vladivostok. Issues of housing comfort are also considered important at this stage of society development.

Sovetsky district was established in 1972. It became the fifth district of Vladivostok. Sovetsky district is the newest in Vladivostok, this territory began developing in the XIX century. Most of Sovetsky district is occupied by sanatoriums, boarding houses, a recreation center and children's health centers.

We have conducted the analysis of all one-room apartments for rent in Sovetsky district. We collected data during November 2023. In total, we processed more than 120 rental offers.

We can clearly see in the diagram that most of the buildings were built in the 60s of the 20th century (Fig.1).

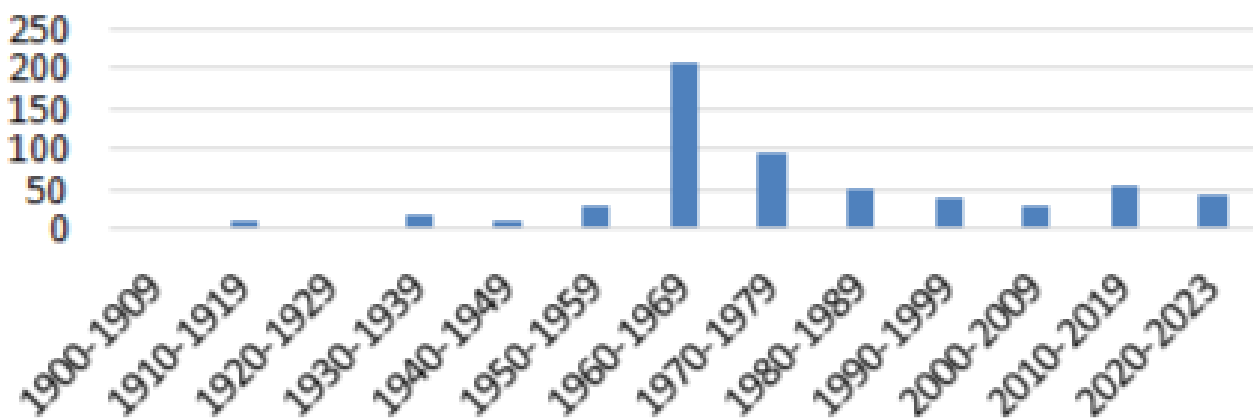


Fig 1. Number of buildings by the year of construction

In this diagram, we can see that most of the buildings are panel ones (Figure 2).

THE 11th ANNUAL STUDENT SCIENTIFIC CONFERENCE IN ENGLISH
Vladivostok, May 2024

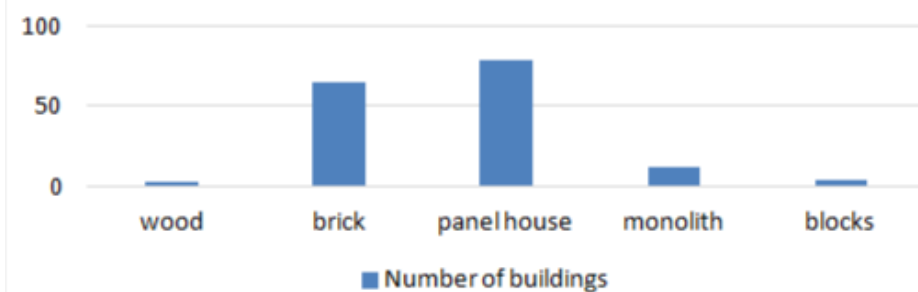


Fig 2. Number of buildings by the type of building material

We evaluated the quality of apartments and looked for a correlation between the characteristics of an apartment and the cost of rent per month. The analyzed comfort indicators are the distance to the supermarket, the number of public transport routes, the floor on which an apartment is located, the number of schools in the area and many others. In total, we analyzed 15 indicators to find a correlation.

Here is an example of one of the analyzed correlations. The diagram shows data on the correlation between the rental price per square meter and the distance from the supermarket. We see that in the area of Second River, the correlation between the two indicators is low, because the factor of distance from the store is not significant in this developed and densely populated area. The opposite situation is observed in Trudovoye area. There is a high correlation between the compared indicators, that is, we can talk about the relationship between the indicators of the cost of renting housing and the distance from the supermarket. There were no ads for renting one-room apartments in Zarya area, so we do not have data to calculate the correlation (Figure 3).

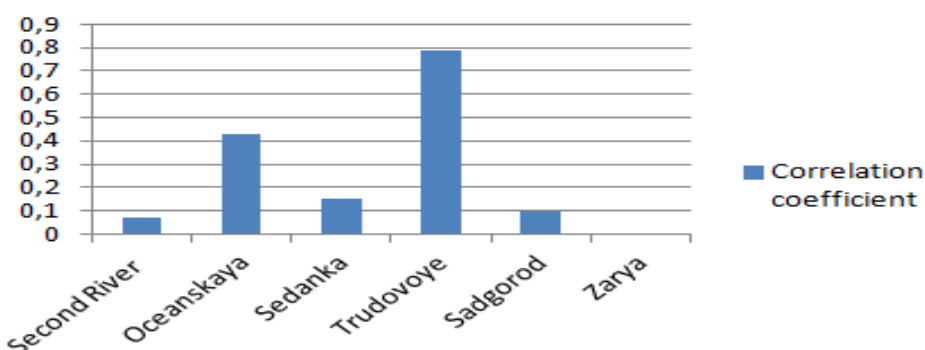


Fig 3. Correlation between the price per m² and the number of supermarkets

As a result of our research, we conclude that, in general, there is a low correlation between the cost of renting a one-room apartment and the indicators of housing comfort in Sovetsky district.

This means that the cost of renting a house does not correlate with its characteristics and is not objective.

References:

1. Rezin, G.I. How the city works / Rezin, G.I. – Moscow. – 2019. – 221 p.
2. Samson, I. Comfort of the environment as a factor of innovative development of the city / Samson, And. – Moscow. – 2013. – 180 p.
3. Adamov, O. I. Formation of a comfortable urban environment / Adamov, O. I. – Moscow. - 2022. – 32 p.
4. Sidorov V.P., Sitnikov P.Yu. Spatial factors for assessing the comfort of the urban environment of a large city // Bulletin of the Polotsk State University. Series D. Economic and legal sciences. – 2021. – 73-81p.
5. Budarov V.P., Dubrovsky A.V. Geoinformation research of indicators of social comfort in rural settlements // In the collection: Information technologies, systems and devices in agriculture. materials of the 5th International Scientific and Practical Conference. Editorial board: Savchenko O.F., Gurova T.A. – 2012. – 205-210 p.

**SPATIAL DIFFERENTIATION OF THE SOCIO-ECONOMIC COMPLEX OF THE COASTAL ZONE
OF PRIMORSKY KRAI**

¹Far Eastern Federal University, Institute of the World Ocean, FEFU

²Far Eastern Federal University, Oriental Institute-School of Regional and International Studies, FEFU

Scientific advisor – A.A. Glushko¹

Scientific consultant – O.K. Titova²

The coastal geographical location is a competitive advantage for the development of the territory. This location makes it possible to develop many sectors of the maritime economy: transport, port facilities, extraction and processing of natural resources (biological, mineral), mariculture, shipbuilding and ship repair. Recently, there has been an urgent need for the development of the Far Eastern territories of Russia. The most populated and economically developed part of the Far Eastern Federal District is Primorsky Krai; it ranks first in the district in terms of GRP (gross regional product), investment inflows, etc. Consequently, its coastal zone (CZ) is especially attractive for priority development. CZ refers to municipal districts and urban districts that have access to the sea coastline. Moreover, this entity has the most profitable economic-geographical location: in relative proximity to CZ of Primorsky Krai there are countries of Asia-Pacific region with the largest urban agglomerations and port-industrial complexes (PIC) in the world, such as Shanghai (PIC cargo turnover – 47 million TEU), Ningbo-Zhoushan (PIC cargo turnover – 47 million TEU), etc. [2].

The total area of the coastal zone in Primorsky Krai is 61.7 thousand km², which is 37.2% of the entire region. CZ can be divided into 2 parts: southern and northern. The first consists of 8 municipalities: 4 municipal districts (Khasansky, Nadezhinsky, Shkotovsky, Partizansky), 3 urban districts (Vladivostok, Artemovsky, Nakhodkinsky) and 2 closed administrative-territorial entities (CATE) (Bolshoi Kamen, Fokino) and covers the area of 13 943 km² or 22.6% of the CZ area. The second includes 5 municipalities: 4 municipal districts (Terneysky, Kavalerovsky, Olginsky, Lazovsky), 1 urban district (Dalnegorsk). It occupies 47 767 km² or 77.4% of the CZ area [1].

The essential factor in the development of any territory is population. The total population of CZ for 2021 is 1170 thousand people, which is 60.7% of the population of Primorsky Krai. At the same time, serious disproportions are observed: 1 076 thousand people or 92% of the population of the coastal zone live in its southern part. To analyze population, it is important to take into account the size of territories, so for this it is better to use the population density indicator. The average for CZ is 19 people/km², which is higher than for Primorsky Krai (11.6 people/km²). The most densely populated areas in CZ are Vladivostok (1121.2 people/km²), Nakhodka (932.3 people/km²) and Artem (391.4 people/km²). The most sparsely populated are Lazovsky (2.7 people/km²), Terneysky (1.4 people/km²) and Olginsky (0.4 people/km²) municipal districts. The demographic situation in the region under consideration is characterized by population decline. In the southern part of the coastal zone, the population loss rate is minus 6.4%, while in the northern part the situation is significantly worse – minus 14.8%. One of the reasons for this situation is the excess of the mortality rate over the birth rate [1].

Migration plays an important role in population number. The average indicator for CZ is 25.5 people/10,000 people, which significantly exceeds the average for Primorsky Krai (-2). Strong differentiations are observed between the southern and northern parts of CZ (33.6 against -66). The leaders are Nadezhinsky (252.3) and Partizansky (86.1) municipal districts, as well as Vladivostok (61.8).

Within CZ, the urban form of settlement predominates. The average urbanization rate in CZ is 86%, that is higher than in Primorsky Krai (77.5%). In the southern part the average is 86%, in the northern part – 71%. In urban districts, urbanization indicators have the highest values: from 85% (Dalnegorsk urban district) to 100% (CATE Fokino). Nadezhinsky, Partizansky municipal district (lack of urban settlements) and Olginsky municipal district (38.7%) are in the rearguard.

THE 11th ANNUAL STUDENT SCIENTIFIC CONFERENCE IN ENGLISH
Vladivostok, May 2024

The indicator of the volume of shipped goods and services was used to analyze the economic situation in municipalities. CZ accounts for 878 965 640 rubles, which is about 80 % of the gross regional product (GRP) of Primorsky Krai. It allows to characterize this territory as the most developed, but in terms of socio-economic development indicators there are significant differences. The largest contribution to this coastal zone comes from Vladivostok (535 587 078 rubles or 61% of the CZ), Nakhodka (153 057 605 rubles or 17.4% of the CZ) and Bolshoi Kamen (65 826 295 rubles or 7.5% of the CZ). Due to the presented data, it is obvious that the southern part of the coastal zone occupies a significantly larger share in the CZ economy than the northern part (96% and 4%) [1].

A significant problem for the development of the territory is the quality of life of the population. To analyze the potential, the volume of shipped goods and services per capita was calculated. The average for CZ is 750 thousand rubles, which is higher than for Primorsky Krai as a whole (583 thousand rubles). The leaders are Bolshoy Kamen (1 668 thousand rubles), Lazovsky (1 181 thousand rubles) and Terneysky (1 086 thousand rubles) municipalities. The lowest figure is for Partizansky (32.9 thousand rubles), Kavalerovsky (49.4 thousand rubles) and Olginsky (114.7 thousand rubles) municipal districts. Such data can be explained not by the high level of industrial development, but by the extremely small population [1].

Another indicator of quality of life is the size of wages. The average salary for CZ as a whole was 65 900 rubles in 2021, which significantly exceeds the average for Primorsky Krai (47 252 rubles). In the southern part of the coastal zone, the average salary was 69 822 rubles, and in the northern part – 58 841 rubles. If to compare the territories, the highest wages are observed in the Bolshoi Kamen CATE (95.2 thousand rubles), Vladivostok urban districts (85.3 thousand rubles) and Shkotovsky district (82.3 thousand rubles). The lowest wages are in Partizansky (49.1 thousand rubles), Olginsky (51.2 thousand rubles) and Kavalerovsky (52.2 thousand rubles) municipal districts [1].

Summing it up, it should be noted the active processes of socio-economic development of the southern part of CZ of Primorsky Krai: the main socio-economic centers are concentrated here, there are maximum indicators of the volume of shipped goods and services, high population density, positive migration growth, high rates of construction of new housing, high wages. Also, conditions have been created here for the influx of investments (regimes of territory of advanced development and free port of Vladivostok), etc. In the northern part of the coastal zone, despite the large size of the territory, most of these advantages are absent, with the exception of higher wages in areas equated to the conditions of the far north. The highest per capita rates in these areas were achieved solely due to the small population and ongoing outmigration.

References

1. Federal State Statistics Service // Municipal Statistician – URL:
<https://rosstat.gov.ru/storage/mediabank/munst.htm>
2. World Shipping Council // Top-50 Ports – URL: <https://www.worldshipping.org/top-50-ports>

Potapov L.O.¹, Makarchuk I.M.¹

ASSESSMENT OF THE MICROCLIMATE OF THE FEFU CAMPUS

¹Far Eastern Federal University, Institute of the World Ocean, FEFU

²Far Eastern Federal University, Oriental Institute-School of Regional and International Studies, FEFU
Scientific supervisor – I. A. Lisina¹
Scientific consultant – O.K. Titova²

An important feature of the influence of conditions created by urban development is the change in the microclimate of small spaces. The study was carried out to assess the difference between the campus climate and the climate of adjacent territories and to form general climatic characteristics of the Muravyov-Amursky Peninsula.

THE 11th ANNUAL STUDENT SCIENTIFIC CONFERENCE IN ENGLISH
Vladivostok, May 2024

Microclimatic differences mainly depend on the heterogeneous influences of the underlying surface, and therefore manifest themselves mainly in the surface layers of air and are smoothed out with height. The ground layer of air occupies an air space two meters above the ground level. Therefore, all instrumental observations were performed at this level.

The goal of the work was a spatiotemporal analysis of changes in meteorological parameters on campus and their comparison with reference observations on the Roshydromet network.

The FEFU campus is located on Russky Island, in the city of Vladivostok, Primorsky Krai. The island is located in Peter the Great Bay of the Sea of Japan, at a distance of about 1.3 km from the city of Vladivostok, which provides unique climatic conditions.

In order to determine the location of reference points for carrying out instrumental observations, a reconnaissance survey of the FEFU campus, located on the coast of Ajax Bay and the area around the Laboratory Building (not far from Novik Bay), was carried out. To establish deviations of the obtained values from climatic characteristics, data from the Vladivostok weather station (Mountain) and an automatic weather station (AMS) installed on the roof of the FEFU Laboratory Building were used.

As a result, 21 reference points were selected (Fig. 1), at each of which the main meteorological parameters were studied: air temperature and humidity, wind direction and speed, and wind gusts were assessed. The work analyzed the results for three dates: April 12, May 13 and May 21, 2024.

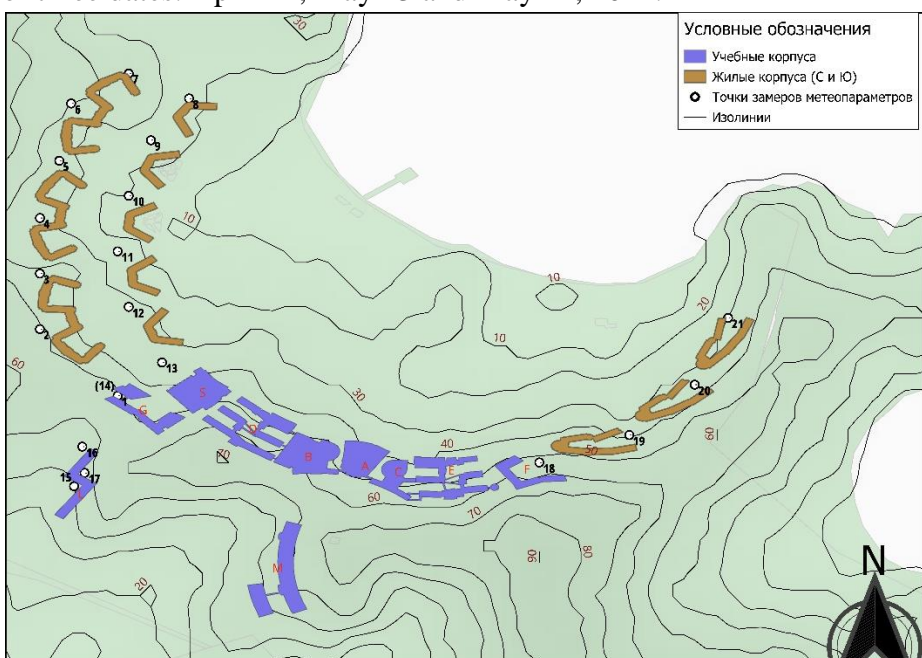


Figure 1 - FEFU campus map with reference points

On April 12, 2024, the air temperature at the Vladivostok weather station was 6.8°C, according to the AMS of the FEFU campus - 6.7°C, the average temperature at the reference points was 7.3°C (Fig. 2 a), the maximum air temperature was recorded at the eastern end of building No.11, and the minimum was recorded on the western side of the transition between buildings 8.1 and 8.2. Air humidity for the last point, on the contrary, was maximum. Its lowest value is typical for this date between buildings 9 and 10 (with an average of 85% for all points, Fig. 2 b). Relative air humidity at stations Vladivostok and AMS at the time of measurements was 100%.

THE 11th ANNUAL STUDENT SCIENTIFIC CONFERENCE IN ENGLISH
Vladivostok, May 2024

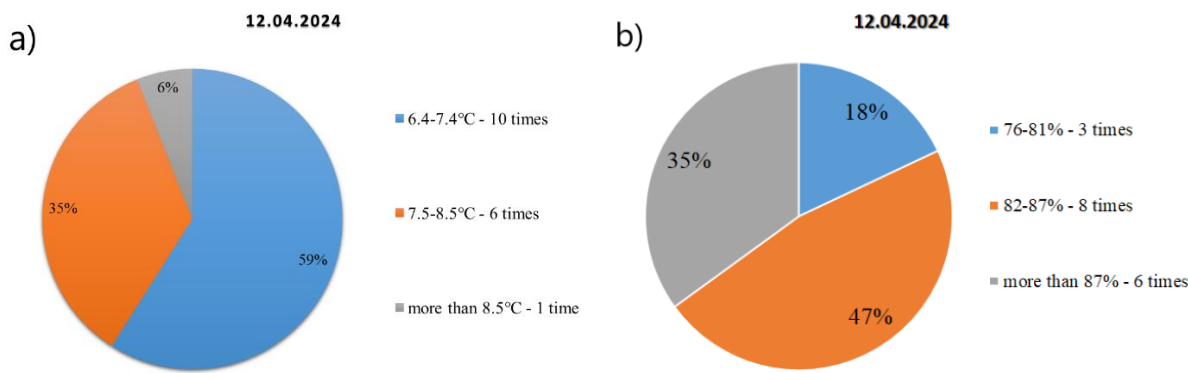


Figure 2 – Relative distribution of measured temperature (a) and air humidity (b) according to selected gradations

The wind at all points was predominantly weak with an average speed of 2.2 m/s (gusts up to 6 m/s), at the Vladivostok weather station - 5 m/s (gusts up to 10 m/s), according to the AMC - 4-5 m/s (gusts 6-7 m/s). The maximum value of the average wind speed was recorded at point 6, and the minimum at point 13.

The wind direction at the Vladivostok weather station is south, according to the AMS it is south-west, the wind direction at the reference points is predominantly south.

On 05/13/2024, the air temperature at the Vladivostok weather station was 16.4°C, at the AMS - 14.8°C, the average temperature for reference points was 18.1°C, with the maximum temperature value typical for point 1, and the minimum for points 19. Relative air humidity at the Vladivostok weather station and at the AMS was 45% and 47%, respectively, and the average at the reference points, as in April, was lower (37%), with prevailing values for the transition between buildings 9 and 10, and the minimum - between buildings 8.1 and 8.2 and the smoking room near building G.

At the Vladivostok weather station and AMS, the wind was recorded in the southwestern direction, and at the reference points it was predominantly southeastern. The quantitative characteristics of the wind differed little from 04/12/2024.

On 05/21/2024, the air temperature at the Vladivostok weather station was 17.7°C, according to the AMS of the FEFU campus - 17.1°C, the average at the reference points was 19.8°C, with the maximum temperature value typical for the northern end of building 5, and the minimum - for the transition between buildings 9 and 10. At point 19, the maximum relative air humidity was observed (with an average of 47%), and at points 8, 12 and 13 - the minimum. Indicators at reference points of the Roshydromet network are 53 and 59%.

The wind, like previous dates, was mostly weak, on average 2.1 m/s (according to the campus reference point), 3 m/s (Vladivostok station) and 4.5 m/s (AMS). Wind gusts in the city reached 11m/s, on the island. Russian – 6-7 m/s. The wind direction at the Vladivostok weather station is southern, according to the AMS it is southwestern, at the reference points it is predominantly southern (Fig. 3).

THE 11th ANNUAL STUDENT SCIENTIFIC CONFERENCE IN ENGLISH
Vladivostok, May 2024

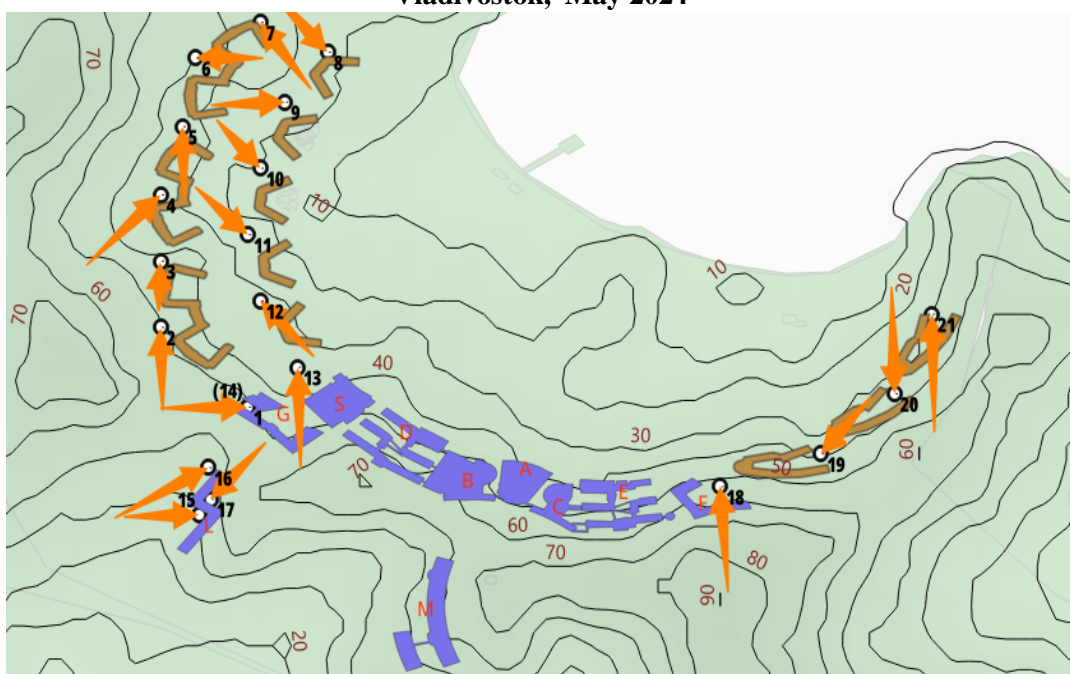


Figure 3 – Wind direction 05/21/2024 (orange arrows indicate wind direction at reference points)

Analysis of the results obtained allowed us to draw the following conclusions:

1. At the reference points, a similar transformation of the wind direction relative to its main vector by campus buildings is observed in spring.
2. The air temperature on campus is generally higher than at the automatic weather station and in the city of Vladivostok, which is due to the presence of heat-intensive materials such as concrete and asphalt surfaces. The campus area, like other urban areas, is hot.
3. Air humidity at the measurement level is lower than at the reference network of Roshydromet and has a significant variability across reference points.

For a more objective conclusion on the influence of the orientation of individual buildings and drawing up recommendations, it is necessary to continue detailed studies in other seasons of the year.

Section IV

MATHEMATICS AND COMPUTER SCIENCES

Alekseitceva N.D.

ANALYSIS AND MODEL CONSTRUCTION FOR DISTRIBUTION OF ANTI-THEFT SYSTEMS **SUBJECT AREA**

Far Eastern Federal University, Institute of Mathematics and Computer Technologies, FEFU
Scientific adviser – E.I. Antonova

Nowadays, insurance for vehicle is not enough to protect yourself from auto theft. It is important to provide additional protection for your car. Currently, there are many innovative means of protection. Anti-theft systems can be ranged from simple mechanical locks to complex electronic circuits [1].

To provide additional protection and convenience of transport, drivers usually contact services of the anti-theft systems distributors. Contacting distributors ensures the quality and provides guarantees the correct work and installation of the purchased anti-theft systems.

Consumers usually interact with online platforms, but simple online store may not be enough: most of the service centers can only be reached by record over the phone, and installers rely on maintaining paper records of installations, which in modern realities has no longer been an effective solution. There also may be a situation in which sales systems, customer bases, devices and installations are maintained separately, which makes it difficult to update them in a right time.

Therefore, for an enterprise specializing in providing the opportunity to purchase and install auto electronics, a flexible approach to interaction with clients is a key factor in the successful development of the business. The categories of users and their tasks of the designed system were established at table 1.

Table 1

User analysis

User type	User tasks
Client	To create orders. To record for installation. To record for a consultation. To record for repairs. To register an account.
Manager	To manage of normative and reference information. To manage warehouse. To fill or update product data. To create reports or infographics.
Specialist	To work on records for install, repair or consultation of anti-theft systems.

To create a domain model, we need to consider the minimum number of objects that provide support for workflows (Table 2). An ER model was chosen to build a model of the subject area, objects, relationships between objects and laws of the subject area. ER model is a data model that allows you to describe the schema of a subject area at various levels: conceptual, logical or physical [2]. The conceptual level is a generalized model for representing the project domain. The classical Chen notation was used in construction of the ER model.

Objects of the distribution of anti-theft systems subject area

Object	Description
Service (Order / Installation / Repair)	Document that defines the needs for sale, repair or installation of products in a fixed quantity.
Manager	User who is responsible for updating data and realization devices.
Specialist	User who can install or repair devices.
Client	User who can view devices, record for device installation or repair, and purchase devices.
Box	Premises, specially equipped for the provision of installation services, part of the company.
Device	Product from a specific list of products.
Device type	Defines the type of device and the estimated time required to install it.
Warehouse	Premises where products and their quantity are stored, part of the company.
Schedule	Defines working days and weekends and working hours for each day for enterprise branches (warehouse, box).
Time for records	Defines time on the time axis, both start and end dates and time for each installation, tied to a specific order and installer, consistent with the work schedule.

Figure 1 reflects the conceptual level model of the subject area.

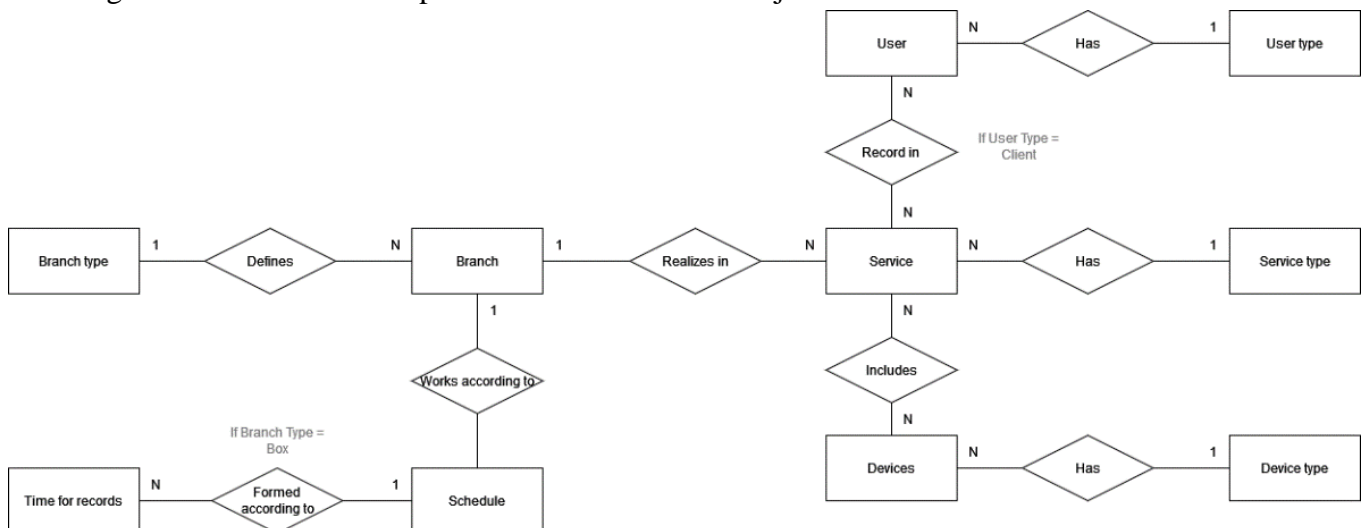


Figure 1. ER model for distribution of anti-theft systems subject area

The model for a subject area was built using the ER model as a result of solving the problem of analysis and model construction for distribution of anti-theft systems subject area. Moreover, the objects of the subject area and relationships between them were defined.

References:

1. Auto anti-theft systems – dzen – Text: electronic // dzen – URL: <https://dzen.ru/a/ZUvtgXDumliTh8dJ> (access date: 04/27/2024).
2. What is ER Modeling? – sql-easy – Text: electronic // sql-easy – URL: <https://www.sql-easy.com/learn/what-is-er-modeling/> (access date: 04/28/2023).

Bakhtin K.E.¹

**GENERALIZATIONS OF KARLSSON-MINTON SUMMATION FORMULAS FOR
 HYPERGEOMETRIC FUNCTIONS OF THE IPD TYPE**

¹Far Eastern Federal University, Institute of Mathematics and Computer Technologies, FEFU

² Far Eastern Federal University, Oriental Institute - School of Regional and International Studies, FEFU

Scientific adviser – E.G. Prilepkina¹

Scientific consultant - E.V. Kravchenko²

In 1970 Minton proved the summation formula (see, for example, [1, (1.2)]).

$${}_pF_{p-1} \left(\begin{matrix} -k, b, \mathbf{f} + \mathbf{m} \\ b+1, \mathbf{f} \end{matrix} \right) = \frac{k!}{(b+1)_k} \frac{(\mathbf{f}-b)_{\mathbf{m}}}{(\mathbf{f})_{\mathbf{m}}}, \quad (1)$$

valid for $k \geq m, k \in \mathbb{N}$ and where $\mathbf{f} \in \mathbb{C}^{p-2}, \mathbf{m} \in \mathbb{N}^{p-2}$. Soon thereafter, his result was generalized by Karlsson, who replaced $-k$ by an arbitrary complex number a satisfying $\operatorname{Re}(1-a-m) > 0$ to get (see, for example [1, (1.3)]).

$${}_pF_{p-1} \left(\begin{matrix} -k, b, \mathbf{f} + \mathbf{m} \\ b+1, \mathbf{f} \end{matrix} \right) = \frac{\Gamma(b+1)\Gamma(1-a)}{\Gamma(b+1-a)} \frac{(\mathbf{f}-b)_{\mathbf{m}}}{(\mathbf{f})_{\mathbf{m}}}. \quad (2)$$

In the article [1] a generalization (2) was obtained by replacing the number b with the vector $\mathbf{b} = (b_1, b_2, \dots, b_l)$. Namely, the formula was proved [1, (2.11)]

$$\frac{1}{\Gamma(1-a)} {}_F \left(\begin{matrix} a, \mathbf{b}, \mathbf{f} + \mathbf{m} \\ \mathbf{b} + \mathbf{p}, \mathbf{f} \end{matrix} \right) = \frac{(\mathbf{b})_{\mathbf{p}}}{(\mathbf{f})_{\mathbf{m}}} \sum_{q=1}^n \frac{\Gamma(\beta_q)(\mathbf{f}-\beta_q)_{\mathbf{m}}}{B_q \Gamma(1+\beta_q-a)}, \quad (3)$$

where $\mathbf{b} = (b_1, b_2, \dots, b_l), \mathbf{p} = (p_1, p_2, \dots, p_l)$ are vectors of positive integers, $n = p_1 + p_2 + \dots + p_l$, and all the coordinates of the vector $\beta = (b_1, b_1+1, \dots, b_1+p_1-1, \dots, b_l, b_l+1, \dots, b_l+p_l-1) = (\beta_1, \beta_2, \dots, \beta_p)$, $B_q = \prod_{v=1, v \neq q}^n (\beta_v - \beta_q)$. Adding additional parameters to the hypergeometric function according to the principle

$$F \left(\begin{matrix} a, b, \mathbf{f} + \mathbf{m} \\ b+3, \mathbf{f} \end{matrix} \right) = F \left(\begin{matrix} a, b, b+1, b+2, \mathbf{f} + \mathbf{m} \\ b+1, b+2, b+3, \mathbf{f} \end{matrix} \right), \quad (4)$$

it is enough to consider the case $\mathbf{p} = \mathbf{1} = (1, 1, \dots, 1)$. Then (3) takes the form

$${}_{l+p-1}F_{l+p-2} \left(\begin{matrix} a, \mathbf{b}, \mathbf{f} + \mathbf{m} \\ \mathbf{b} + \mathbf{1}, \mathbf{f} \end{matrix} \right) = \frac{\Gamma(1-a)(\mathbf{b})_1}{(\mathbf{f})_{\mathbf{m}}} \sum_{q=1}^l \frac{\Gamma(b_q)(\mathbf{f}-b_q)_{\mathbf{m}}}{\alpha_q \Gamma(1+b_q-a)}, \quad (5)$$

where $\mathbf{b} = (b_1, b_2, \dots, b_l), \alpha_q = \prod_{v=1, v \neq q}^l (b_v - b_q)$. In this report, we will talk about generalizing (5) to the case of identical vector coordinates \mathbf{b} .

Theorem 1. Let

$\mathbf{b} = (b_1, b_2, \dots, b_l), n = n_1 + n_2 + \dots + n_l, \operatorname{Re}(n-1-m) > 0, (-1+a, -\mathbf{b}, -\mathbf{b}+a-1, -\mathbf{f}) \notin \mathbb{N}_0^{2l+p-1}$.

Then:

$$F \left(\begin{matrix} a, & b_1, \dots, b_1, & b_2, \dots, b_2, & b_l, \dots, b_l, \mathbf{f} + \mathbf{m} \\ & \underbrace{b_1+1, \dots, b_1+1}_{n_1-times}, & \underbrace{b_2+1, \dots, b_2+1}_{n_2-times}, & \underbrace{b_l+1, \dots, b_l+1}_{n_l-times}, \mathbf{f} \end{matrix} \right) = \frac{\Gamma(1-a)}{(\mathbf{f})_{\mathbf{m}}} \sum_{i=1}^l \sum_{k_i=1}^{n_i} \frac{(-1)^{k_i+1} \alpha_{k_i}^i}{(k_i-1)!} \left(\frac{\Gamma(x)(\mathbf{f}-x)_{\mathbf{m}}}{\Gamma(x-a+1)} \right)_{x=b_i}^{k_i-1}, \quad (6)$$

where $\alpha_{k_i}^i$ coefficients of decomposition $\prod_{i=1}^l \frac{b_i^{n_i}}{(b_i+x)^{n_i}}$ into simple fractions,

THE 11th ANNUAL STUDENT SCIENTIFIC CONFERENCE IN ENGLISH

Vladivostok, May 2024

$$\prod_{i=1}^l \frac{b_i^{n_i}}{(b_i + x)^{n_i}} = \sum_{i=1}^l \sum_{k_i=1}^{n_i} \frac{a_{k_i}^i}{(b_i + x)^{k_i}}. \quad (7)$$

The work was carried out at the Far Eastern Center for Mathematical Research with the financial support of the Ministry of Education and Science of the Russian Federation, Agreement No. 075-02-2024-1440 dated February 28, 2024 on the implementation of programs for the development of regional scientific and educational mathematical centers.

References:

1. Karp D.B. and Prilepkina E.G. Extensions of Karlsson–Minton summation theorem and some consequences of the first Miller–Paris transformation, *Integral Transforms and Special Functions*, Vol. 29, Issue 12 (2018). – p. 955-970.
2. Andrews G.E., Askey R. and Roy R. *Special functions*: Cambridge University Press, 1999.
3. Miller A.R., Paris R.B. Transformation formulas for the generalized hypergeometric function with integral parameter differences. *Rocky Mt. J. Math.* 43(1), 291–327 (2013).

Cherkasov M.D.¹

THE PRINCIPLE OF OPERATION OF THE PARALLEL TEMPERING ALGORITHM IN THE ISING MODEL

¹Far Eastern Federal University, Institute of High Technology and Advanced Materials, FEFU

² Far Eastern Federal University, Oriental Institute - School of Regional and International Studies, FEFU

Scientific adviser – Y.A. Shevchenko¹

Scientific consultant - Y.O. Kamornaya ²

The Ising Model [1] is a mathematical model of statistical physics in which spins can take 2 states: -1 and 1. In Ising Model to compute the energy and the capacity of the system directly, we need to iterate 2^N states of system that limits computational powers. One approach, that could help us in solving this problem is parallel tempering.

Parallel tempering [2] is an approach that allows to ignore the canonical ensemble and can overcome the energy trap at low temperatures. Energy trap is main problem for many Metropolis algorithms in particular for Monte-Carlo algorithm. This trap gives big inaccuracy for low temperatures that distorts the results. By overcoming the trap, we get more accurate results.

The essence of this algorithm is as follows: choose the initial temperature and generate for it initial random state from our canonical ensemble. Then we create N copies of initial state and place them at a certain temperature distance. Next, we execute the Metropolis algorithm for each temperature.

The Metropolis algorithm works to these principles: at first, we compute the energy of our incoming state using this formula:

$$E = -J \sum_{i,j=0}^n s_i s_j,$$

where s_i, s_j – spin moment $\epsilon [-1, 1]$, in our case $J = 1$ (ferromagnetic). Then we flip one random particle (change it to the opposite sign) and compute energy of our new state. And according to this the probability of acceptance of the new state:

$$p(E_1 \rightarrow E_2) = \begin{cases} 1, & \text{if } E_1 > E_2 \\ e^{\frac{E_2 - E_1}{T}}, & \text{if } E_2 > E_1, \end{cases}$$

where T is our current temperature. This procedure repeats M times, and then we write mean energy

THE 11th ANNUAL STUDENT SCIENTIFIC CONFERENCE IN ENGLISH
Vladivostok, May 2024

in energy array from the Metropolis algorithm.

After one work of the Metropolis algorithm, replicas are exchanged among themselves with probability:

$$p_{swap} = \min[1, \exp[(\beta' - \beta)(E' - E)]],$$

where $\beta = \frac{1}{kT}, k = 1$. After replicas exchange the Metropolis algorithm works again and again replicas exchanges happen. And it works the specified number of times.

Then we compute mean energy from energy array and compute the capacity using this formula:

$$C(T)_i = \frac{(E^2)_i - \langle E \rangle^2_i}{kT^2 N},$$

where $k = 1, E$ – mean energy for M steps i copy, N – quantity of particles in the system.

For more accurate results, the probability of an exchange between replicas of 20% is best suited in [3].

If we want to achieve 20% of replicas exchange, we need to push them to a certain distance.

We used linear interpolation method for energy curve, without considering energy in final results while interpolation works. At first, we start common Metropolis algorithm for certain temperatures and write energy array, then we calculate a probability of exchange of two neighboring copies, where the first copy is the next one from initial temperature, and the second copy is the next one from first copy. If probability of exchange of the first copy with second one is higher than 20%, then we take the second copy as the next one from the array of temperatures, and we push second copy in array of temperatures until probability becomes lower than 20%. If second copy will go to the end of temperature array, we use linear interpolation method.

If probability of replica exchange is still higher than 20%, we add a constant to the second (last) temperature (the rate of convergence to 20% depends on it) and write this value to T_k , else subtract a constant from second temperature. Then we compute E_k using this formula:

$$E_k = \left[\frac{E_2 - E_1}{T_2 - T_1} \right] (T_k - T_1) + E_1,$$

where T_2 - accepted as a second temperature (last in temperature array), T_1 – accepted as a first copy (still next one from initial temperature), E_k – interpolated energy in a straight line. And we repeat this certain times until we get the probability of about 20%.

After that we accept new first copy next one last first copy and second copy next one new first copy and we repeat this algorithm for new first and second copies and thus we are moving along temperature array.

After this algorithm we start the Metropolis algorithm again and repeat interpolation and so on until we get the probability of 20%. When we got probability of 20% we start parallel tempering and begin to take into account the energy in results.

Our parallel tempering algorithm is ready, but taking into account the manual temperature selection. For automatic temperature selection we need to use interpolation algorithm, which is currently under development. To make sure that the algorithm works, the figures below are, but excluding 20% of probability of replicas exchange.

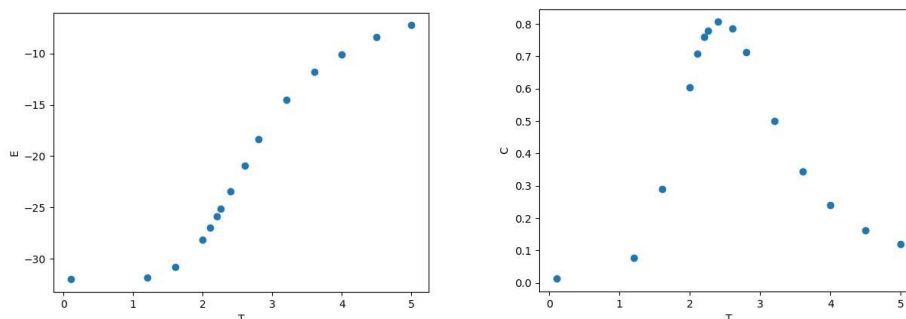


Fig.1. dependence of energy from temperature is on the left, and the heat capacity from temperature is on the right

THE 11TH ANNUAL STUDENT SCIENTIFIC CONFERENCE IN ENGLISH

Vladivostok, May 2024

Another advantage of our algorithm is that it uses OOP. Thus, it simplifies the integration of code into other codes and makes it possible to conveniently select parameters for our system. The program is written using C++ programming language and is being tested on a FEFU supercomputer cluster.

References:

1. Janke W. Monte Carlo methods in classical statistical physics //Computational many-particle physics. – Berlin, Heidelberg : Springer Berlin Heidelberg, 2008. – C. 79-140.
 2. Patriksson A., van der Spoel D. A temperature predictor for parallel tempering simulations //Physical Chemistry Chemical Physics. – 2008. – T. 10. – №. 15. – C. 2073-2077.
 3. Earl D. J., Deem M. W. Parallel tempering: Theory, applications, and new perspectives //Physical Chemistry Chemical Physics. – 2005. – T. 7. – №. 23. – C. 3910-3916.

Daquan Yu^{1,2}

THE METHOD OF TORQUE CONTROL FOR UPPER LIMB REHABILITATION ROBOT

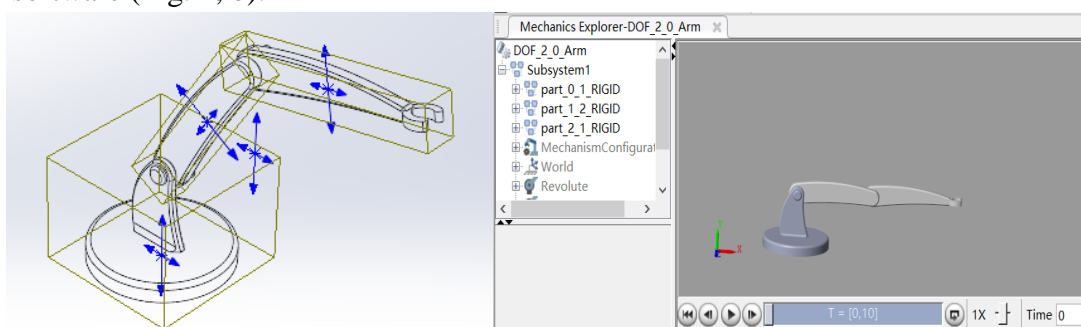
¹Far Eastern Federal University, School of Mathematics and Computer Technologies, FEFU

²Heilongjiang University of Technology, School of Electrical and Information Engineering, HUT

Scientific adviser - E.V. Pustovalov¹

With the progress of technology and the development of society, the standard of people's material living is getting higher, and the problem of population aging is prominent¹. Therefore, there is a significant increase in the number of people with upper limb dysfunction caused by apoplexy and external injuries. To solve this problem, the method of torque control for the upper limb rehabilitation robot is proposed. Through the development of the simulation program and the experimental verification of the upper limb rehabilitation robot, it can help patients recover their upper limb abilities.

First, it is necessary to build the upper limb rehabilitation robot model in SOLIDWORKS software. The model has two degrees of freedom, which include both the upper and lower arms (Fig. 1, a). Then, we should import the model into MATLAB software and construct the control system of the rehabilitation robot in Simulink software (Fig. 1, b).



a) Model of the robot

b) Import model into

Fig. 1. Model of the robot and the simulation of environment

Finally, we simulate motion using Simulink software and verify the effectiveness of the rehabilitation robot. At the same time the security of patient rehabilitation training is improving.

The tensosensors are placed on the controlled object to establish a dynamic relationship between torque and position, by adjusting the relationship state of parameters to achieve the purpose of indirect adjustment torque control and position control of the rehabilitation robot. In the Mass-Spring-Damping system, the output torques at the end of the node of system can establish a relationship with the functions of displacement, velocity, and acceleration. Therefore, it can be used by the Mass-Spring-Damping system instead of the

process of measuring the tensosensors' impedance².

We should establish Second-Order Differential Equation for the Mass-Spring-Damping system by equation (1).

$$K_d X + B_d \dot{X} + M_d \ddot{X} = F_e \quad (1)$$

M_d , K_d and B_d are parameters of the tensosensor's system. Among them, M_d is the inertia coefficient; K_d is the stiffness of the spring; B_d is the damping of the damper; X is the position of the object; \dot{X} is the speed of the object; \ddot{X} is the acceleration of the object; F_e is the external force. When the external force changes from F_e to F_d , the position, velocity and acceleration values of the object are separately changed by E , \dot{E} and \ddot{E} . By using E , \dot{E} and \ddot{E} as the values of position, speed and acceleration, we form a new equation.

$$K_d E + B_d \dot{E} + M_d \ddot{E} = F_e - F_d \quad (2)$$

The equation (2) is named the equation of impedance, and to get the transfer function, we need to transform equation (2) by using Laplace to get equation (3).

$$E(s) = \frac{F_e(s)}{M_d s^2 + B_d s + K_d} \quad (3)$$

During rehabilitation training, the interaction force between the patient and the rehabilitation robot may suddenly increase, which can cause secondary damage to the patient's upper limb³. Therefore, on the basis of combining trajectory tracking and human-machine interaction security, we proposed a method of upper limb rehabilitation robot compliance control based on the force sensor. The upper limb rehabilitation robot is designed to provide precise and comfortable assistance to patients during rehabilitation training while ensuring security and effectiveness.

When the interaction torque exceeds the set value, the damage to the patient caused by the interaction force is reduced by improving compliance. The controller structural diagram is shown in Figure 2. Using this method, we can optimize the rehabilitation process and improve the overall effectiveness of rehabilitation training for patients.

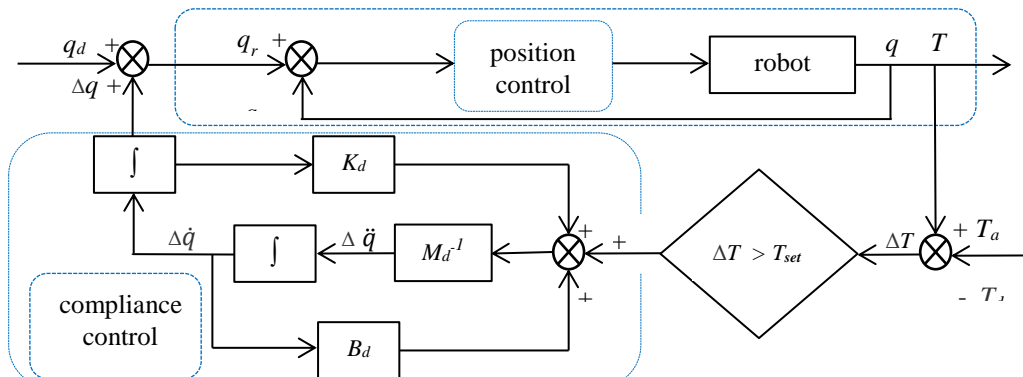


Fig. 2. Structural diagram of the controller

In Figure 2, two PID controllers form a position control system of front feedback, where q_d is the expected angular displacement; Δq is the displacement offset converted by the impedance controller; q_r is the corrected trajectory value; q is the angular displacement feedback from the robot; T_a is the torque value detected by the torque sensor; T_d is the expected torque value; ΔT represents the human-machine interaction force; T_{set} is the set value for compliance control; M^{-1} is the inertia coefficient; B_d is the environmental damping coefficient; K_d is the environmental stiffness coefficient.

According to Figure 2, we obtain the impedance equations (4) and (5).

$$M_d(\ddot{q} - \ddot{q}_d) + B_d(\dot{q} - \dot{q}_d) + K_d(q - q_d) = T_a - T_d \quad (4)$$

$$\Delta \ddot{q} = M^{-1}[T_a - T_d - B_d(\dot{q} - \dot{q}_d) - K_d(q - q_d)] \quad (5)$$

The controller structure is made up of an inner loop of position control and an outer loop of tensosensor control. When the interaction force is less than the set value, control of the position is performed. If the interaction force exceeds the set value, tensosensor control starts to work and converts the interaction torque

that exceeds the set value into a trajectory in order to reduce the interaction torque between robot and patient and ensure the security of patient rehabilitation training. When the interaction force falls below the set value, the rehabilitation robot will return to the original planned trajectory of position control to continue trajectory tracking training.

To verify its practical effectiveness, it is assumed that the robot for upper limb rehabilitation is drawing a circular trace on a plane with a center coordinate of (1,1) and a semidiameter of 0.5 m. When $T = 3S$ and $T = 6S$, the human-machine interaction torque exceeds the set value, lasts for 0.2 seconds, and sets the simulation time to 7 seconds.

In Figure 3, x_d and y_d are the set values of joint angular displacements, while x_a and y_a are the actual measured values of joint angular displacements. Where $T = 3s$ and $T = 6s$, the excess torques are converted into joint angular displacements.

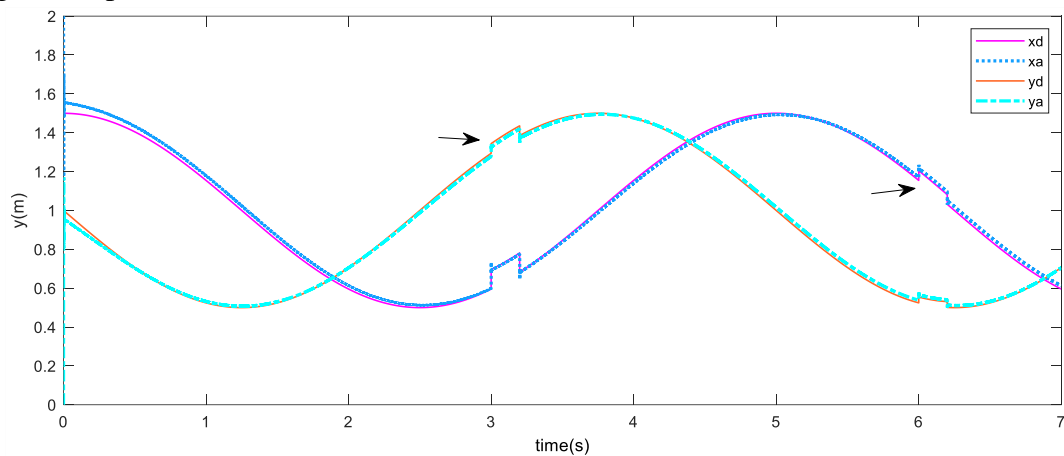


Fig. 3. The design and the actual joints angles of robot

In Figure 4, the upper limb rehabilitation robot converts excess torques into joint angular displacements to avoid patients suffering damage caused by excess torques. When the torque returns to its normal value, the robot continues to perform rehabilitation training according to the set trajectory.

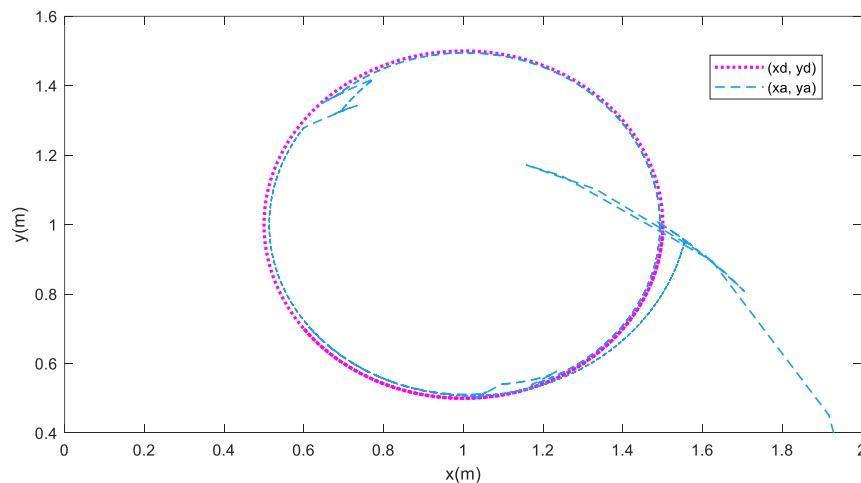


Fig. 4. The design and the actual terminal trajectories of robot

The purpose of this article is to develop a method of torque control that will enable the robot to be better controlled during upper limb rehabilitation training. By using this method, patients could avoid secondary injuries to the upper limb caused by excess torques from the rehabilitation robot when using the robot for rehabilitation training. The simulation results show that this method can achieve the purpose of compliant control for the rehabilitation robot and improve the level of security while patients are doing rehabilitation training.

THE 11th ANNUAL STUDENT SCIENTIFIC CONFERENCE IN ENGLISH

Vladivostok, May 2024

References:

1. Guo Fumin, Zhang Hua, Xu Yilu, Xiong Genliang & Zeng Cheng. (2023). Isokinetic Rehabilitation Trajectory Planning of an Upper Extremity Exoskeleton Rehabilitation Robot Based on a Multistategy Improved Whale Optimization Algorithm. *Symmetry*(1). doi:10.3390/SYM15010232.
2. Yu W, Rosen J. Neural PID control of robot manipulators with application to an upper limb exoskeleton[J]. *IEEE Transactions on Cybernetics*, 2013, 43(2): 673-684.
3. Zhang Pengfei, Gao Xueshan, Miao Mingda & Zhao Peng. (2022). Design and Control of a Lower Limb Rehabilitation Robot Based on Human Motion Intention Recognition with Multi-Source Sensor Information. *Machines*(12). doi:10.3390/MACHINES10121125.

Dranov S.V.¹, Afanasyeva S.D.¹

NUMERICAL SIMULATION OF NAVIER-STOKES BLOOD FLOW MODEL IN AN ARTERY WITH A NARROWING CHANNEL USING NEURAL NETWORKS AND FINITE ELEMENT METHOD

¹Far Eastern Federal University, Institute of Mathematics and Computer Technologies, FEFU,

² Far Eastern Federal University, Oriental Institute - School of Regional and International Studies, FEFU
Scientific adviser – K.S. Kuznetsov ¹
Scientific consultant - I.N. Lazareva²

In recent years, number of studies of blood flow in an artery with a narrowing channel has increase due to the importance of this problem in modern medicine. Simulation of blood flow in narrowing artery helps diagnose and treat cardiovascular diseases such as ischemia or myocardial infarction. The Navier-Stokes system of differential equations is often used for blood flow simulation [3]. The most popular methods for solving differential equations include numerical finite element method and the method utilizing neural networks - Physics Informed Neural Networks (PINN) [2].

The system of equations describing the unsteady motion of a viscous Newtonian fluid in a cylindrical coordinate system with rotational symmetry in the angular direction can be expressed as follows:

$$\frac{\partial u_r}{\partial t} + u_r \frac{\partial u_r}{\partial r} + u_z \frac{\partial u_r}{\partial z} + \frac{1}{\rho} \frac{\partial p}{\partial r} - \frac{\mu}{\rho} \left[-\frac{u_r}{r^2} + \frac{1}{r} \frac{\partial u_r}{\partial r} + \frac{\partial^2 u_r}{\partial r^2} + \frac{\partial^2 u_r}{\partial z^2} \right] = 0, \quad (1)$$

$$\frac{\partial u_z}{\partial t} + u_r \frac{\partial u_z}{\partial r} + u_z \frac{\partial u_z}{\partial z} + \frac{1}{\rho} \frac{\partial p}{\partial z} - \frac{\mu}{\rho} \left[\frac{1}{r} \frac{\partial u_z}{\partial r} + \frac{\partial^2 u_z}{\partial r^2} + \frac{\partial^2 u_z}{\partial z^2} \right] = 0, \quad (2)$$

$$\frac{1}{r} u_r + \frac{\partial u_r}{\partial r} + \frac{\partial u_z}{\partial z} = 0, \quad (3)$$

$$r \in [0; R], z \in [0; Z], t \in [0, T]$$

where u_r – is the radial velocity, $\left[\frac{m}{s}\right]$, u_z – is the axial velocity, $\left[\frac{m}{s}\right]$, p – is the pressure, $[Pa]$, ρ – is the density, $\left[\frac{kg}{m^3}\right]$, μ – is the dynamic viscosity, $[Pa \cdot s]$, R – is the radius of the artery, $[m]$, Z – is the artery length, $[m]$, T – is the overall time of process, $[s]$.

For the solution, it is necessary to non-dimensionalize the system by introducing the following variables:

$$r = \frac{\tilde{r}}{R}, \quad z = \frac{\tilde{z}}{Z}, \quad t = \frac{\tilde{t}}{T}, \quad u_r = \frac{\tilde{u}_r}{U_r}, \quad u_z = \frac{\tilde{u}_z}{U_z}, \quad p = \frac{\tilde{p}}{P}$$

where U_r, U_z, P – are relative values of velocity components u_r, u_z and pressure p respectively.

Let's introduce the following dimensionless quantities:

THE 11th ANNUAL STUDENT SCIENTIFIC CONFERENCE IN ENGLISH

Vladivostok, May 2024

$$Sh_r = \frac{TU_r}{R}, \quad Sh_z = \frac{Tu_z}{z}, \quad \frac{Sh_z}{Sh_r} = \frac{U_z R}{U_r Z}, \quad V = \frac{U_z}{U_r}, \quad d = \frac{R}{Z}, \quad \nu = \frac{\mu}{\rho}$$

$$Eu_r = \frac{P}{U_r^2 \rho}, \quad Eu_z = \frac{P}{U_z^2 \rho}, \quad Re_r = \frac{RU_r}{\nu}, \quad Re_z = \frac{RU_z}{\nu}$$

where Sh_r, Sh_z – are Strouhal numbers for the velocity component u_r, u_z respectively, Eu_r, Eu_z – are Euler numbers for the velocity components u_r, u_z respectively, ν – is the kinematic viscosity, Re_r, Re_z – are Reynolds numbers for the velocity components u_r, u_z respectively, d – is the ratio of the radius to the length of the channel.

The system of equations in the new dimensionless variables with the boundary conditions has the following form:

$$\frac{\partial u_r}{\partial t} + Sh_r u_r \frac{\partial u_r}{\partial r} + Sh_z u_z \frac{\partial u_r}{\partial z} + Sh_r Eu_r \frac{\partial p}{\partial r} - \frac{Sh_r}{Re_r} \left[-\frac{u_r}{r^2} + \frac{1}{r} \frac{\partial u_r}{\partial r} + \frac{\partial^2 u_r}{\partial r^2} + \frac{\partial^2 u_r}{\partial z^2} \right] = 0 \quad (4)$$

$$\frac{\partial u_z}{\partial t} + Sh_r u_r \frac{\partial u_z}{\partial r} + Sh_z u_z \frac{\partial u_z}{\partial z} + Sh_z Eu_z \frac{\partial p}{\partial z} - \frac{Sh_z}{Re_z} \left[\frac{1}{r} \frac{\partial u_z}{\partial r} + \frac{\partial^2 u_z}{\partial r^2} + \frac{\partial^2 u_z}{\partial z^2} \right] = 0 \quad (5)$$

$$\frac{1}{r} u_r + \frac{\partial u_r}{\partial r} + \frac{Sh_z}{Sh_r} \frac{\partial u_z}{\partial z} = 0, \quad (6)$$

The boundary conditions can be written as follows:

$$u_r|_{r=R} = 0, \quad u_z|_{r=R} = 0,$$

$$u_r|_{r=0} = 0, \quad \frac{\partial u_z}{\partial n}|_{r=0} = 0,$$

$$u_r|_{z=0} = 0, \quad u_z|_{z=0} = 0,7 - 0,7r,$$

$$\frac{1}{Re_z} \frac{\partial u_z}{\partial z}|_{z=z} - Eu_z p|_{z=z} = 0, \quad \frac{\partial u_z}{\partial n}|_{z=z} = 0$$

The numerical solution of the problem is carried out using the finite element method using of the FreeFem++ software [1]. The geometry of the narrowing artery is shown in Figure 1.

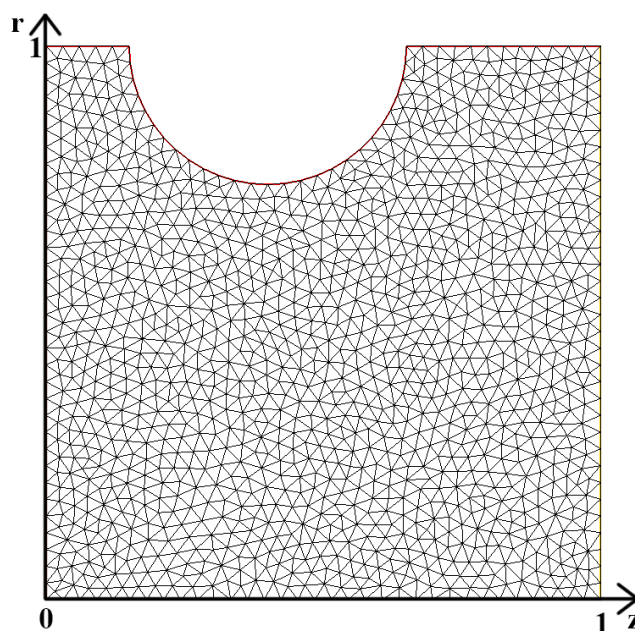


Figure 1. Computational domain for finite element method

The method PINN was used to solve the task using a neural network. The following functional J was proposed, incorporating quadratic terms of the residuals of the equations as well as initial and boundary conditions:

THE 11th ANNUAL STUDENT SCIENTIFIC CONFERENCE IN ENGLISH

Vladivostok, May 2024

$$J = J_r + J_0 + J_{b_1} + J_{b_2} + J_{b_3} + J_{b_4},$$

$$J_r = \frac{1}{N_r} \sum_{i=1}^{N_r} \sum_{k=1}^3 r_k^2(z_i^r, r_i^r, t_i^r),$$

$$J_0 = \frac{W_0}{N_0} \sum_{i=1}^{N_0} [\hat{u}_r(z_i^0, r_i^0, t_i^0)]^2 + [u_z|_{t=0}(z_i^0, r_i^0, t_i^0) - \hat{u}_z(z_i^0, r_i^0, t_i^0)]^2,$$

$$J_{b_1} = \frac{W_b}{N_{b_1}} \sum_{i=1}^{N_{b_1}} [\hat{u}_r(z_i^{b_1}, r_i^{b_1}, t_i^{b_1})]^2 + [\hat{u}_z(z_i^{b_1}, r_i^{b_1}, t_i^{b_1})]^2 + \left[\frac{\partial \hat{p}(z_i^{b_1}, r_i^{b_1}, t_i^{b_1})}{\partial n} \right]^2,$$

$$J_{b_2} = \frac{W_b}{N_{b_2}} \sum_{i=1}^{N_{b_2}} [\hat{u}_r(z_i^{b_2}, r_i^{b_2}, t_i^{b_2})]^2 + \left[\frac{\partial \hat{u}_z(z_i^{b_2}, r_i^{b_2}, t_i^{b_2})}{\partial n} \right]^2,$$

$$J_{b_3} = \frac{W_b}{N_{b_3}} \sum_{i=1}^{N_{b_3}} [\hat{u}_r(z_i^{b_3}, r_i^{b_3}, t_i^{b_3})]^2 + [u_z|_{z=0}(z_i^{b_3}, r_i^{b_3}, t_i^{b_3}) - \hat{u}_z(z_i^{b_3}, r_i^{b_3}, t_i^{b_3})]^2 \\ + [\hat{p}(z_i^{b_3}, r_i^{b_3}, t_i^{b_3}) - 1]^2,$$

$$J_{b_4} = \frac{W_b}{N_{b_4}} \sum_{i=1}^{N_{b_4}} \left[\frac{\partial \hat{u}_r(z_i^{b_4}, r_i^{b_4}, t_i^{b_4})}{\partial n} \right]^2 + \left[\frac{\partial \hat{u}_z(z_i^{b_4}, r_i^{b_4}, t_i^{b_4})}{\partial n} \right]^2,$$

where r_1, r_2, r_3 – are the residuals of the equations (1)-(3) respectively, $\hat{u}_r, \hat{u}_z, \hat{p}$ – are approximations of unknown functions by neural networks.

The minimization of the functional J was performed using the TensorFlow library in the Python programming language. To solve the task, a training dataset was generated uniformly inside and on the boundaries of the computational domain, as shown in Figure 2.

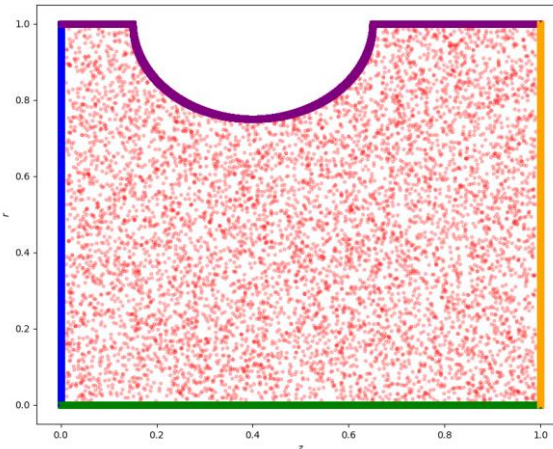


Figure 2. Training dataset for neural network

References:

1. Hecht, F. New development in FreeFem++. Journal of numerical mathematics, 2012, 20(3-4), 251-266.
2. Pokhrel, P., Kafle, J., Kattel, P., Gaire, H. Analysis of Blood flow Through Artery with Mild Stenosis // Journal of Institute of Science and Technology. 2020. V. 25. P. 33-38.
3. Raissi M., Perdikaris P., Karniadakis G.E. Physics-informed neural networks: A deep learning framework for solving forward and inverse problems involving nonlinear partial differential equations // Journal of Computational Physics. 2019. V. 50. No. 3. P. 686–707.

Frolov A.A.¹

AI-BASED CHEATING PREVENTION ON E-LEARNING PLATFORMS

¹Far Eastern Federal University, Institute of Mathematics and Computer Technologies, FEFU

² Far Eastern Federal University, Oriental Institute - School of Regional and International Studies, FEFU

Scientific adviser – G.P. Ozerova¹

Scientific consultant – I.F. Veremeeva²

E-learning has become more popular since Internet's growth. There are plenty of online courses and platforms, where one is able to learn any topic he or she wants to learn. Nevertheless, some people got used to cheating on their online tests, and interactive trainers. It is a huge problem since cheating decreases e-learning efficiency [1][2].

Although some cases of cheating may not have serious consequences, there are tests that should not be answered in such ways. For example, tests in medical universities.

Students have become much better at cheating since GPT-based models were released to the public in November 2022. GPTs or Generative pre-trained transformers are able to understand any popular human language and answer questions and problems from many different subjects. GPTs are now used by students to answer online tests as well.

Hence, there must be some methods to prevent cheating via generative transformers and to make e-learning platforms more cheating-sustainable. E-learning platforms deal with this differently:

1. Creating plagiarism search systems – some online platforms are able to search through the Internet to find similar texts and phrases. Since GPTs are trained on data from public sources, including books, websites, and articles, they usually output exact text fragments, which are effortless to detect and handle [3].

2. Creating GPT guidelines – there are platforms that created guidelines about how students may and may not use GPT in their courses, and tests. It may help, but people are used to not reading online platform guidelines [4].

3. Making questions and tasks hard to parse for artificial intelligence models – making question texts obscure for AIs is a great approach against cheating. It may be achieved by making them interactive, which often confuses AIs and forces them either to give wrong answers or to make it even impossible to understand [5].

The most important flaw of the major part of e-learning platforms is the absence of task obfuscation. The obfuscation could help prevent cheating.

Let us compare two forms of one math problem, which is memorizing math formulas. The first form would contain just plain text, such as "What is the math formula of rectangle area?" and one text input for the answer. The second form is much more complex: the formula parts are draggable elements, with which the student must create the formula.

Table

Comparison of GPT-3.5 abilities to solve two types of tasks

	Plain text	Obfuscated and interactive
GPT-3.5 Success rate	100.0%	5.0%

It is plain to see how to solve the problem in the first form; it is enough to copy the problem text. The AI success rate here is 100%. However, the second form appears much more sustainable against AI cheating. Sometimes GPT-3.5 cannot understand the task or gives a wrong answer. Moreover, the task is harder to copy and paste to GPT, which prevents cheating even better.

Summing up all the AI cheating prevention methods, developing a platform using all these methods would help make online education more efficient by reducing AI-based cheating.

THE 11th ANNUAL STUDENT SCIENTIFIC CONFERENCE IN ENGLISH

Vladivostok, May 2024

References:

1. Jean Underwood, Attila Szabo. Academic offences and e-learning: individual propensities in cheating // British Educational Research Association, 2003. – URL: <https://berajournals.onlinelibrary.wiley.com/doi/10.1111/1467-8535.00343>
2. Zeenath Reza Khan, Sreejith Balasubramanian. Students go click, flick and cheat: E-cheating, technologies and more, 2009 // Journal of Academic and Business Ethics. – URL: <https://repository.mdx.ac.uk/download/198ea4868cc9449b397c5d32d48a4f8d6633e1a5aa5ea49de07b3551b7d68e9a/473464/121192.pdf>
3. Debby R. E. Cotton, Peter A. Cotton, J. Reuben Shipway. Chatting and cheating: Ensuring academic integrity in the era of ChatGPT, 2024 // Innovations in education and teaching international. – URL: <https://www.tandfonline.com/doi/epdf/10.1080/14703297.2023.2190148?needAccess=true>
4. Tobias Greitemeyer, Andreas Kastenmüller. HEXACO, the Dark Triad, and Chat GPT: Who is willing to commit academic cheating?, 2023 // ScienceDirect – URL: [https://www.cell.com/heliyon/pdf/S2405-8440\(23\)07117-7.pdf](https://www.cell.com/heliyon/pdf/S2405-8440(23)07117-7.pdf)
5. Kalepesh Krishna, Yixiao Song, Marzena Karpinska, John Wieting, Mohit Iyyer. Paraphrasing evades detectors of AI-generated text, but retrieval is an effective defense, 2023. - URL:https://proceedings.neurips.cc/paper_files/paper/2023/file/575c450013d0e99e4b0ecf82bd1afaa4-Paper-Conference.pdf

Gerus P.A.1, Protsenko D.V.¹

DEVELOPMENT OF A PROTOTYPE SOFTWARE SYSTEM FOR TEACHING WRITTEN ENGLISH

¹Far Eastern Federal University, Institute of Mathematics and Computer Technologies, FEFU

² Far Eastern Federal University, Oriental Institute - School of Regional and International Studies, FEFU

Scientific adviser – O.A.Krestnokova¹

Scientific consultant – B.F. Veremeeva²

The sphere of international communications and business relations is constantly expanding in the modern world. In this regard, knowledge of the English language becomes an essential tool for successful communication and business management. A huge amount of communication and solutions to important issues occur through e-mail, messengers, and other means of online communication. Thus, mastering written English nowadays is a key component of personal and professional success.

The basic writing skills include: abstract presentation, taking notes, writing essays, articles, reports, conducting business and non-business correspondence by e-mail, two-way translation. There are various forms of written works that students can study during the educational process. All this includes communicative competence, which is aimed at the application of the English language in life [1].

It is important that the application not only checks spelling and literacy in the text, but also is a tool for learning, that is, there should be tasks and their verification. Also, the software tool should provide detailed visual statistics to the user on the mistakes he made in various aspects of the language and display progress; allow you to choose the type of letter (postcard, essay, email, etc.) and its style; be able to customize tasks, which will allow you to take into account the level of the student, his age, and the task that he faces, for example, passing an English exam.

One of the popular platforms for checking grammar, spelling and stylistics of text in English are such platforms as Grammarly [2], Linguiix [4], Write&Improve [5], Hemingway [3], Ginger [6], LanguageTool [7]. But only Write&Improve positions itself as a learning platform.

THE 11th ANNUAL STUDENT SCIENTIFIC CONFERENCE IN ENGLISH

Vladivostok, May 2024

A comparative analysis of the software tools presented in the table showed that there is no system that would allow not only to simplify the writing of concise and literate texts, but was aimed at teaching and training writing, as well as had detailed statistics and additional learning tools.

Table

Platform comparison

Platform Functions \ Platform	Grammarly	Linguix	Write&Improve	Hemingway	Ginger	LanguageTool
Checking the style of the text	-	+	+	+	-	-
Checking the spelling of the text	+	+	+	+	+	+
Checking grammar in the text	+	+	+	+	+	+
Detailed statistics	+	+	-	-	-	-
Analysis and explanation of mistakes made	-	-	-	-	-	-
Writing training Tasks	-	-	+	-	-	-
The ability to customize tasks	-	-	+	-	-	-

The considered software tools are not positioned as educational and, therefore, do not solve the problem facing the user. Thus, it is relevant to develop a software tool that will meet all the requirements presented in the comparative table. It is planned to implement the following tasks: writing a text on a given topic and training written assignments from English language exams (IELTS, TOEFL, USE).

In the first type of tasks, the user, depending on the selected level, is offered to write: an email, an essay, describe a story from pictures, an email, a resume, a report, a plan, an article, a post for a social network on a given topic. After completing the task, the program will check compliance with grammatical and spelling rules, as well as with the specified style. The mistake locations will be highlighted, and you will also be able to view the correct version with its analysis in accordance with the rules of the English language.

In the second type of tasks, the user will need to select the exam he is interested in and complete the available tasks in the allotted time. After execution, the application will display the mistake locations with their explanation and give an assessment.

During training, it is important to see not only your mistakes, but also your progress, so detailed user statistics on completed tasks will be implemented. This will allow you to track changes in your level, which aspects you should pay attention to, set goals and achieve them.

References:

1. Smirnova E. V. Actual aspects of improving foreign language written speech when using information and communication technologies // Baltic Humanitarian Journal. 2015. №4 (13). P. 102–105.
2. Grammarly [Electronic resource] – URL: <https://app.grammarly.com/>
3. Hemingway [Electronic resource] – URL: <https://hemingwayapp.com>
4. Linguix [Electronic resource] – URL: <https://linguix.com/>
5. Write&Improve [Electronic resource] – URL: <https://writeandimprove.com/>
6. Ginger [Electronic resource] – URL: <https://www.gingersoftware.com/grammarcheck>
7. LanguageTool [Electronic resource] – URL: <https://languagetool.org/>

THE USE OF AUGMENTED REALITY IN APPLICATIONS WITH MOVABLE CAMERA

¹Far Eastern Federal University, Institute of Mathematics and Computer Technologies, FEFU

²Far Eastern Federal University, Oriental Institute – School of Regional and International Studies, FEFU

Scientific adviser – A.A. Antonova¹

Scientific consultant – E.V. Kravchenko²

Augmented reality (AR) is a technology that lies at the intersection of virtual and real spaces, facilitating their mutual integration. Therefore, its application holds significant potential both at the macro level, in conditions of human interaction with other people or the surrounding environment, and at the micro level, such as in the execution of high-precision processes. This paper examines the usage of augmented reality within urban environment, particularly in the context of interaction between a spectator and architectural forms. Digital content that is demonstrated within the mentioned interaction primary serves the purpose of human navigation in urban areas and is also an integral component of the process of gamifying the surrounding space. Consequently, a device intended for augmented reality implementation should possess high mobility and processing power. At the current level of technological development, a smartphone satisfies these requirements. Leading companies such as Apple and Google provide opportunities for creating augmented reality applications, however, the final products demonstrate unstable results when dealing with a moving camera. Displaying digital content based on architectural forms requires high precision in spatial placement to create the desired impression on the user, and therefore, it is necessary to explore ways of enhancing this aspect.

One of the most common methods of placing virtual objects in the urban space is to associate them with geographic coordinates. This process involves converting the virtual Cartesian coordinate system into geodetic coordinates. Even though the inverse operation seems to be simple from a differential geometry perspective, the conversion itself can only be achieved through sequential approximation methods and requires the use of a reference datum that is unique to each application development platform [3]. Additionally, tracking geodetic coordinates are derived from data obtained from GPS (Global Positioning System), which can result in significant errors when positioning virtual content in real space [4]. The magnitude of these errors increases directly with the altitude of the digital objects being placed, limiting this method to visualizing ground-level objects, such as navigation lines.

It is more accurate to display content associated with spatial 2D markers. This is based on an analysis of the image stream received from the smartphone camera. The target object may be a QR code, but it is also common to use an image of the area in which the content should be visualized. In this case, the developer determines in advance the location and orientation of the smartphone to ensure a positive user experience with the application. However, this method is highly dependent on environmental weather conditions and the time cycle. Changes in ambient lighting can affect the identification of feature points, leading to errors in image recognition. In addition, the use of 2D markers imposes limitations on the user's freedom of movement within the area. The angle of the camera can introduce errors into the projection of three-dimensional virtual objects onto the flat smartphone screen [1]. Therefore, despite the availability of image stabilization and filtering techniques, this method may not be suitable for application within an urban environment.

The use of 3D marks has significant potential. These are created using photogrammetry, which involves scanning a real-world scene and placing it into virtual space. To visualize content, the application must not only search for a match among feature points, but rather analyze their clusters and calculate planes based on them, comparing with the geometry of the scan. This method is less dependent on environmental factors and provides greater camera mobility, however it does require a more complex application architecture. To recognize 3D shapes, the image captured by camera must contain not only color channels but also a depth

THE 11th ANNUAL STUDENT SCIENTIFIC CONFERENCE IN ENGLISH

Vladivostok, May 2024

channel, which allows the position of object in space to be calculated. Most often, this channel is created by combining images captured from several spatially distributed cameras, which can either be integrated into the smartphone or separated into a standalone sensor device, such as Kinect. To facilitate use, the depth channel can be created as a separate map, allowing for object analysis without considering the color of the original image. An example of this solution is Apple's FaceID technology. However, due to limitations imposed by the design on camera performance, the accuracy of object positioning is not always ideal. This is particularly evident in the recognition of highly detailed objects. The boundaries of depth areas may be uneven, hindering the user's immersion in virtual reality.

It is necessary to examine the existing methods for generating depth maps to determine the preferred one. In this regard, the use of LiDAR (Light Detection and Ranging) is considered advanced. The device emits laser pulses into the surrounding space and measures the time it takes them to return. The software associated with LiDAR can perform calculations based on either a full-fledged emission wave map, which would be problematic within the context of smartphone-based technologies, or discrete values [8]. LiDAR sensors have been integrating into the design of Apple's latest-generation devices, enabling the ARKit toolkit to perform enhanced depth map calculations. The advantage of this method lies in its ability to rapidly scan a large area, which can be implemented in scientific research of ecosystems. However, within the urban environment, the error obtained during discretization is sufficiently high to disrupt the immersion effect [5]. Furthermore, the integration of LiDAR into the device necessitates significant investment, both technically and financially.

Another method of calculating depth map is applied in Google smartphones, which are predisposed to use the ARCore toolkit. Despite the possibility of using data from specialized sensors, such as time-of-flight (ToF) sensor, this technology builds the depth map based on occlusion calculations. Given an image stream received from camera, the system search for visually similar elements, supplemented with data on the position and orientation of the smartphone. Therefore, camera movement is a necessary condition for implementing this technology. Nevertheless, the highest accuracy in depth determination is achieved when the device is located within 5 meter range from the target object, with a maximum distance of 65 meters [2]. The key feature of this method, expressed in the necessity of movement, also presents a significant obstacle. Due to the requirement to process a large number of images individually to build the depth map, the speed of building is extremely low. This makes it difficult to quickly move the smartphone, which is frequently applied as a gameplay element in gamified spaces. Additionally, using this number of images necessitates the allocation of an equal amount of device memory to store depth map, making the application inefficient for use in urban environment.

A possible solution to this issue is the application of machine learning technologies to reduce the quantity of images. Niantic has developed the SimpleRecon system, which enables the determination of spatial depth based on a single image [6]. The underlying neural network of the system, while convolutional, requires fewer implementation resources compared to analogs. Its purpose is not to entirely reconstruct the real world in virtual space but rather to predict the position of significant elements, which is achieved through the integration of geometrical metadata into the image recognition process. Machine learning is also used in occlusion calculation [7]. The bitmask needed for displaying 3D objects in augmented reality is generated using data derived from the image of the intended scene, rather than the complete depth map of the surroundings. This, in theory, allows for complete elimination of the need for such a depth map. The considered technology can be implemented on Apple and Google devices, and also does not necessitate the usage of complex sensor designs.

Therefore, the current level of technological advancement allows for the development of applications that integrate virtual elements into the urban environment with high accuracy. To ensure the necessary object placement, a viable method is to locate them based on comprehensive analysis of data received from GPS and smartphone sensors. Random camera movements occurring as user moves within the urban space can be

THE 11th ANNUAL STUDENT SCIENTIFIC CONFERENCE IN ENGLISH

Vladivostok, May 2024

compensated for using machine learning technologies. The ongoing decrease in devices load, combined with the improvement of their technical capabilities, makes augmented reality available for providing a sufficient degree of user immersion in the digital space.

References:

1. Batkova, Y.S. A particle filtering method to enhance marker recognition in augmented reality / Y.S. Batkova, D.G. Shtennikov // International Scientific and Practical Conference "Science Today: Global Challenges and development mechanisms". – 2019. – P. 12-14.
2. Depth adds realism [Electronic resource]. – Google for Developers. – Mode of access: <https://developers.google.com/ar/develop/depth>
3. Kurosheev, G.D. Methods of transformation of geodetic and spatial rectangular coordinates, their algorithms, parameters, accuracy / G.D. Kurosheev, A.A. Harunzhii // Vestnik SPbSU. – 2012. – Book 7. – №3. – P. 79-90.
4. Lee, G.A. CityViewAR: A Mobile Outdoor AR Application for City Visualization / G.A. Lee, A. Dünser, S. Kim, M. Billinghurst // 11th IEEE International Symposium on Mixed and Augmented Reality (ISMAR 2012) – Arts, Media, and Humanities. – 2012. – P. 57-64.
5. Quito, B. Compare and Contrast LiDAR and Non-LiDAR Technology in an Autonomous Vehicle: Developing a Safety Framework / B. Quito, L. Esmahi // Open Journal of Safety Science and Technology. – 2013. – №13. – P. 101-131.
6. SimpleRecon: 3D reconstruction without 3D convolutions / M. Sayed, J. Gibson, J. Watson, et al. // Proceedings of the European Conference on Computer Vision (ECCV). – 2022.
7. Virtual occlusions through implicit depth / J. Watson, M. Sayed, Z. Qureshi, et al. // Computer Vision and Pattern Recognition Conference (CVPR). – 2023.
8. Wasser, L.A. The Basics of LiDAR - Light Detection and Ranging - Remote Sensing [Electronic resource]. – Neon. – 2024. – Mode of access: <https://www.neonscience.org/resources/learning-hub/tutorials/lidar-basics>

Kuchapina S.S.¹

THE DEVELOPMENT OF A RECOMMENDATION SYSTEM FOR PREDICTING THE OCCURRENCE OF FOREST FIRES USING METEOROLOGICAL DATA

¹Far Eastern Federal University, Institute of Mathematics and Computer Technologies, FEFU,

² Far Eastern Federal University, Oriental Institute - School of Regional and International Studies, FEFU

Scientific adviser – I.L. Artemeva¹

Scientific consultant - I.N. Lazareva²

Fires are known as a dangerous phenomenon causing enormous and often irreparable damage to nature and humans. Despite the dangers, fires occur regularly, even though it is within our power to control this phenomenon by taking timely measures to manage fire-prone situations. The main cause of fires is human activity, but weather conditions also significantly contribute to the occurrence of fires, particularly in forests.

The primary direct cause of initial forest fire outbreaks is improper actions by people visiting the forest for economic or recreational purposes. However, hydrometeorological factors can significantly influence the spread of fires. For instance, a fire caused by natural (lightning strike) or anthropogenic reasons (careless handling of fire) spreads faster with lower relative humidity and higher wind speeds. Conversely, weather can also prevent the spread of fires: prolonged rains and damp, inclement weather prevent forest fires. Moreover, weather is the most unpredictable factor affecting fire danger: depending on the area, weather can change

THE 11th ANNUAL STUDENT SCIENTIFIC CONFERENCE IN ENGLISH

Vladivostok, May 2024

quickly. A light breeze can turn into strong gusts, or the wind direction may change. Therefore, it is crucial to consider current weather conditions to increase the effectiveness of forest fire control measures.

In the last decade, the growth rate of forest fires has slowed. Statistics on forest fires in Russia over the past five years show that their number is within historical minimums and maximums. However, over the past five years, the area affected by forest fires has significantly increased.

Data for assessing the fire situation include: a geometric map of the fire area, type of fire, wind speed, relative humidity, fuel load, etc. People spend a significant amount of time assessing and predicting fire occurrences, and since key factors can change over time, the results become outdated. Hence, systems are being developed to automate the process of calculating fire danger.

Today, several software tools can detect forest fires at an early stage. These systems can monitor multiple areas and detect early fire outbreaks in real time using sensitive sensors, photo and video cameras, and fire recognition algorithms with trained models.

However, an analysis of the software tools shows that none of the existing solutions meet all functional criteria. Particular attention should be given to the "Fire Occurrence Prediction" function. Only the Canadian Forest Fire Danger Rating System (CFFDRS) possesses this functionality, fulfilling the need for software tools. But CFFDRS is only available in Canada. Therefore, to solve the problem of predicting forest fire occurrences, an application is needed that can predict their occurrence based on meteorological data.

Currently, there are several algorithms to determine the comprehensive fire danger index based on meteorological data.

Until 1949, the combustibility index was assessed based on a single hydrometeorological value. This situation persisted until Nesterov published his research. Based on the analysis of more than 600 experiments, he hypothesized that forest combustibility increases with the duration of the dry period. During this period, it is proposed to consider not a single meteorological characteristic, but a complex of them. Nesterov's complex includes air temperature at a height of 2 meters, dew point deficit at a height of 2 meters, and their product. As a result of the calculations, a formula was derived to identify the comprehensive index:

$$K\Pi_n = K\Pi_{n-1} * K_{oc} + (T_0 - T_d) * T_0$$

In this formula, shortcomings were identified by other scientists, who then supplemented it. L.I. Sverdlova identified the influence of wind speed on combustibility. M.A. Sofronov introduced an adjustment for the hygroscopicity of forest fuels, noting that certain fuels (mosses, lichens) do not fully evaporate water but reach equilibrium moisture. At 85% humidity, they lose the ability to burn, although Nesterov's combustibility index continues to rise. Thus, to account for all features and adjustments, a non-primitive ontology model was constructed, based on generalizing methods for determining the threat level, which are modifications of Nesterov's method. A formal grammar was developed for working with formulas and calculating values. Technical documentation for the developed system was also described.

The system can be used as a standalone module in the development of an integrated forest fire control system. The software will automatically collect meteorological data from rp5.ru or similar services. The main meteorological data collected for further prediction processes include ambient and soil temperature, relative air temperature, wind speed and direction, humidity, precipitation probability, and atmospheric pressure. Processing this data will help identify areas at risk of fire outbreaks.

References:

1. Ladokhina E.M., Aniskina O.G., 2019. Fire hazard forecast for the European territory of Russia based on the hydrodynamic forecast of fields of meteorological quantities, Proceedings of the main Geophysical Observatory named after A.I. Voeikov, 113-128 p.
2. Simonenko V.V., Kozhenikova N.Yu. Forest fires, classification, statistical data for 2017-2021. - 2021 - pp. 344-349. – URL:// https://www.elibrary.ru/download/elibrary_48576135_94192025.pdf

ENERGY DISTRIBUTION OF APAMEA LATTICE VERTICES FOR SPIN ICE

¹ Far Eastern Federal University, Institute of High Technology and Advanced Materials, FEFU

² Institute of Applied Mathematics, Far East Branch of the RAS

³ Far Eastern Federal University, Oriental Institute - School of Regional and International Studies, FEFU

Scientific adviser – Y.A. Shevchenko¹

Scientific consultant - Y.O. Kamornaya ³

In the middle of the last century, the similarity between pyrochlore lattice and water ice lattice was discovered [1]. Ising antiferromagnetic spin nanosystems of similar structure were named “spin ice” [2]. XMCD images of lithographically created spin ice on the Apamea lattice were examined (Figure 1a, 1b). There are 100 pieces for each temperature in the range from 240K to 290K in 10K increments. Figure 1c lists, in order of increasing energy, all types of lattice vertices and also indicates the relative energies. The energy of a vertex is calculated using the formula:

$$E = \sum_{\langle i,j \rangle} \left(\frac{(\vec{m}_i \vec{m}_j)}{|\vec{r}_{ij}|^3} - 3 \frac{(\vec{m}_i \vec{r}_{ij})(\vec{m}_j \vec{r}_{ij})}{|\vec{r}_{ij}|^5} \right),$$

where $\langle i,j \rangle$ means the summation over all unique pairs of spins near a given vertex, \vec{m}_i and \vec{m}_j are their magnetic moments, \vec{r}_{ij} is the distance between them. It was calculated that for types alpha, beta and a, b the number of high-energy vertex configurations decreases with temperature decreasing (Figure 2). But for vertices with three and four adjacent particles, the types close in energy alternate in the temperature range from 250K to 290K.

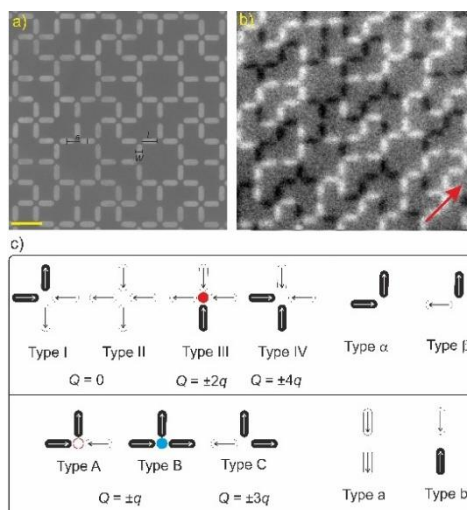


Figure 1. Apamea lattice vertices [3]

(a) Scanning electron microscopy image of the Apamea lattice consisting of nanomagnets with length $L = 360$ nm, width $W = 120$ nm and thickness $d = 2.6$ nm with lattice parameter $a = 500$ nm.

The yellow scale bar indicates a length of 600 nm. (b)

XMCD image of the low-energy moment configuration obtained after thermal annealing. (c)

Vertex types at two-, three-, and four nanomagnetic edges.

Listed in the order corresponding to the increase in dipole energy

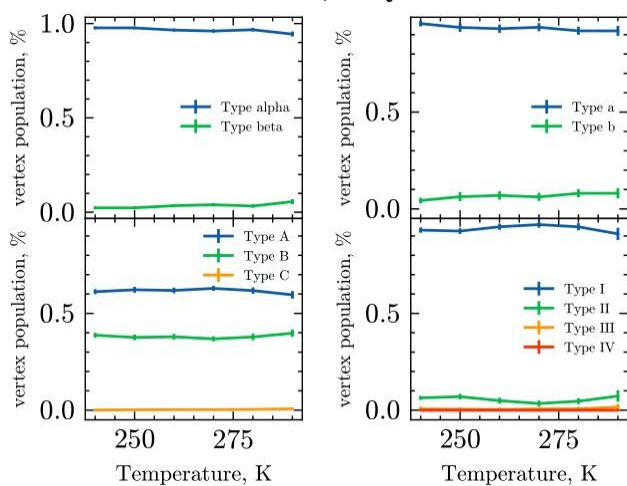


Figure 2. Populations of vertex types as a function of temperature

References:

- Anderson P. W. Ordering and antiferromagnetism in ferries // Physical Review.— 1956. — Vol. 102, no. 4. — P. 1008.
- Geometrical Frustration in the Ferromagnetic Pyrochlore Ho₂Ti₂O₇ / M. J. Harris [et al.] // Physical Review Letters. — 1997. — Vol. 79, issue 13. — P. 2554–2557.
- Saccone, M., Caravelli, F., Hofhuis, K. et al. Real-space observation of ergodicity transitions in artificial spin ice. Nat Commun 14, 5674 (2023). <https://doi.org/10.1038/s41467-023-41235-4>

Malikov V. P.¹

MODEL OF AUTONOMOUS DRIVING USING OBSTACLE DETECTION BASED ON RAY TRACING AND NEURAL NETWORK

¹Far Eastern Federal University, Institute of Mathematics and Computer Technologies, FEFU

² Far Eastern Federal University, Oriental Institute - School of Regional and International Studies, FEFU
Scientific consultant – I.F. Veremeeva²

Autonomous driving technologies have been rapidly developing in recent years, and they have the potential to revolutionize not only the automotive industry, but also the way people get around and interact with their environment. A crucial aspect of autonomous driving systems is their ability to perceive and understand the environment, enabling safe and efficient navigation on the road. This project proposes to apply a neural network that utilizes ray tracing techniques to detect obstacles and perceive the environment, allowing the vehicle to learn autonomous driving in a simple simulation model.

The proposed algorithm uses neural network algorithms and ray tracing to train the car to drive on roads in a simulated environment. The car is equipped with a set of sensors that emit rays to measure the distance to obstacles, allowing it to “see” its surroundings. This information is then used by a neural network to make decisions about how to navigate the environment, such as adjusting speed, steering angle or braking.

Using the ray tracing method allows to measure distances to the nearest obstacles. This information then can be used as input to a neural network, providing it with a real-time understanding of its surroundings. The neural network makes movement decisions based on the data received from the ray sensors. Each beam is assigned an action based on the distance to the object the beam is aimed at. It is a self-learning algorithm, meaning that the next action is determined independently by rewarding the car for fulfilling some necessary requirements, such as not colliding with other cars, not driving off the road, and maintaining a decent speed.

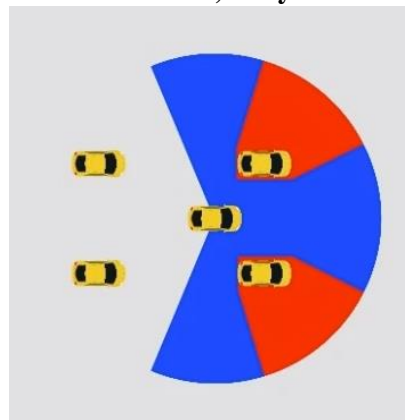


Figure 1. Ray tracing

The effectiveness of the algorithm can be evaluated by the ability of the vehicle to travel safely and efficiently in the simulation environment. This would include measuring the number of successful trips, time taken and any collisions.

In this project, an unsupervised neural network for autonomous driving is developed utilizing ray tracing to detect obstacles and perceive the environment. By utilizing the power of ray tracing and the ability of neural networks to learn, the road to the future with self-driving cars will be paved.

References:

1. Deep Learning //Goodfellow I., Bengio Y., Courville A. Deep learning. – MIT press, 2016.
2. Schmidhuber J. Deep learning in neural networks: An overview //Neural networks. – 2015. – T. 61. – pp. 85-117.

Moiseev D.A.¹, Vayay M.S.¹

DEVELOPMENT OF A SOFTWARE TOOL FOR ANALYSING ARBITRAGE SITUATIONS ON FINANCIAL MARKETS OF "ARBITRUM"

¹Far Eastern Federal University, Institute of Mathematics and Computer Technologies, FEFU

²Far Eastern Federal University, Oriental Institute – School of Regional and International Studies, FEFU

Scientific adviser – I.L. Artemyeva¹

Scientific consultant – N.S. Fedchenko²

In today's financial market, there are many money services that help users to make buy and sell transactions in the most expeditious manner., arbitrage as an investment strategy becomes a useful tool in conditions of constant price volatility. Its essence is to exploit differences in the prices of the same assets in different markets in order to make a profit.

There have been seen many instances of arbitrage in the financial markets for the last twenty years. For example, RUSAL stocks which are listed in Hong Kong. The ratio of securities was stable. In April 2018, after getting into the sanctions SDN-list, the price of shares in Hong Kong fell down quickly. The value of securities of the Russian aluminum company collapsed, hitting an all-time low, by 20.1% to HK\$1.63 USD a share. When sanctions were lifted in early 2019, the spread between the shares levelled out over several days. The papers moved towards each other, with stocks on the Moscow Exchange declining and those in Hong Kong rising. The movement was predictable, which allowed short-term speculators who understood this relationship to make money on such a convergence [1].

There are many platforms for analyzing arbitrage opportunities, and the choice of the most suitable one depends on the required functionality and personal preferences (MetaTrader 4, Interactive Brokers, P2P.Army,

THE 11th ANNUAL STUDENT SCIENTIFIC CONFERENCE IN ENGLISH
Vladivostok, May 2024

QUIK, Bloomberg Terminal)[2-3].

The features of P2P.Army [4]:

1. Tracking arbitrage situations, the difference in price of the same cryptocurrency asset on direct currency exchanges.

2. Large amount of price data. P2P.Army contains a large number of opportunities to monitor the current prices of crypto-assets on various sites, as well as offers to buy or sell cryptocurrency with the display of popular payment directions.

3. Intuitive interface. All found opportunities for arbitrage deals are summarised in a table and shown to a user. Information about the platforms for the transaction, the asset, the purchase and sale price, the authors of the ads and their payment systems for the exchange are indicated.

The disadvantages of P2P.Army:

1. High cost of use. For user access to arbitrage signals it is necessary to purchase one of two tariffs with monthly payment.

2. There is no mobile version of the service.

3. There is no analysis of arbitrage situations on the stock market of Russian assets.

Each trading service includes the ability to monitor asset price quotes and place orders, the availability of technical indicators, the display of a short news feed, and the control of a personal investment portfolio.

Having analysed the existing solutions, let's make a table comparing the functionality of these software on their ability to automatically detect arbitrage situations.

Table

Comparison of trading platforms

Platform Function / features	MetaTrader 4	P2P.Army	QUIK	Interactive Brokers	Bloomberg Terminal
Interface customisation	+	-	-	+	+
Connection of external plugins	+	-	-	+	+
Graphical display of prices at the current moment of time	+	-	+	+	+
Monitoring of investment portfolio status	+	-	+	+	+
Registration of Russian users	+	+	+	-	-
Automatic detection of arbitrage situations on the stock and currency markets	-	-	-	-	-

Based on the comparative analysis, these systems lack the function of automatic search for arbitration situations. Therefore, it is urgent to develop a software system that has this function.

The "ARBITRUM" system under development will have a number of anticipated features that will make it unique and useful to users. Some of them are as follows:

1. Availability of filtering and sorting by different sites and assets according to specific preferences and

THE 11th ANNUAL STUDENT SCIENTIFIC CONFERENCE IN ENGLISH
Vladivostok, May 2024

criteria of a user.

- 2.Built-in statistical and graphical tools that provide access to data on asset prices over different time periods.
- 3.Profit calculator to calculate the potential profit after the realisation of the selected bundle.
- 4.A tab with arbitrage situations, providing users with information about possible differences in asset prices on different platforms.
- 5.Automatic arbitrage search, saving the user from manual monitoring of asset price dynamics.
- 6.Visual and audible notification system, alerting information about potential profitable operations.
- 7.Cross-platform and cross-browser functionality, ensuring the possibility of using the system on various devices.

References:

1. News portal BKS EXPRESS [Electronic resource] // Access mode: <https://bcs-express.ru/novosti-i-analitika/chto-takoe-arbitrazh-i-gde-investoru-ego-iskat?ysclid=lqet13o5w0707033167/>
2. Educational portal #investing [Electronic resource] // Access mode: <https://www.hashtaginvesting.com/blog/best-forex-scanners-in-2023>.
3. Educational portal "The Best Arbitrage Scanners" [Electronic resource] // Access mode: <https://top-arbitrazhskaner.ru/>
4. Web platform P2P.Army [Electronic resource] // Access mode: <https://p2p.army/ru>.

Moskovchenko Z.A.¹

**DEVELOPMENT OF A PROGRAM FOR CONTROLLING A ROBOTIC TRAINER USING
ROBOTICS OPERATING SYSTEM**

¹Far Eastern Federal University, Institute of Mathematics and Computer Technologies, FEFU

² Far Eastern Federal University, Oriental Institute - School of Regional and International Studies, FEFU

Scientific advisor – E.V. Pustovalov¹

Scientific consultant – I.F. Veremeeva²

According to statistical data, approximately 15 million people worldwide experience a stroke each year. In Russia, this number is around 450 thousand people. However, a stroke does not have severe consequences and ends in complete recovery only in 8-10% of all cases [1]. In the remaining cases, the ability to move one or more limbs is often lost. Robotic trainers can be used for the rehabilitation of those patients.

There are several types of robotic trainers that can be used for the rehabilitation of post-stroke patients: Biodex, Artomot, Amadeo, and ExoAtlet. Among these trainers, only multi-purpose ones (such as Biodex) can be used for treatment of arms, but they usually require significant funds. The rest of the trainers can only be used for rehabilitation of other limbs.

The small enterprise “Trenazher” is developing a robotic trainer called RoboTrainer, designed for the rehabilitation of arms after a stroke. The prototype of the trainer has two degrees of freedom - one for the shoulder joint, and one for the elbow joint. The trainer is oriented towards passive movement, during which the patient does not exert any effort.

To improve the prototype of the trainer, it is necessary to add feedback to the system and create a control system that operates with it in mind. Since the trainer is intended for medical use, feedback will ensure the safety of its operation.

Robotics Operating System (ROS) is a middleware for robotics programming that is used to develop the control system for the robotic trainer. This system is the most common in the field of robotics and supports the

THE 11th ANNUAL STUDENT SCIENTIFIC CONFERENCE IN ENGLISH
Vladivostok, May 2024

largest number of peripheral devices compared to alternatives.

The following sensors are planned to be used to provide feedback: a strain gauge to determine the force in the joint and an angle sensor to determine the angle of joint flexion.

The GTK library of GUI elements is used to develop the user interface. The layout of the user interface is presented in Figure 1.

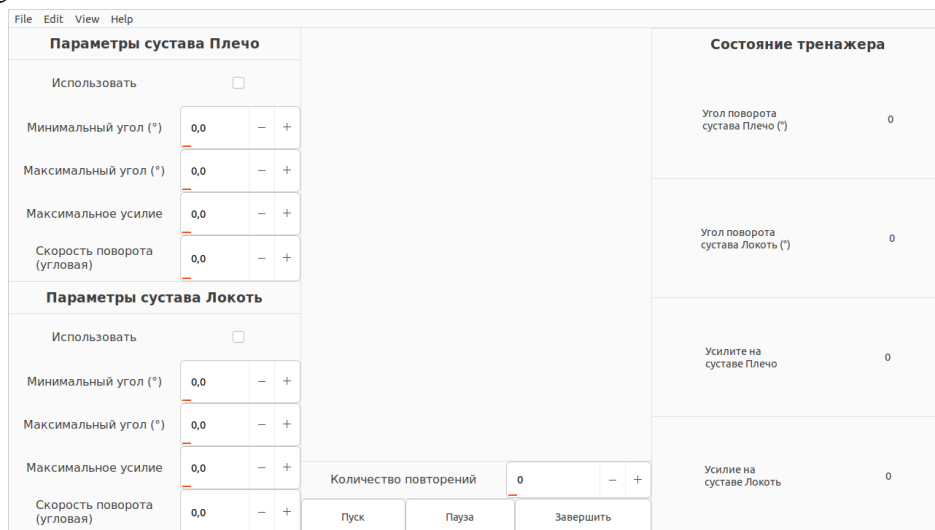


Figure 1. User interface layout of the control system

The control system consists of two components. The server component includes the user interface, which sends commands to the trainer and receives feedback from it. The client directly controls the trainer according to the control input from the server.

References:

1. Kostiv, E. P. Method of restoring joint function / E. P. Kostiv, V. M. Zanin, B. B. Kuryshev // Man and Medicine: Materials of the VI Far Eastern Regional Congress with international participation, supplement to the Pacific Medical Journal 2009, No. 4, Vladivostok, September 24–25, 2009. – Vladivostok: Medicine DV, 2009. – P. 85–86.

Nazarov M.S., Kurbanov M.M., Pestryak N.E.

VST PLUGIN FOR AUTOMATIC EQUALIZATION

Far Eastern Federal University, Institute of Mathematics and Computer Technologies, FEFU
Scientific advisor - I.L. Artemyeva

The need for high-quality processing of voice recordings is steadily growing in the world of modern audio engineering. With the development of music production and recording technologies, the demand for instruments that can provide the best sound of voice tracks is growing too.

One of these tools is VST plugins. VST (Virtual Studio Technology) is a standard developed by Steinberg for use in audio editors and DAW (Digital Audio Workstation), which are used to create and edit music. VST plugins are small programs that can be loaded into a DAW and used to process audio tracks.

Such plug-ins can provide various audio processing capabilities, such as equalizer, compressor, reverb, delay, and others. The main purpose of such plugins is to improve the sound quality of an audio track, create interesting effects and additional features for musicians and sound engineers.

Equalizer is one of the most important types of VST plugins. Equalizer is a tool for controlling the frequency balance in an audio track, which is used to correct the frequency level in a signal in order to achieve a certain sound effect or bring the sound to an ideal one (Fig.1).

THE 11th ANNUAL STUDENT SCIENTIFIC CONFERENCE IN ENGLISH
Vladivostok, May 2024



Figure 1. Examples of simple VST plugins

Equalization is a frequency correction of sound. The principle of equalization is to lower or increase the volume level of certain frequencies to achieve a “pure” sound.

Traditionally, the voice equalization process is performed manually. The sound engineer analyzes the audio track and manually adjusts the frequency levels according to the desired effect. This process can be very time-consuming and demanding for the professionalism of the sound engineer.

References:

1. Official VST website : https://www.steinberg.net/VST_sdk.html
2. General information about audio plugins: https://en.wikipedia.org/wiki/Audio_plugin
3. Information about the DAW: https://en.wikipedia.org/wiki/Digital_audio_workstation
4. Information about the standard equalization process: [https://en.wikipedia.org/wiki/Equalization_\(audio\)](https://en.wikipedia.org/wiki/Equalization_(audio))
5. Description of the automatic voice equalization process: <https://pdfs.semanticscholar.org/34c6/86a0fc1ecdd5fb17b5eeb64107010f177a95.pdf>

Sakharov I.A.¹

DEGREES OF SEMANTIC AND SYNTACTIC RIGIDITY OF CONNECTED UNARS WITHOUT LEAVES

¹Far Eastern Federal University, Institute of Mathematics and Computer Technologies, FEFU

²Far Eastern Federal University, Oriental Institute – School of Regional and International Studies, FEFU

Scientific advisor — A.A. Stepanova¹

Scientific consultant – P.S. Minakova²

In this paper we study semantic and syntactic rigidity of structures such as unars. Syntactic rigidity shows the extent to which elements of a structure can be interconnected by automorphisms. Semantic rigidity shows how adding constants to a structure signature affects the syntactic rigidity of that structure. The following concepts from model theory can be found in [1], from unar theory – in [2, 3].

Let A be a set in a structure \mathcal{M} . The structure \mathcal{M} is called *semantically A-rigid* if any A -automorphism $f \in Aut(\mathcal{M})$ is identical. The structure \mathcal{M} is called *syntactically A-rigid* if $\mathcal{M} dcl(A)$. The structure \mathcal{M} is called \exists -semantically (respectively \exists -syntactically) n -rigid, $n \in \omega$, if \mathcal{M} is a semantically (syntactically)

THE 11th ANNUAL STUDENT SCIENTIFIC CONFERENCE IN ENGLISH

Vladivostok, May 2024

A-rigid structure for some of its subset A of cardinality n . The least n such that \mathcal{M} is \exists -semantically (\exists -syntactically) n -rigid structure is called the \exists -semantic (\exists -syntactic) degree of rigidity of the structure \mathcal{M} and is denoted by $\deg_{rig}^{\exists\text{-sem}}(\mathcal{M})$ ($\deg_{rig}^{\exists\text{-synt}}(\mathcal{M})$). If such n does not exist, then we put $\deg_{rig}^{\exists\text{-sem}}(\mathcal{M}) = \infty$ ($\deg_{rig}^{\exists\text{-synt}}(\mathcal{M}) = \infty$).

The structure $\mathcal{A} = (A; f)$, where f is a unary operation on A , is called a *unar*. A unar \mathcal{A} is called *connected* if for any $a, b \in A$ there exist $n, m \in \omega$ such that $f^n a = f^m b$. A unar $\mathcal{C} = (C; f)$ is called a *chain* if $C = \{c_i \mid i \in Z\}$ and $fc_i = c_{i+1}$. A unar $\mathcal{C} = (C; f)$ is called a *cycle (of length n)* if $C = \{c_i \mid 0 \leq i \leq n - 1\}$, $fc_{n-1} = c_0$ and $fc_i = c_{i+1}$ for any i , $1 \leq i < n - 1$. A cycle of length 1 is called a *loop*. An element $a' \in A$ is called the n th preimage of an element $a \in A$ if $f^n a' = a$. The first preimage of a is called the *preimage* of a . Let $f^{-n}(a)$ denote the set of all n th preimages of a . Let denote $\bigcup_{n \in \omega} f^{-n}(a)$ by $\langle a \rangle_-$. An element $a \in A$ is called a *leaf* if it has no preimages. Any unar without leaves contains a chain or a cycle. An element $a \in A$ is called *cyclic* if there exists $t \geq 1$ such that $f^t a = a$, otherwise it is called *acyclic*. An element $a \in A$ is called a *branching* if it has two different preimages, at least one of which is acyclic. Let us denote the set of all branchings of \mathcal{A} by $B(\mathcal{A})$. The *distance* between elements $a, b \in A$ is the number $d = \min\{n + m \mid n, m \in \omega, f^n a = f^m b\}$. Denoted by $d(a, b)$. If $a \in A$ is an acyclic element, then a *branch* of the element a is called $\langle a \rangle_-$. If $a \in A$ is a cyclic element, then the *branch* of the element a is the set $\{a' \in \langle a \rangle_- \mid d(a', a) \leq d(a', c), \forall c \in C\}$, where C is the set of all cyclic elements of A . We denote the branch of the element a by $b(a)$. The *tail* of an element $a \in A$ is called $\{a\} \cup b(a')$, where $a' \in A$ is the acyclic preimage of a and $b(a')$ does not contain any branchings. The number of all tails of element a is denoted by $N_t(a)$.

Theorem. Let \mathcal{A} be a connected unar without leaves. If there exists a cycle or a chain $C \subseteq \mathcal{A}$, $C = \{c_i \mid i \in I\}$, $I \in \omega \cup \{\omega\}$, such that

\mathcal{C} is not a loop,

there exists a positive n , $n < |I|$ for $|I| < \omega$, such that for any $i, j \in I$

$(C \cup b(c_i); f) \cong (C \cup b(c_j); f)$, if $i \equiv j \pmod{n}$,

then

$$\deg_{rig}^{\exists\text{-sem}}(\mathcal{A}) = \deg_{rig}^{\exists\text{-synt}}(\mathcal{A}) = \max\{1, \sum_{b \in B(\mathcal{A})} \max\{0, N_t(b) - 1\}\}.$$

Otherwise

$$\deg_{rig}^{\exists\text{-sem}}(\mathcal{A}) = \deg_{rig}^{\exists\text{-synt}}(\mathcal{A}) = \sum_{b \in B(\mathcal{A})} \max\{0, N_t(b) - 1\}.$$

The paper was carried out at the Far Eastern Centre for Mathematical Research with the financial support of the Ministry of Education and Science of Russia, Agreement No. 075-02-2024-1440 dated 28 February 2024 on the implementation of programs for the development of regional scientific and educational mathematical centers.

References:

1. Sudoplatov S. V. Variations of Rigidity // Известия Иркутского государственного университета. Серия Математика. 2024. Т. 47. С. 119–136. <https://doi.org/10.26516/1997-7670.2024.47.119>
2. Skornyakov, L. A. Elements of general algebra / L. A. Skornyakov. — M.: Nauka, 1983. — 272 p.
3. Jungabel E. Quasi-projective monounary algebras // Eotvos Lorand University. – 2020. – 20p. – (Prepr./ Eotvos Lorand University).

CREATING AN ARCHITECTURAL SOLUTION FOR DRONE CONTROL IN AUTONOMOUS AND REMOTE MODES

¹Far Eastern Federal University, Institute of Mathematics and Computer Technologies, FEFU

² Far Eastern Federal University, Oriental Institute - School of Regional and International Studies, FEFU

Scientific adviser – V.M. Grinyak¹

Scientific consultant - E.V. Kravchenko²

To date, the creation and integration of drones is the object of close attention from researchers and engineers. Historically, drones have been developed for specific purposes and to operate in areas that are dangerous for humans. Currently, there are attempts to use them in a variety of industries: video surveillance, delivery of large and small cargo, agricultural work, monitoring of environmental parameters, warehouse tasks, etc. Drones are divided into the following types: ground, aerial, surface, and underwater.

From the perspective of implementing drone control processes, there are four modes of operation can be identified [1, 2]:

1. manually operated system – the operator (captain) is located on the board and controls the drone either alone or with a crew;
2. fully autonomous system – the system operates without any human intervention (for example, on the high seas) and does not require the presence of an operator;
3. remotely controlled system – the drone is operated by an operator who is located outside of the board;
4. system with a combined mode of operation – combines autonomous and remote modes, as well as allowing you to quickly switch between them. This is useful in case of an emergency, where remote control may be necessary.

Remote control of the drone can be a difficult task due to delay. It takes time for a signal to pass through satellites, the Internet, or other means. Too much delay may hinder the implementation of practical tasks. Therefore, the combined mode of operation provides the greatest research and practical interest [3].

Now, a software platform has not been developed with proven architectural solutions for combined mode of operation, there are no well-established standard solutions for drones. It is also important for this software platform to ensure modularity, weak dependence of system components, and the possibility of their interchangeability. But first, it is necessary to ensure the interchangeability of behavior in the autonomous mode so that control algorithms can be easily replaced during operation of the drone.

To implement an autonomous mode of operation and ensure the interchangeability of the behavior model, it is worth paying attention to the use of neural networks. Neural networks provide a powerful tool for creating adaptive systems capable learning from experience and adapting to changing conditions.

Artificial intelligence has significant potential in the field of drone control, especially in the context of ships that are heavily influenced by wind, waves, currents, and other environmental disturbances and have very complex nonlinear characteristics for course control systems. Despite the increasing interest in artificial intelligence technologies, there is a lack of scientific research. Traditional drone control methods do not always provide the right quality and reliability. Intelligent algorithms that mimic the behavior of experts can be key in improving the quality of control, therefore it is necessary to develop and improve algorithms and control systems specially adapted for drones [4, 5].

In conclusion, drones are a promising technology with a wide range of potential applications. The combined mode of operation is particularly significant, but there are currently no standard solutions yet. Neural networks provide high adaptability to changing conditions, which will allow to implement the autonomous mode of operation with the possibility of replacing the behavior model. Thus, the main purpose of the work is

THE 11th ANNUAL STUDENT SCIENTIFIC CONFERENCE IN ENGLISH

Vladivostok, May 2024

to develop an architectural solution for combined drone control.

References:

1. Epikhin A.I., Heckert E.V., Movina M.A. Analysis of the safety of unmanned vessels based on the structure of the Bayes network-based risk model // Marine intelligent technologies. – 2021. – №2–4(52). – pp. 38–46.
2. Bratić K., Pavić I., Vukša S. and Stazić L. Review of Autonomous and Remotely Controlled Ships in Maritime Sector // Transactions on Maritime Science. – 2019. – №8(2). – pp. 253–265.
3. Jalonens R., Tuominen R., Wahlström M. Safety of Unmanned Ships: Safe Shipping with Autonomous and Remote Controlled Ships // Aalto University Publication Series Science + Technology. – 2017. – №5.
4. Luo Z., Qian T., Ye X., Huang J., Yu L. Research on a course control strategy for unmanned surface vessel // Journal of Physics: Conference Series. – 2021. – №1948(012106).
5. Epikhin A.I., Kondrat'ev S.I. Artificial intelligence, application prospects in ship power plant management // Operation of maritime transport. – 2020. – №4(97). – pp. 95-100.

Simakov V.K.

ČECH COHOMOLOGIES OF A SINGLE-ELEMENT FAMILY

¹Far Eastern Federal University, Institute of Mathematics and Computer Technologies, FEFU,

² Far Eastern Federal University, Oriental Institute - School of Regional and International Studies, FEFU

Scientific adviser – E.E. Skurikhin¹

Scientific consultant - I.N. Lazareva²

An arbitrary abelian presheaf $A: K^{op} \rightarrow Ab$ from the category K in which products and coproducts exist is considered. Let there $\alpha = \{f_i \mid i \in I\}$ be a family of morphisms $f_i: k_i \rightarrow k$, $i \in I$ from the category K to a fixed object k . The n-dimensional cochains $C^n(\alpha, A)$ of the family α with coefficients in the abelian presheaf A are defined as follows:

$$C^n(\alpha, A) = \prod_{s: [n] \rightarrow I} A(\alpha_s),$$

where α_s is the fibered product of objects $k_{s(0)}, k_{s(1)}, \dots, k_{s(n)}$ over k corresponding to a finite sequence of indices $s: [n] \rightarrow I$, $[n] = \{0, 1, \dots, n\}$. The operator $d_\alpha^n: C^n(\alpha, A) \rightarrow C^{n+1}(\alpha, A)$ for taking n-dimensional coboundaries is defined as follows:

$$(d_\alpha^n(c))_{t: [n+1] \rightarrow I} = \sum_{l=0}^{n+1} (-1)^l (A(p_{t(l)}^{\alpha_t})) (c_{\widehat{t(l)}}),$$

where $c \in C^n(\alpha, A)$, $p_{t(l)}^{\alpha_t}: \alpha_t \rightarrow \alpha_{\widehat{t(l)}}$ is the canonical morphism from α_t to $\alpha_{\widehat{t(l)}}$, $\widehat{t(l)} = t|_{[n+1] \setminus \{l\}}$, $c_{\widehat{t(l)}} = \pi_{\alpha_{\widehat{t(l)}}}^n(c)$, and $\pi_{\alpha_{\widehat{t(l)}}}^n: C^n(\alpha, A) \rightarrow A(\alpha_{\widehat{t(l)}})$ is also a canonical morphism. The pair $(C^*(\alpha, A), d_\alpha^*) = \{(C^n(\alpha, A), d_\alpha^n) \mid n \in \mathbb{Z}\}$, where $d_\alpha^n \circ d_\alpha^{n+1} = 0$ for any $n \in \mathbb{Z}$, is called a cochain complex. The cohomologies of this cochain complex are denoted by $H^n(\alpha, A)$.

A family α is canonically associated with the family $\beta = \{f\}$ consisting of a single morphism $f: \coprod_{i \in I} k_i \rightarrow k$ to the object k , where $\coprod_{i \in I} k_i$ is the coproduct of objects k_i , $i \in I$. Due to the properties of coproducts, there exists a canonical morphism $w_s: \alpha_s \rightarrow \beta_n$ from the fibered product α_s , $s: [n] \rightarrow I$, to the $(n+1)$ -fold fibered product β_n of objects $\coprod_{i \in I} k_i$ over k . This morphism defines a homomorphism $h_A^n: C^n(\beta, A) \rightarrow C^n(\alpha, A)$ of cochains and a homomorphism $h_A^*: \{h_A^n: C^n(\beta, A) \rightarrow C^n(\alpha, A) \mid n \in \mathbb{Z}\}$ of

THE 11th ANNUAL STUDENT SCIENTIFIC CONFERENCE IN ENGLISH
Vladivostok, May 2024

cochain complexes.

The presentation demonstrates that if the category K is distributive and the presheaf possesses the property $A(\coprod_{i \in I} k_i) = \prod_{i \in I} A(k_i)$, then the homomorphism h_n^* of cochain complexes is an isomorphism. This isomorphism, in turn, establishes an isomorphism of the cohomologies $H^n(\alpha, A) \cong H^n(\beta, A)$ of the family alpha and the single-element family beta with coefficients in the abelian presheaf A.

The work was performed at the Far Eastern Center for Mathematical Research with the financial support of the Ministry of Science and Higher Education of the Russian Federation, agreement No. 075-02-2024-1440 dated February 28, 2024, for the implementation of programs for the development of regional scientific-educational mathematical centers.

References

1. Skurikhin E.E. Sheaf cohomologies and the dimension of uniform spaces // Advances in Mathematical Sciences. 2003. Vol. 58. No. 4 pp. 157–158.

Vasileva N.B.¹, Pugach P.A.¹

**TRAINING OF THE APPLIED AI "RAZUM AI" ALGORITHMS FOR FINDING
THE SHORTEST SPANNING TREES**

¹Far Eastern Federal University, Institute of Mathematics and Computer Technologies, FEFU

² Far Eastern Federal University, Oriental Institute - School of Regional and International Studies, FEFU
Scientific adviser – A.L. Abramov ¹
Scientific consultant - E.V. Kravchenko²

Graph shortest spanning tree is subgraph an acyclic, connected subgraph of a graph that contains a set of vertices of the original graph [1, c. 10; 2, c. 43; 3, c. 18, c. 26].

In 2023-2024 work was carried out to train the applied AI “BAUM AI” on algorithms for finding the shortest spanning trees. In 2023, the BAUM AI system came under the management of AiB LLC and became a part of the RAZUM AI software.

The RAZUM AI platform, which included the AI “BAUM AI”, uses a combination of an optimized hardware platform and unique software for processing structured and unstructured data, that allows everyone train artificial intelligence models to solve problems of creating knowledge bases, predictive analytics in the field of industry, education, healthcare and others [4].

Pipelines and algorithms for automation of processing, transformation of graph data and interactive problem solving on networks and graphs and their visualization, hosted on an artificial intelligence platform and/or framework, are created for forecasting and planning in the field of national economy, bioeconomy, protection and management of natural bioresources (hereinafter - PAIA) [5-8].

PAAI is a universal tool designed to find the shortest spanning tree and visualize it.

The following operations are performed as part of the pipeline blocks:

1. Loading adjacency matrix block settings.
2. Adding a *.xlsx file for download.
3. Algorithm block settings.
4. Visualization block settings.
5. Start testing the algorithm.
6. View a graph with the shortest spanning tree.
7. View a report on the work of the algorithm.

Based on the graph adjacency matrix, the following search algorithms are used to find the shortest

THE 11th ANNUAL STUDENT SCIENTIFIC CONFERENCE IN ENGLISH

Vladivostok, May 2024

spanning tree of the original graph, which work with undirected graphs – MST (Kruskala) and MST (Prima) [9; 10; 11, c. 492—498].

It is possible to build a complex pipeline with the same initial conditions, but different algorithms (Fig.1).

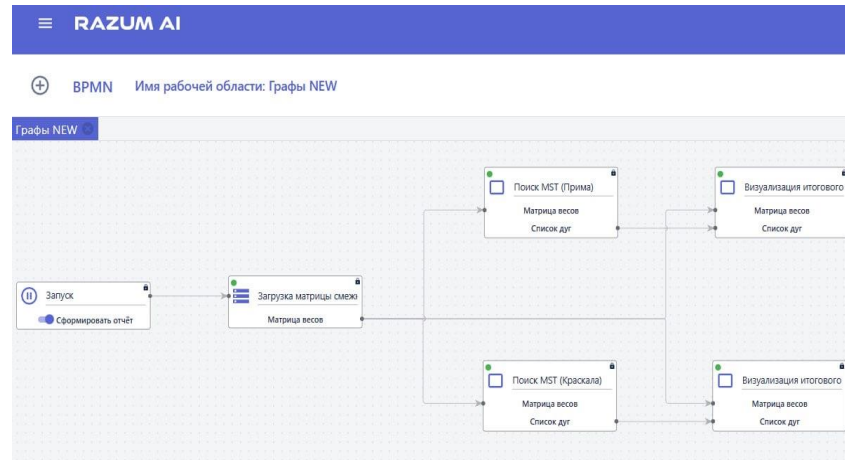


Figure 1. View of the complex pipeline

We should click the “Start” button to start the algorithm run. The process of running the algorithm is sequential. Indication on the block informs about the status of the block: "yellow" - the block is working, "green" - the block has completed its work.

The visualization block builds a graph (MST (Prima)), which is located in the upper right corner in the “Images” section. The graph with the shortest spanning tree is highlighted in green (Fig. 2).

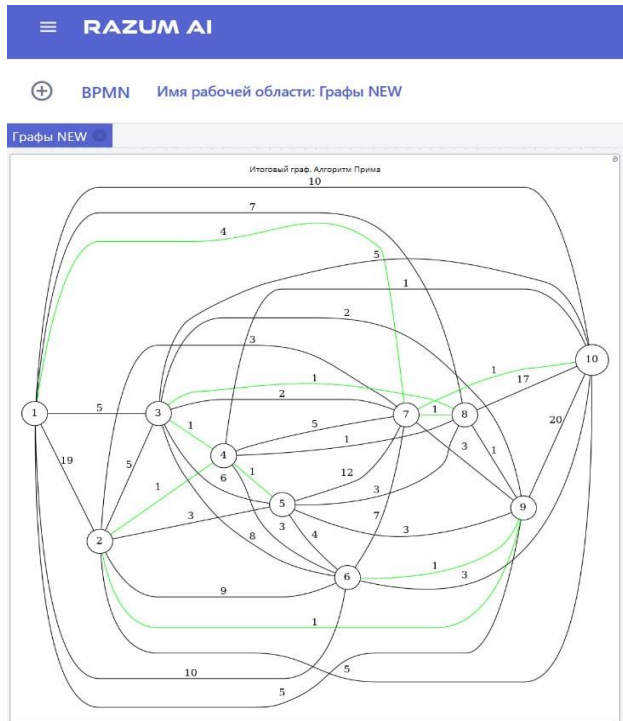


Figure 2. The graph with the shortest spanning tree

The developed pipeline blocks provide the following capabilities to users:

- interactive search for the shortest chains and the shortest spanning tree using artificial intelligence;
- loading initial tabular data with information;
- visualization of an interactive solution to the problems of finding the shortest chains and the shortest spanning tree in the form of graph models using artificial intelligence [12].

Further use of the results obtained is expected in relation to forecasting and planning in the field of regional and municipal management, national economy, bioeconomy, protection and management of natural

THE 11th ANNUAL STUDENT SCIENTIFIC CONFERENCE IN ENGLISH
Vladivostok, May 2024

biological resources in the Far East.

The work was carried out with the financial support of the Ministry of Science and Education of the Russian Federation and the achievement of the results of the federal project "Advanced Engineering Schools" (No. 075-15-2022-1143 dated 07/07/2022) within the framework of an agreement concluded by the Advance Engineering School "Institute of Biotechnology, Bioengineering and Food Systems" of the Far Eastern Federal University and Bauman Moscow State Technical University.

References:

1. Alekseev V.E., Zakharova D.V. Graph theory: Textbook // Nizhny Novgorod: Nizhny Novgorod State University. 2017. 119 p.
2. Omelchenko A. V. Graph theory // M.: MTsNMO. 2018. 416 p.
3. Karpov D.V. Graph theory// M.: MTsNMO. 2022. 555 p.
4. RAZUM AI // Of. RAZUM AI website. URL: <https://ai-aib.ru/> (access date: 05/01/2024).
5. Vasileva N.B. "BAUM AI" applied artificial intelligence training on graph models for cities / The 10 th annual student scientific conference in English, Vladivostok, May 2023 [Electronic resource]: conference proceedings / Chief editor V.Y.Ermachenko. Electr. dat. Vladivostok: Far Eastern Federal University, 2023. Uniform Resource Locator: https://www.dvfu.ru/institute_of_high_technologies_and_advanced_materials/Conferences/. p 111 – 113.
6. Vasilyeva N. B., Pugach P. A. Applied AI "BAUM AI" training on graph models of cities / Materials of the Regional scientific and practical Conference of students, postgraduates and young scientists in natural sciences, Vladivostok, April 15 – May 10, 2023 [Electronic resource] / Ed. by V.Y. Ermachenko. Electron. dan. Vladivostok: Far Eastern Federal. Univ., 2023. Access mode https://www.dvfu.ru/institute_of_high_technologies_and_advanced_materials/Conferences/ / p. 139 – 141.
7. Certificate of state registration of a computer program RU 2023682957. Interaktivnii poisk kratchaishih putei v graphovih modelyah gorodov dlya apparatnoi platformi iskusstvennogo intellekta BAUM AI [Interactive search for shortest paths in graph city models for the BAUM AI hardware artificial intelligence platform]. Abramov A. L., Vasilyeva N. B., Velichko A. S., Pugach P. A. Declared 20.02.2012. Published 01.11.2023. (In Russian).
8. Database Registration Certificate RU 2023623074. Baza graphovih modelei gorodov Rossii s chislennost'yu naseleniya sviske 100 tisyach chelovek [Database of the Russian cities graph models with a population over 100 thousand people]. Abramov A. L., Vasilyeva N. B., GORIK Y.R., Pugach P. A. Declared 28.08.2023. Published 11.09.2023. (In Russian).
9. Joseph. B. Kruskal. On the Shortest Spanning Subtree of a Graph and the Traveling Salesman Problem // Proc. A.M.S. 1956. Vol 7, No. 1. pp. 48-50.
10. Belousov A.I., Tkachev S.B. Discrete mathematics // M.: MSTU, 2006. 744 p.
11. Cormen, Thomas H., Leiserson, Charles I., Rivest, Ronald L., Stein, Clifford. Algorithms: construction and analysis, 2nd edition // Transl. from English M.: Williams Publishing House, 2011. 1296 p.
12. Velichko, A.S. Abramov, A.L. Anferova, E.N. Matvienko, N.N. Vasilyeva, N.B. Gorik, Yu.R. Pugach, P.A. Podgorny, A.S. Zgurya, D.S. Nedoshivina, A.A. Syzhipova, S.O. Ogneva, M.G. Research report. Development of system analysis and applied artificial intelligence algorithms for forecasting and planning in the field of national economy, bioeconomy, protection and management of natural biological resources. Stage 2. Code 9N: Advanced engineering schools. State program of the Russian Federation “Scientific and technological development of the Russian Federation” // Vladivostok: Far Eastern Federal University, 2023. 363 p.

Section V PHYSICS

Amelkina N.O.¹

META-SUBJECT PHYSICAL TASKS

¹Department of General and Experimental Physics of the FEFU Institute of Computer Science and Mathematics

²Far Eastern Federal University, Oriental Institute School of Regional and International Studies, FEFU

Scientific supervisor - T.N. Gnitetskaya¹

Scientific consultant – Yu.O. Kamornaya²

The most important task of the modern education system is the formation of a set of interdisciplinary concepts and "universal educational activities". The former determines the development of interdisciplinary knowledge by students that forms a worldview, the latter ensures the ability to learn. The Federal State Educational Standards of Secondary Education give this concept through the introduction of meta-subject results.

Meta-subject result is the skills formed in the process of learning, advanced to the level of abilities to perform purposeful independent actions resulted in skills to establish meta-subject connections. [1]

Meta-subject connection arises between the subject content and the element of meta-subject content (or meta-subject situation), and is performed through the system of inter-subject connections. [1]. Fig.1 provides an illustration of the definition of meta-subject connection (MSC) in the form of a construction of the following components: an element of meta-subject content (meta-subject situation), the content of the subject, the object of communication (OC), the communication channel (CC). Meta-subject is a life situation, the outcome of which can be predicted with the help of subject knowledge

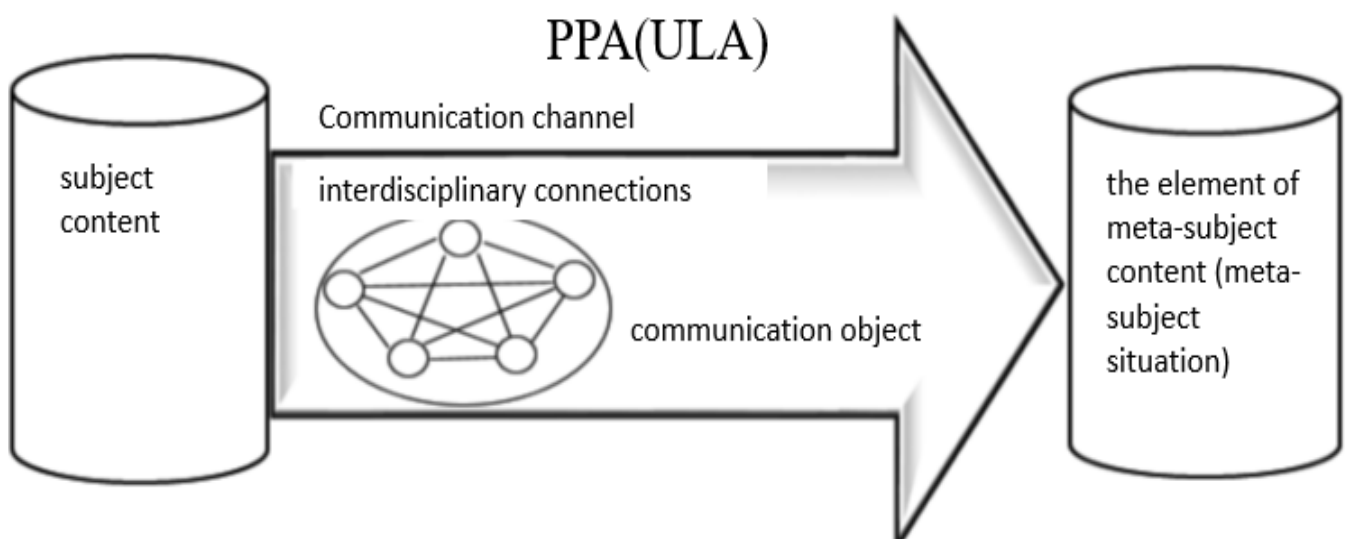


Fig.1. Illustration of the definition of meta-subject connection.

Let's apply this model to a specific meta-subject problem, in which a connection is established between physics and the meta-subject situation where the painter performs his professional actions. The problem goes as follows: "Sergey the painter rocks in the boatswain's chair year after year. Its weight is 500 N, and the rope on the chair has a tensile strength of 300 N. Why doesn't the rope break when it is supported on the left, as shown in Fig.2? One day, Sergey draws near the flagpole and, for a change, ties the free end of the rope to the flagpole, and not to his seat, as shown in Fig. 2 on the right. Why did Sergey eventually leave his job ahead of schedule?"

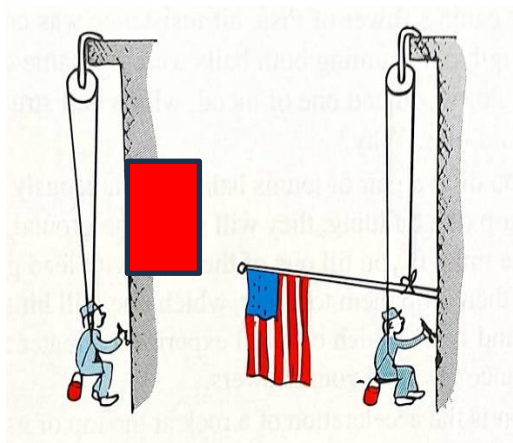


Fig.2. Image of a painter in a chair in different

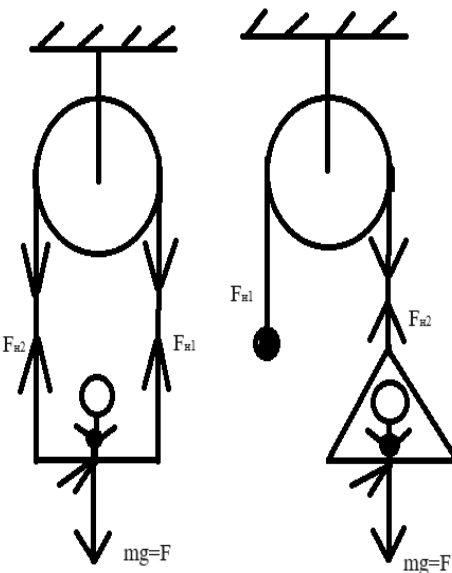


Fig.3. Suspension scheme in two versions suspension options

In order to solve this problem (to obtain a meta-subject result), it is necessary to know that in both the first and second variants of attachment the chair is under the influence of tension forces of the rope directed upwards, and the force of gravity or the weight of the painter directed downwards. In the first case (see Fig. 3 on the left), the sum of the tension forces (250 N each) is 500 N, and the weight of the painter which is 500 N are balanced, so the painter works calmly. In the second case (Fig. 3, on the right), the result of two forces (weight -500 N and thread tension - 300 N) is 200 N and is directed downwards, so the rope breaks, and the fall of the painter is inevitable. Consider the consequences of the painter falling, his retirement ahead of schedule is understandable.

This meta-subject situation can arise in three cases. The first is that the painter did not study physics (meta-subject connection-1). The second one: he did not study safety precautions (meta-subject connection-2), which should contain warning provisions when working at height. The third case: he studied both physics and safety properly, but did not establish obvious interdisciplinary links between them. One of the interdisciplinary connections is established through the concept of the gravitational force of the load acting on the suspension, which must always be equal to or less than the maximum possible tension force of the suspension, otherwise the rope breaks.

Thus, by solving this kind of problems, it is possible to teach the way of establishing of meta-subject connections. Which is considered as the organization of students' achievement of meta-subject results.

References:

1. Gnitetskaya T.N. Model of Meta-Subject Communication on the Example of Physics University in the Era of Pedagogical Innovations: Collection of Articles on the Results of the Second Professorial Pedagogical Forum June 1–4, 2023 Moscow: Russian Professorial Assembly, 2023. 360 p. ISBN 978-5-907588-04-2 (P.113-122).
2. Gnitetskaya T.N., Reznik B.L., Chebotarev A.Yu. - Vladivostok : Dalnevost. Federal. University, 2022. – 254 p. : ill. ISBN 978-5-7444-5142-4. <https://doi.org/10.24866/7444-5142-4>
<https://www.dvfu.ru/upload/medialibrary/66e/whfsjtestvzgzl30h7wksz5qai2vjvv8/МЕТАПРЕДМЕТНОСТЬ%20В%20ОБУЧЕНИИ%20ФИЗИКЕ.pdf>

SEMANTIC STRUCTURING OF THE HALL EFFECT AND ELECTRICAL CONDUCTIVITY¹Department of General and Experimental Physics of Institute of High Technologies and Advanced Materials²Far Eastern Federal University, Oriental Institute School of Regional and International Studies, FEFUScientific supervisor – T.N. Gnitetskaya¹Scientific consultant – Yu.O. Kamornaya²

The presentation of the physical picture of the world plays an important role in the methodology of science teaching. It is not enough to have only general ideas about this or that phenomenon - it is necessary to know the limits of its application and to establish connections with other phenomena. This idea can be demonstrated on the example of kinetic phenomenon in conductors - electrical conductivity, which has both classical theoretical justification and quantum one. The problem to be solved can be formulated as follows: to analyze and structure the way the authors like V. L. Bonch-Bruevich and S. G. Kalashnikov represent the Hall Effect in conductors in the book 'Physics of Semiconductors' [1].

The Hall phenomenon is the emergence of electromotive force ϵ and, as a consequence, the electric field strength \vec{E}_y inside an isotropic homogeneous current – carrying conductor when introduced into an external magnetic field with magnetic induction vector \vec{B} . In the presence of a magnetic field, the Lorentz force \vec{F}_{\perp} , acts on the moving charges perpendicular to the velocity vector and the magnetic induction vector, causing the disorder in electrons motion. In other words, this force does work on the particles, which is the Hall Effect in itself. Fig.1 shows the representation of the Hall Effect by the method of semantic structures [2].

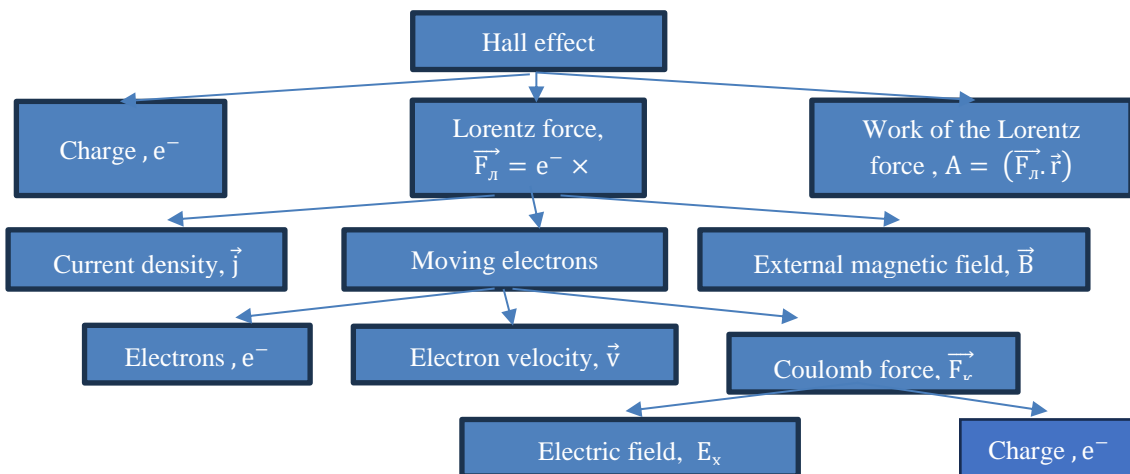


Fig. 1 - semantic structure of the Hall effect

From the Figure it can be seen that the concept of electrical conductivity is not included in the structure. Let us turn to the vector representation of the considered quantities. Before the conductor is introduced into the external magnetic field, there is only an electric field \vec{E}_x , co-directed with the current density vector \vec{j} , but when the transverse field \vec{B} is added to the system under consideration, there is a shift of the resulting intensity vector from the initial direction by an angle φ , called the Hall angle. To determine it, we apply Ohm's law in differential form, where the coefficient of proportionality between the vectors \vec{j} and \vec{E} is the electrical conductivity tensor $\sigma_{\alpha\beta}$. Thus, the phenomenon of electrical conductivity is related to the effect in terms of physical explanation of the possibilities of its application. Figure 2 shows the semantic structure of physical explanation of technical application of the Hall Effect. It is clearly shown that the tensor character of electrical conductivity in conjunction with differential form of Ohm's law determines the applied transformations of the effect, which are practically useful and used in engineering.

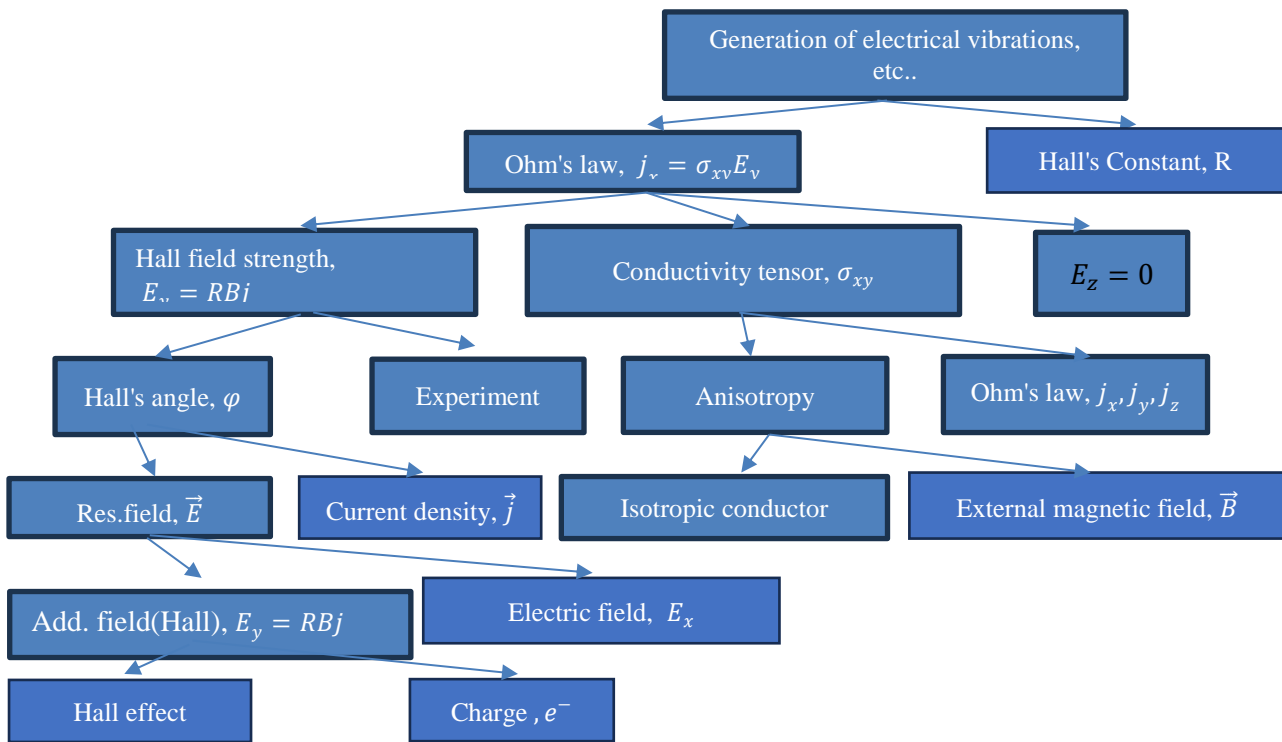


Fig. 2 - structure of physical explanation of technical application of the Hall Effect using electrical conductivity

These include: measuring magnetic field strength, generating and modelling electrical oscillations, amplifying electrical signals, and so on. Thus, the phenomenon of electrical conductivity does not play an important role in the theoretical explanation of the Hall Effect, but it is the leading one in the field of technical applications.

References:

1. V. L. Bonch-Bruevich, S. G. Kalashnikov Physics of Semiconductors / Moscow: Nauka, 1977. - 677 c.
2. Gnitetskaya T.N. Theory of intra-subject and inter-subject links. Monograph / L.L. Afremov, T.N. Gnitetskaya - Vladivostok: Far East University Press, 2005, 176 p.

Gordienko Y.D.¹

ON THE CONCEPTS OF INERTIA AND INERTNOST IN SCHOOL PHYSICS TEXTBOOKS BY DIFFERENT AUTHORS

¹Department of Theoretical and Experimental Physics of Institute of High Technologies and Advanced Materials

²Far Eastern Federal University, Oriental Institute School of Regional and International Studies, FEFU

Scientific supervisor – T.N. Gnitetskaya¹

Scientific consultant – Yu.O. Kamornaya²

In English the physical terms *inertia* and *inertnost* do not differ. Physics courses use a single term *inertia* to describe the inertial properties of bodies.

In Russian physics textbooks introduce two physical concepts, namely *inertia* and *inertnost*, to describe the same properties. Let's look at this problem using the example of a school physics course.

School physics textbooks use the concept of *inertnost* to introduce another physical concept of body mass which different authors determine as a measure of a body. After the introduction of mass, the term *inertnost* disappears from the physics textbooks completely. All the further discussions use the *inertia* term to deal with.

How close is the meaning of the two terms *inertnost* and *inertia*? Do they have the same or different

THE 11th ANNUAL STUDENT SCIENTIFIC CONFERENCE IN ENGLISH
Vladivostok, May 2024

semantics? How do these concepts relate in terms of intra-subject relationships [10]? To answer these questions, we analyzed the definitions of terms given by different authors in physics textbooks for secondary and higher education. We have summarized the definitions themselves in two tables: one for *inertnost* and the other for *inertia*. Considering *inertnost* the definitions can be divided into three groups (see Table 1).

Table 1

Definitions of the concept of *inertnost* by different authors

No	Content of the definition	Source
Group 1. <i>Inertnost</i> as the ability to resist changes in speed		
1	Every body "resists" attempts to change its state of motion. This property of bodies is called <i>inertnost</i> .	I.V. Saveliev
2	Every body resists attempts to set it in motion or change the modulus or direction of its velocity. This property of bodies is called <i>inertnost</i> .	D.V. Sivukhin
3	<i>Inertnost</i> is the property of a body itself to prevent a change in speed.	A.E. Gurevich
Group 2. <i>Inertnost</i> as a result of the interaction of bodies		
4	<i>Inertnost</i> is the property of bodies to change their velocity in different ways during interaction.	A.V. Peryshkin
5	Bodies have some property characterizing their ability to change speed in different ways during interaction. This property of bodies is called <i>inertnost</i> .	N.S. Purysheva
Group 3. <i>Inertnost</i> as a result of external influence		
6	<i>Inertnost</i> is the property of different bodies to change their velocity differently under the same external influence.	V.A. Kasyanov
7	<i>Inertnost</i> is the property of bodies to change their velocity differently under the action of the same force.	G.Y. Myakishev

It should be noted that the interpretation of *inertnost* as the "property of bodies to resist" is given by the authors D.V. Sivukhin [8, p. 69] and I.V. Saveliev [9, p. 58] in the course of general physics, where special explanations are no longer required – the concept was introduced at school. The second group includes the definitions of the authors of textbooks for grades 7 such us A.V. Peryshkin [3, p. 54], N.S. Purysheva [4, p. 52]. These definitions do not specify how bodies interact exactly: between each other or with other bodies. The third group consists of two definitions given by G.Y. Myakishev [2, p. 66] and V.A. Kasyanov [1, p. 77]. Kasyanov's definition is more preferable because it clarifies that the interacting bodies must be different.

The first four definitions in Table 2 are taken from physics textbooks of different years of study: 10th grade [1, p. 84], [2, p. 69], 7th grade [3, p. 57], [4, p. 53], [6, p. 45] and 9th grade [5, p. 49]. They are all the same in meaning and have a complete form: the phenomenon of preserving the velocity of a body in the absence of external influence. The definition given by V.A. Kasyanov is questionable because it includes the term "Inertial frame of reference" which is studied later in the course.

Table 2

Definitions of the concept of *inertia* by different authors

No	Content of the definition	Source
1	The property of bodies to maintain their velocity in the absence of other bodies acting on them is called <i>inertia</i> of bodies.	G.S. Landsberg
2	The phenomenon of preserving the velocity of a body in the absence of other bodies acting on it is called <i>inertia</i> .	A.V. Peryshkin, N.S.Purysheva, V.V.Belaga
3	The phenomenon of <i>inertia</i> : bodies can move not only under the influence of other bodies, but also by themselves, by <i>inertia</i> .	A.E. Gurevich
4	The phenomenon in which a body retains velocity when other bodies do not act on it is called the phenomenon of <i>inertia</i> .	G.Y. Myakishev

THE 11th ANNUAL STUDENT SCIENTIFIC CONFERENCE IN ENGLISH
Vladivostok, May 2024

5	<i>Inertia</i> is the phenomenon of maintaining a state of motion or rest in relation to an inertial frame of reference in the absence of external influences.	V.A. Kasyanov
---	--	---------------

It can be seen that the meanings of the concepts of *inertnost* and *inertia* are closely related to each other. A new question arises: is it necessary to introduce a local concept of *inertnost* if after the introduction of mass concept, it disappears from the content of physics textbooks? Maybe we can limit ourselves to the concept of *inertia* for the introduction of mass? It can be answered by examining the semantic content of the concept of mass which is the subject of further research.

References:

1. Kasyanov, V. A. PHYSICS. Advanced level. 10th grade / V. A. Kasyanov — 8th ed., stereotypical. — Moscow: BUSTARD, 2020 — 480 c.
2. Myakishev, G. Y. PHYSICS. 10th grade. Textbook for general education organizations / G. Y. Myakishev, B. B. Bukhovtsev, N. N. Sotsky — Moscow: Enlightenment, 2014 — 416 p.
3. Peryshkin A.V. PHYSICS. 7th grade. Textbook for general education institutions / Peryshkin A.V. — 2nd ed., stereotypical. — Moscow: BUSTARD, 2013 — 221 c.
4. Purysheva, N. S. PHYSICS. 7th grade. Textbook for general education institutions / N. S. Purysheva, N.E. Vazheevskaya — 2nd ed., stereotypical. — Moscow: BUSTARD, 2013 — 222c.
5. Gurevich, A. E. PHYSICS. 9th grade. Textbook for general educational institutions / A. E. Gurevich — Moscow: BUSTARD, 2001 — 288 p.
6. Belaga, V. V. PHYSICS. 7th grade. Textbook for general educational institutions / V. V. Belaga, I. A. Lomachenkov, Yu. A. Panebrattsev — 2nd ed., stereotype. — Moscow: Prosveshchenie, 2014 — 144 p.
7. Elementary physics textbook: Textbook. In 3 vols. Vol. 1. Mechanics. Warmth. Molecular Physics / Edited by G.S. Landsberg. - 14th ed. — M.: FIZMATLIT, 2010. — 612 p.
8. Sivukhin D. V. General course of physics. Study guide: for universities. In 5 vols. T. I. Mechanics. - 4th ed., stereot. — M.: FIZMATLIT; MIPT Publishing House, 2005. - 560 p.
9. Saveliev, I. V. Course of general physics, volume 1, Mechanics. Textbook / I. V. Savelyev — 6th ed., stereotypical. — St. Petersburg: Lan, 2021 — 340 p.
10. Gnitetskaya T.N. Intrasubject connections in teaching physics: monograph / T.N. Gnitetskaya, Yu.E. Shutko ; D— Vladivostok : Publishing House of the Far Eastern Federal. unita, 2023. — 212 with DOI <https://doi.org/10.24866/7444-5575-0>

Didenko Y. P.¹, Shut M. V.¹, Sorokin M. A.^{1,2}

HYDROLOGY INHOMOGENEITY INFLUENCE ON SOUND PROPAGATION IN SHALLOW SEA WAVEGUIDES

¹Far Eastern Federal University, the Institute of Mathematics and Computer Technologies

² Pacific Oceanological Institute FEB RAS

³Far Eastern Federal University, Oriental Institute School of Regional and International Studies, FEFU

Scientific advisor - V. I. Il'ichev²

Scientific consultant – Yu.O. Kamornaya³

Underwater sound propagation is mainly influenced by two factors: bathymetry, i.e. the relief of the ocean bottom, and hydrology, i.e. sound speed distribution in water column, including the depth of underwater sound channel. Despite the fact that in shallow sea waveguides the main influence on sound propagation is caused by the bottom shape [1], heterogeneity of the underwater environment plays an important role in forming the sound field

**THE 11th ANNUAL STUDENT SCIENTIFIC CONFERENCE IN ENGLISH
Vladivostok, May 2024**

too. This, in its cases, is very important for the problems related to underwater navigation.

The goal of the current research was to investigate how changing the parameters of underwater sound channel depth affects the sound propagation in shallow sea waveguide with the flat bottom. The modelling [2] of sound propagation was performed with varying the parameter z , which corresponds to the depth of the minimum of underwater sound channel. In all the cases sound source was placed at the fixed depth. Then the shape of underwater sound channel was varied whilst keeping its minimum at a constant depth.

The relation of sound field $TL(z)$ at the depth of the signal source was researched for different waveguide configurations. It was found that the sound field $TL(z)$ depends on the depth of the minimum of underwater sound channel (Fig.1). An unusual effect of propagation loss being lower when the sound channel minimum is higher than the signal source was discovered. The application of such physical effects in problems of acoustical navigation has been discussed.

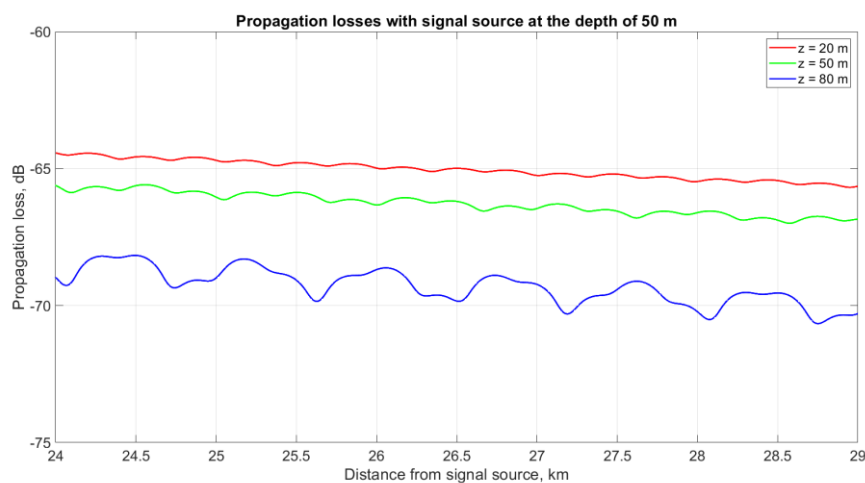


Fig.1. Propagation losses with respect to the depth of underwater sound channel's minimum z .
Signal source is at the depth of 50 m.

References:

1. Experimental and Theoretical Study on Arrival Times and Effective Velocities in the Case of Long-range Propagation of Acoustical Pulses along the Shelf Edge in a Shallow Sea, Petrov P. S. Golov A.A. Bezotvetnykh V. V., Burenin A. V., Kozitskiy S.B., Sorokin M. A., Morgunov Yu.N. // Acoustical Physics. 2020. V. 66. № 1. p. 20-33.
2. F. Jensen, W. Kuperman, M. Porter, H. Schmidt. Computational ocean acoustics. - Springer, New-York et al, 2011. - 794 p.

Sokirkina D. V.¹, Tkachenko P. D.¹, Skorobogatov D. E.¹, Sorokin M. A.^{1,2}

**BATHYMETRY INHOMOGENEITY INFLUENCE ON SOUND PROPAGATION IN SHALLOW SEA
WAVEGUIDES**

¹ Far Eastern Federal University, the Institute of Mathematics and Computer Technologies

²Pacific Oceanological Institute FEB RAS

³Far Eastern Federal University, Oriental Institute School of Regional and International Studies, FEFU

Scientific advisor - V. I. Il'ichev²

Scientific consultant – Yu.O. Kamornaya³

Underwater sound propagation is influenced by two main factors: bathymetry, or seabed topography, and hydrology. It is considered that the bathymetry inhomogeneities have more significant influence on sound

THE 11th ANNUAL STUDENT SCIENTIFIC CONFERENCE IN ENGLISH
Vladivostok, May 2024

propagation [1], than the hydrological inhomogeneities. The goal of the study was to give a qualitative description of this influence.

The modelling of sound propagation [2] was performed for the shallow sea waveguide with complex bottom. The sound speed in the water column and the source depth were constant, and the bottom shape was described by equation (1), where A is a magnitude of bathymetry disturbance:

$$h = h_0 + A * \sin\left(2\pi * \frac{x}{L}\right) \dots \quad (1)$$

The mechanism of sound field formation in ocean waveguides with complex seabed was studied, and the results for different values of parameter A were obtained (Fig.1). Canalization of sound field was detected near peaks of bathymetry. With increasing of curvature, the area occupied by geometrical shadow, where an absence of sound can be noted, is noted to also increase.

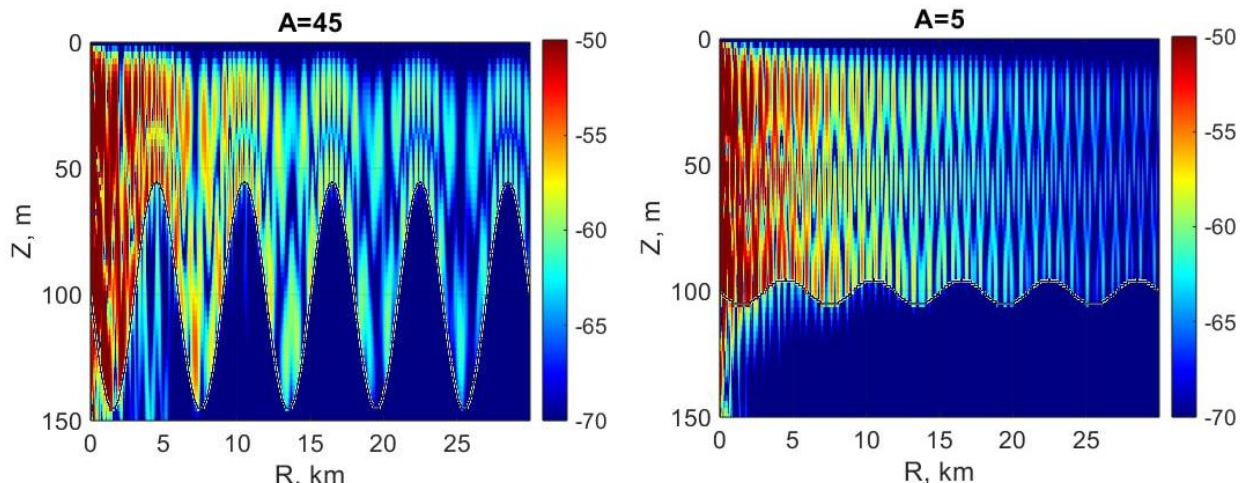


Fig. 1. Sound propagation for different values of parameter A.

References:

1. Experimental and Theoretical Study on Arrival Times and Effective Velocities in the Case of Long-range Propagation of Acoustical Pulses along the Shelf Edge in a Shallow Sea, Petrov P. S. Golov A.A. Bezotvetnykh V. V., Burenin A. V., Kozitskiy S.B., Sorokin M. A., Morgunov Yu.N. // Acoustical Physics. 2020. V. 66. № 1. p. 20-33.
2. F. Jensen, W. Kuperman, M. Porter, H. Schmidt. Computational ocean acoustics. - Springer, New-York et al, 2011. - 794 p.

Lisovitckii.A.S.¹

POSSIBLE EARTHQUAKE PRECURSORS IN THE EARTH'S CRUST MICRO DEFORMATIONS

¹Far Eastern Federal University, Institute of the World Ocean, FEFU

²Institute of High Technologies and Advanced Materials, FEFU

Scientific adviser –L.G. Moskovchenko²

Scientific consultant - L.G. Moskovchenko²

Fractal analysis of time series of micro-deformations of the Earth's crust was performed. The data are recorded by laser strainmeters during seismic quiet and active periods. The data are studied to identify long-term effects associated with changes in the Earth's crust during the preparation period of tectonic earthquakes. The analysis is performed by the multifractal analysis of fluctuations (MF-DFA) method, as well as by one of the methods for measuring fractal lengths developed by Higuchi.

The Earth's crust exists in the state of self-organized criticality (SOC), meaning it evolves to a stable state

THE 11th ANNUAL STUDENT SCIENTIFIC CONFERENCE IN ENGLISH
Vladivostok, May 2024

characterized by fractality, where parts of the object resemble the whole. Time series of crustal micro-displacements reflect this characteristic property, which stipulates the importance of studying their fractal characteristics [1].

The data were taken from three strainmeters of the Pacific Oceanological Institute. V.I Ilyichev, located at the M. Schultz." The strainmeters are located as follows: the first one is oriented in the north-south direction and is located on a sandy base; the second one is in the west-east direction and is located on a sandy base; the third is similar to the first, but is located on a rocky base [3]. Data obtained during quiet seismic periods from 01.04 to 31.06.2017 and active periods from 1.01 to 31.03.2022, 1.12 to 28.02.2023, and 1.12 to 29.02.2024, during which earthquakes of magnitude up to 6 occurred, was selected for the analysis. The collected data underwent decimation and then underwent special filtration to remove device voltage drops.

The analysis of the time series is conducted using the MF-DFA method, which consists of several stages [2].

Stage 1: Compute the fluctuation profile.

$$Y(k) = \sum_{i=1}^k [z(i) - \bar{z}] \quad (1)$$

Stage 2: Divide the profile Y(k) into non-overlapping segments of equal length s. The same procedure is repeated from the opposite end.

Stage 3: Calculate the local trend for each of the 2Ns segments using the method of least squares. Then, determine the variance F^2(v,s).

Stage 4: Average all segments to obtain q-th order fluctuation functions.

$$F_q(s) \equiv \left\{ \frac{1}{s} \sum_{v=1}^{2N_s} [F^2(v,s)]^{q/2} \right\}^2 \quad (2)$$

Where q can only take real values.

The value of h(0) cannot be directly determined; instead, a logarithmic averaging procedure is used.

$$F_0(s) \equiv \exp \left\{ \frac{1}{4N_s} \sum_{v=1}^{2N_s} \ln[F^2(v,s)] \right\} \quad (3)$$

Stage 5: Determination of the scaling behavior of the fluctuation functions by analyzing the plots of each q value plotted against F_q(s) and s on logarithmic scales [2]. Determination of multifractal characteristics (scaling exponents, singularity exponent, generalized fractal dimensions).

$$F_q(s) \sim s^{h(q)}; \tau(q) = h(q) * q - 1; h(q) = \frac{d\tau(q)}{dq} \quad (4)$$

The method of fractal lengths belongs to the group of fractal analysis methods based on measuring the length of a fractal curve. In the variant proposed by T. Higuchi, for each δ, the calculation of L(δ) is performed δ times. For each Xmk, the length of the curve is determined as follows:

$$L_m(k) = \left\{ \left(\sum_{i=1}^{\left[\frac{N-m}{k} \right]} |X(m + ik) - X(m + (i-1) \cdot k)| \right) \frac{N-1}{\left[\frac{N-m}{k} \right] \cdot k} \right\} / k \quad (5)$$

N is the number of points, m is the initial displacement, and k is the scale (time interval). Finally, the length of the curve for the time interval k is determined as the arithmetic mean.

THE 11th ANNUAL STUDENT SCIENTIFIC CONFERENCE IN ENGLISH
Vladivostok, May 2024

$$\langle L(k) \rangle = \frac{\sum_{m=1}^k L_m(k)}{k} \quad (6)$$

The length of the curve is determined as the arithmetic mean over k points, each of which is equal to $L_m(k)$ [2].

As a result, a series of graphs describing the behavior of multifractal characteristics of the time series from each strainmeters during both quiet and active periods were obtained, as well as a series of graphs depicting fractal dimensions obtained from the Higuchi method. Dates and energies of the earthquakes that occurred were added to the graphs.

$$E = 10^{\frac{3}{2}M+4.8} \quad (7)$$

Where E is the energy of the earthquake in J, and M is the magnitude of the earthquakes.

The series of graphs, presented in Figure 1, were obtained as a result of the study. The following conclusions can be drawn:

1. From the series of graphs obtained using the Higuchi method, as seen in Figure 1, there is an increase in fractal dimensionality preceding all earthquakes.
2. One of the significant precursors identified by multifractal analysis is the sharper behavior and increase in oscillation amplitude during the active period preceding earthquakes compared to the seismic quiet period.

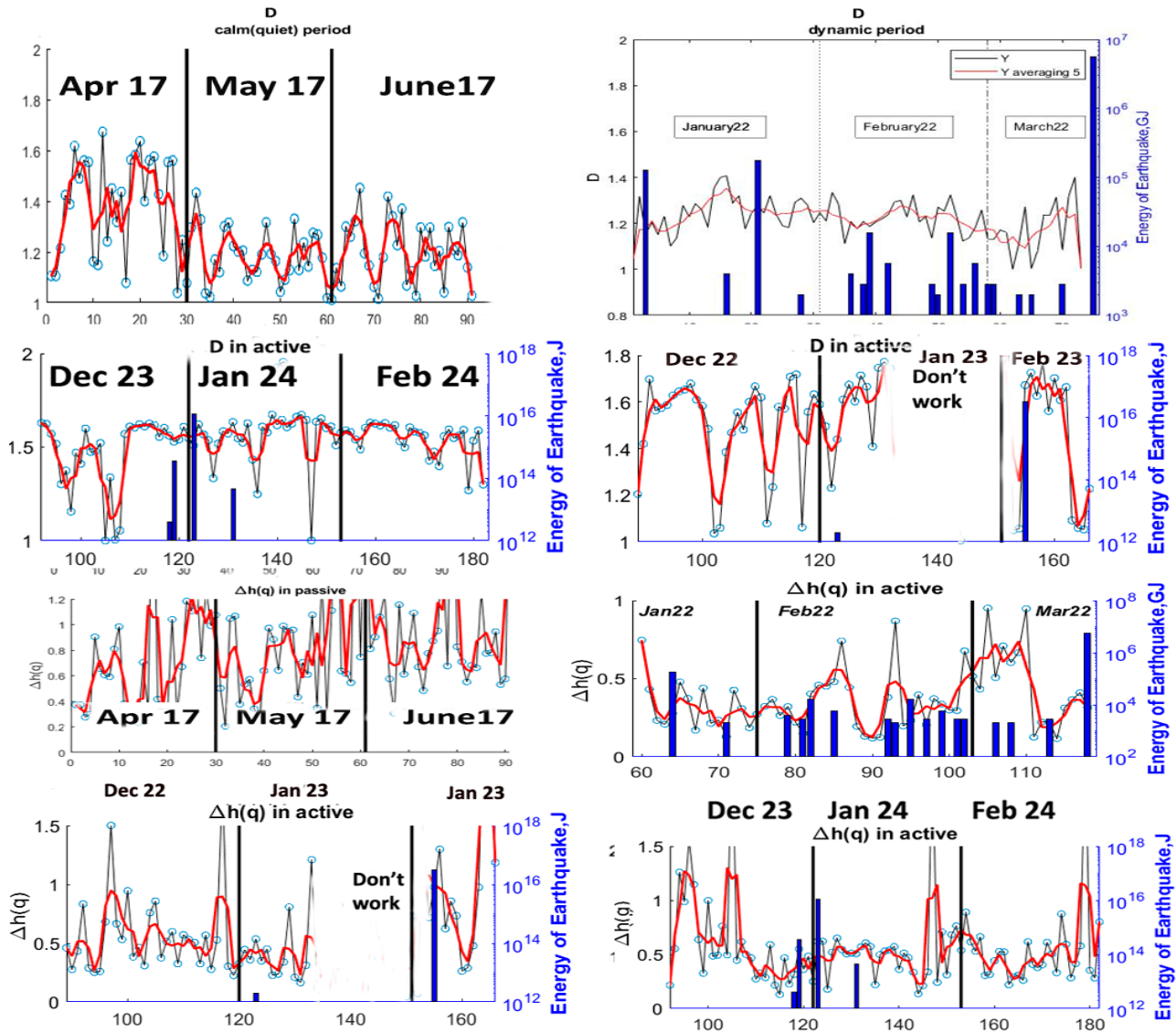


Fig 1. The results of the data analysis from the first strainmeter

THE 11th ANNUAL STUDENT SCIENTIFIC CONFERENCE IN ENGLISH
Vladivostok, May 2024

These conclusions require further refinement and a more detailed investigation. The research findings can be used to enhance the predictive information about impending earthquakes.

References:

1. Bak P., Tang C., Wiesenfeld K. Self-organized criticality — Phys. Rev. B. 1988. —P. 364–374
2. Krylov S.S., Bobrov N.Yu. Fractals in geophysics /Krylov S.S., Bobrov N.Yu. - SPb .: Publishing house of St. Petersburg University, 2004. 132 p
3. G.I.Dolgikh, V.E.Privalov. Laser Physics. Basic and Applied research. – Vladivostok: Reya, 2016. 352p

Stepanov D. V.¹

INVESTIGATION OF THE DIRAC OPERATOR SPECTRUM IN TWO PHASES OF MATTER

¹Far Eastern Federal University, Institute of High Technology and Advanced Materials, FEFU

²Far Eastern Federal University, School of Medicine and Life Sciences, FEFU

³Far Eastern Federal University, Oriental Institute School of Regional and International Studies, FEFU

Scientific adviser - V. A. Goy²

Scientific consultant – Yu.O. Kamornaya³

The fundamental structure of the universe is based on two types of particles: fermions and bosons. In 1928, Paul Dirac derived a relativistic wave equation describing particles with spin $1/2$. The Dirac equation has the following form:

$$\left(mc^2 \alpha_0 + c \sum_{j=1}^3 \alpha_j p_j \right) \psi(\mathbf{x}, t) = i\hbar \frac{\partial \psi}{\partial t}(\mathbf{x}, t),$$

The wave function can be represented as $\psi(\mathbf{x}, t) = \psi_0(\mathbf{x}) e^{-iEt/\hbar}$. Considering this fact, we solve the stationary equation:

$$H\psi_0(\mathbf{x}) = E\psi_0(\mathbf{x}),$$

where $H = mc^2 \alpha_0 + c \sum_{j=1}^3 \alpha_j p_j$.

Hence the energy spectrum of solutions to the Dirac equation:

$$E_{\pm}(p) = \pm \sqrt{(mc^2)^2 + (pc)^2}$$

The Dirac equation is used to describe the dynamics of quarks in the theory of strong interaction (quantum chromodynamics – QCD), which is based on the local symmetry group SU(3). It is impossible to build an analytical solution in the field of a strong coupling constant, therefore numerical research methods are used to study such systems. One of these methods is the lattice regularization of quantum field theory. In this formalism, a discrete Wilson Dirac operator is introduced [1], which has the following form:

$$D(n|m)_{\alpha \beta} = (m + d) \delta_{\alpha, \beta} \delta_{a, b} \delta_{n, m} - \sum_{\mu=\pm 1}^{\pm 4} \frac{1}{2} \left[(1 - \gamma_\mu)_{\alpha \beta} U_\mu(n)_{a b} \delta_{n+\hat{\mu}, m} + (1 + \gamma_\mu)_{\alpha \beta} U_\mu(n - \hat{\mu})^\dagger_{a b} \delta_{n-\hat{\mu}, m} \right]$$

where α, β – Dirac indexes, a, b – color indexes, n, m – space-time coordinates, $U_\mu(n)$ – link variable. The link variable is associated with the 4-potential of the field [2] and has the form:

$$U_\nu(n) = e^{ia A_\nu(n)},$$

**THE 11th ANNUAL STUDENT SCIENTIFIC CONFERENCE IN ENGLISH
Vladivostok, May 2024**

where a – length of the lattice edge, $A_\nu(n)$ – 4-potential.

The spectra of the eigenvalues of the Wilson Dirac operator were found on the $8 * 32$ lattice for the case of free fermions (link variables $U_\mu(n) = 1$) (Fig.1), for the case of the confinement phase (Fig. 2) and deconfining (Fig.3).

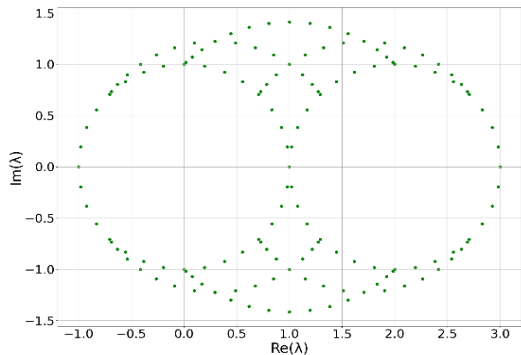


Figure 1 – Spectrum of eigenvalues for the case of free fermions

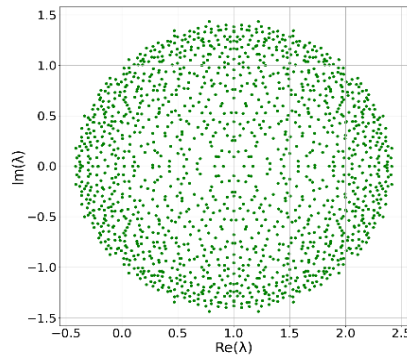


Figure 2 – Spectrum of eigenvalues at $\beta = 0.1$

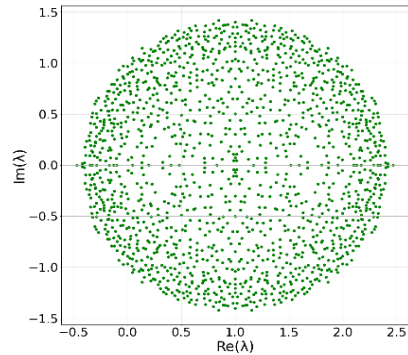


Figure 3 – The spectrum of eigenvalues at $\beta = 100$

The image of the spectrum of eigenvalues of the Dirac operator for the phase of confinement (Fig. 2) and deconfining (Fig. 3) is presented in the form of a circle with a certain internal structure. To identify the existence of a dependence of the internal structure on the phase, the density of the distribution of eigenvalues for 50 link configurations was constructed at $\beta = 100$ (Fig. 4) and $\beta = 0.1$ (Fig. 5). As a result, it was found that the internal structures do not differ at different values of β .

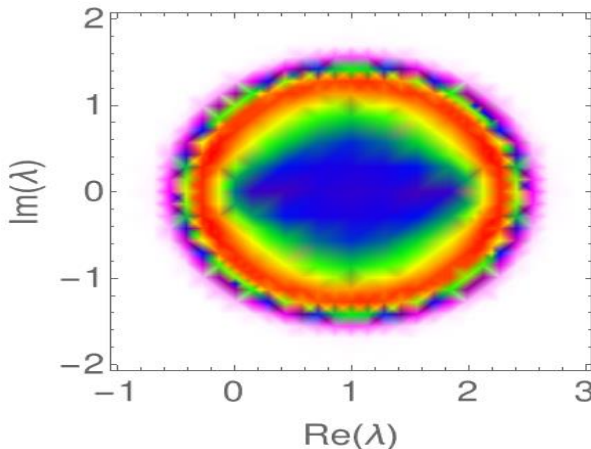


Figure 4 – density of the distribution of eigenvalues at $\beta = 0.1$

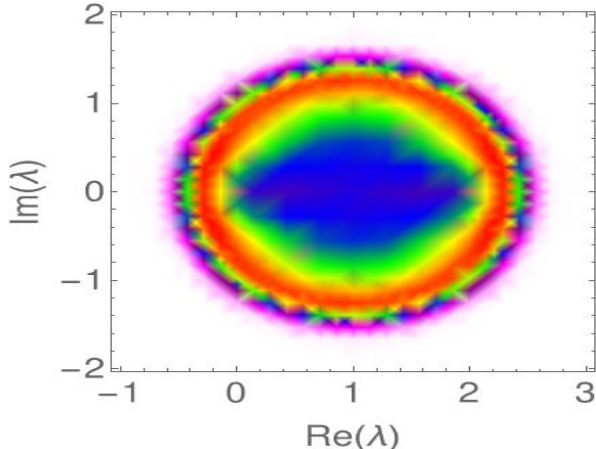


Figure 5 – density of the distribution of eigenvalues at $\beta = 100$

The spectra of the eigenvalues of the Dirac operator within the limits of strong and weak coupling were also obtained. As a result of the analysis of the density distribution of the spectrum of eigenvalues, it was revealed that with a small value of the coupling constant, the spectrum acquires a similar appearance to the spectrum for the case of free fermions.

Within the framework of the lattice gauge theory «1+1» on a lattice with dimensions of $8 * 32$, calculations of the spectrum of eigenvalues of the Wilson Dirac operator at the phases of confinement and deconfining, as well as in the limit of strong and weak coupling, were performed using numerical modeling. As a result of the analysis of the data obtained, it was revealed that the spectrum of eigenvalues of the Dirac operator does not distinguish between the confinement/deconfining phases and senses a change in the coupling constant.

Completed within the framework of the state task of the Ministry of Education and Science of the Russian Federation №FZNS-2024-0002.

THE 11th ANNUAL STUDENT SCIENTIFIC CONFERENCE IN ENGLISH

Vladivostok, May 2024

References:

1. Smit, J. Introduction to Quantum Fields on a Lattice / J. Smit – Cambridge university press, 2003. – 271 p
 2. Gatringer, C. Quantum Chromodynamics on the Lattice / C. Gatringer, C. B. Lang. – Springer, 2010. – 343 p
-

Pochinok A.S.¹, Goy V.A.¹

PARAMETRIZATION OF COUPLE CONSTANTS IN THE ANISOTROPIC LATTICE MODEL

¹Far Eastern Federal University, Pacific Quantum Center

²Université de Tours, Institute Denis Poisson

Scientific adviser – Dr. A.V. Molochkov¹

Scientific adviser – Dr. M.N. Chernodub²

Currently, the investigation of the early Universe, including quark-gluon plasma, stands as one of the forefront tasks in contemporary physics. This field often demands the utilization of non-standard approaches in lattice computations, such as employing asymmetric lattice models. This paper presents the computation of coupling constants on a spatial-temporal lattice exhibiting anisotropy along one of the four designated directions.

In the continuum limit, physical quantities in asymmetric lattices with distinct periods in spatial (a_σ) and temporal (a_τ) directions should be independent of the anisotropy factor $\xi = a_\sigma/a_\tau$. To achieve this, two coupling constants need to be introduced in the lattice action [1, 2]:

$$S = \beta_\sigma \sum_x \sum_{i>j=1}^3 P_{x,ij} + \beta_\tau \sum_x \sum_{i=1}^3 P_{x,4i}, \quad (1)$$

where $P_{x,\mu\nu}$ represents the plaquette variable, β_σ and β_τ the spatial and temporal coupling constants, which are parameterized as:

$$\beta_\sigma = \frac{1}{g_\sigma^2(a, \xi) \xi}, \quad \beta_\tau = \frac{\xi}{g_\tau^2(a, \xi)}. \quad (2)$$

In the symmetric case where $\xi = 1$, the theory reduces to the Euclidean formulation $g_\sigma^{-2}(a, 1) = g_\tau^{-2}(a, 1) = g_E^{-2}(a)$ and

$$\beta_\sigma(a, 1) = \beta_\tau(a, 1) = \frac{\beta}{6} = \frac{1}{g_E^2(a)}, \quad (3)$$

where a represents the lattice spacing, and β the coupling constant of the Euclidean lattice.

For an asymmetric lattice where $\xi \neq 1$, the equality in equation (3) is violated. However, in the weak coupling limit, the coefficients $g_{\sigma;\tau}^{-2}$ can be expanded around the symmetric value g_E^{-2} :

$$\frac{1}{g_\sigma^2(a, \xi)} = \frac{1}{g_E^2(a)} + c_\sigma(\xi) + O(g_E^3), \quad (4a)$$

$$\frac{1}{g_\tau^2(a, \xi)} = \frac{1}{g_E^2(a)} + c_\tau(\xi) + O(g_E^3). \quad (4b)$$

In equations (4 a, b), the term $O(g_E^3)$ is neglected, following the approach in reference [1], while the coefficients $c_\sigma(\xi)$ and $c_\tau(\xi)$ are computed as:

THE 11th ANNUAL STUDENT SCIENTIFIC CONFERENCE IN ENGLISH
Vladivostok, May 2024

$$c_\sigma(\xi) = 4N \left[\frac{N^2 - 1}{24N^2} \left\{ I_1(\xi) - \frac{3}{4} \right\} - \frac{5}{288} I_{2a}(\xi) + \frac{1}{48} I_3(\xi) + \frac{1}{128} I_4(\xi) + \frac{11}{12} FIN(\xi) + 0.010245 \right], \quad (5a)$$

$$c_\tau(\xi) = 4N \left[\frac{N^2 - 1}{16N^2} \left\{ \frac{1}{3\xi^2} I_1(\xi) + \frac{1}{\xi} I_5(\xi) - \frac{1}{2} \right\} + \frac{1}{64} I_{2b}(\xi) - \frac{5}{576} I_{2a}(\xi) + \frac{1}{256\xi^2} I_4(\xi) - \frac{1}{48\xi^2} I_6(\xi) - \frac{1}{192\xi^2} I_7(\xi) + \frac{11}{12} FIN(\xi) + 0.010245 \right], \quad (5b)$$

The integrals $I_1(\xi) - I_7(\xi)$ in equations (5a) and (5b) are provided in references [1, 2], while $FIN(\xi)$ represents the difference of divergent integrals $FIN(\xi) = DIV(\xi) - DIV(1)$:

$$DIV(\xi) = (2\pi)^{-4} \int_{-\pi/2}^{\pi/2} d^3x \int_{-\pi\xi/2}^{\pi\xi/2} dx_4 \left(\sum_{i=1}^3 \sin^2 x_i + \xi^2 \sin^2(x_4/\xi) \right)^{-2}. \quad (6)$$

Spatial and temporal coupling constants for the anisotropic lattice were computed for β ranging from 5.6924 to 6.5, akin to the methodology outlined in reference [3], within the range of ξ from 0.9 to 1.1 with a step of 0.01. The results are depicted in Figure 1.

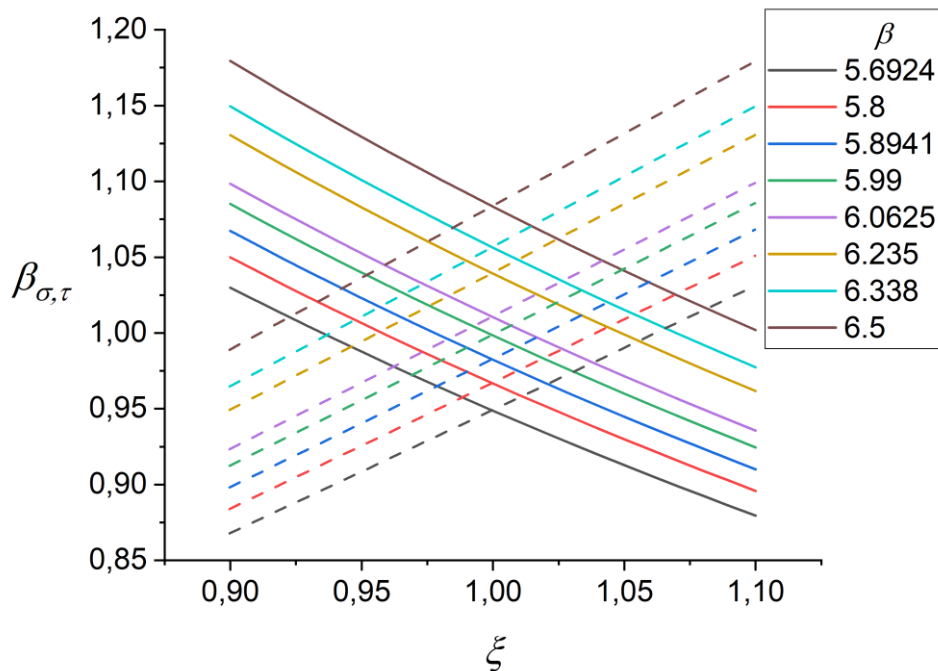


Fig. 1. Distribution of spatial and temporal coupling constants for the asymmetric lattice
(solid line - β_σ , dashed line - β_τ).

References:

1. Karsch F. SU (N) gauge theory couplings on asymmetric lattices //Nuclear Physics B. – 1982. – T. 205. – №. 2. – C. 285-300.
2. Hasenfratz A., Hasenfratz P. The scales of Euclidean and Hamiltonian lattice QCD //Nuclear Physics B. – 1981. – T. 193. – №. 1. – C. 210-220.
3. Athenodorou A., Teper M. The glueball spectrum of SU (3) gauge theory in 3+ 1 dimensions //Journal of High Energy Physics. – 2020. – T. 2020. – №. 11. – C. 1-77.

Tsuranova M.E.¹

PHOTOMETRIC STUDIES OF THE CATACLYSMIC VARIABLE YZ CNC STAR

¹Far Eastern Federal University, Institute of High Technologies and Advanced Materials, FEFU

²Far Eastern State Technical Fisheries University, FESTFU

³Far Eastern Federal University, Oriental Institute, School of Regional and International Studies, FEFU

Scientific adviser - L.G. Moskovchenko^{1,2}

Scientific consultant – Yu.O. Kamornaya ³

The process of photometric research aimed at studying of changes in the luminosity of the cataclysmic variable YZ Cnc star in the constellation Cancer is represented.

Cataclysmic variable stars (CVSs) are physical variable stars that have the following features:

- a close binary system composed of a white dwarf and a main sequence star or a slightly evolved subgiant;
- the presence of regular or single (depending on the type of CVS) flares;
- accretion from a companion star onto a white dwarf.

The causes of outbreaks differ for different types of CVSs. For example, the flare activity of novae and supernovae is caused by thermonuclear reactions on the surface or inside the star. The change in the luminosity of dwarf novae (UG) is the result of an unstable flow of mass in the accretion disk around the white dwarf [4].

There are three subtypes depending on the nature of the change in the luminosity of dwarf novae - UGSS, UGZ and UGSU. Each of them is characterized by regularity of outbursts, the intervals between which for one star cannot be predicted accurately, but for each there is an average value of the cycle. The YZ Cnc star studied in this work belongs to the latter. This type, as well as the UGSS type, is characterized by an increase in brightness of 2-6^m, but several times later “superflares” occur, which are 2^m brighter than usual.

In order to trace the dynamics of changes in brightness, it is necessary to obtain a light curve. For this purpose, photometric studies are carried out, which can be divided into the following stages: 1) observations; 2) photo calibration, noise elimination; 3) photometry, calculation of instrumental magnitude (IM); 4) conversion to real magnitude and construction of a light curve.

In the period from 02.02.2024 to 17.03.2024, the observations of a fragment of the starry sky, including YZ Cnc star were made using the ASTROSIB RC500 telescope located at the Ussurisk Astrophysical Observatory (43°41'58" N 132°09'48" E). The star has coordinates (RA=08 10 56.63, δ= +28 08 33.3) and an average cycle of 12 days.

Over the entire period, due to unfavorable conditions for shooting, it was possible to obtain data from eighteen nights in total. For some nights two series of observations were carried out, for others - one (about forty frames).

Frames ready for photometric analysis, were obtained after calibration, which is carried out by removing noise of a different nature from the image. However, this point of research may also include frame alignment (each star should have the same rectangular coordinates in all images) followed by median averaging of a series of images. These actions were also performed to obtain more compact and visual results.

In order to perform aperture photometry, it is necessary to select several stars on the image with constant magnitude similar to that of the star under study and within close proximity to it to perform comparison. Data on rectangular coordinates are processed automatically. Next, using image analysis tools, the annular aperture of the object and the background aperture are selected (in order to exclude the values of the second from the first). The result of all these procedures is a text file with an estimate of the instrumental magnitudes of all selected stars.

Without considering in detail the process of operation of the CCD matrix used to register radiation, we will limit ourselves to the statement that the instrumental magnitude is a value that depends logarithmically on the flux (accumulated charges converted into a numerical value - counts). The IM must be converted into a real magnitude, knowing the IM of the variable star and comparison stars, as well as their real magnitudes from the catalog.

**THE 11th ANNUAL STUDENT SCIENTIFIC CONFERENCE IN ENGLISH
Vladivostok, May 2024**

After performing all the necessary mathematical calculations, a graph of the dependence of the real stellar magnitude on the HJD value was constructed (Fig. 1).

It is worth noting that the data obtained in the graph, with an error of up to 0.07m, is consistent with the information in the catalog, as well as with theoretical ideas about the type to which the star belongs. Having analyzed the curve, we can assume that all maxima are ordinary flares, and “superflares” characteristic of the UGSU type were not observed during this period.

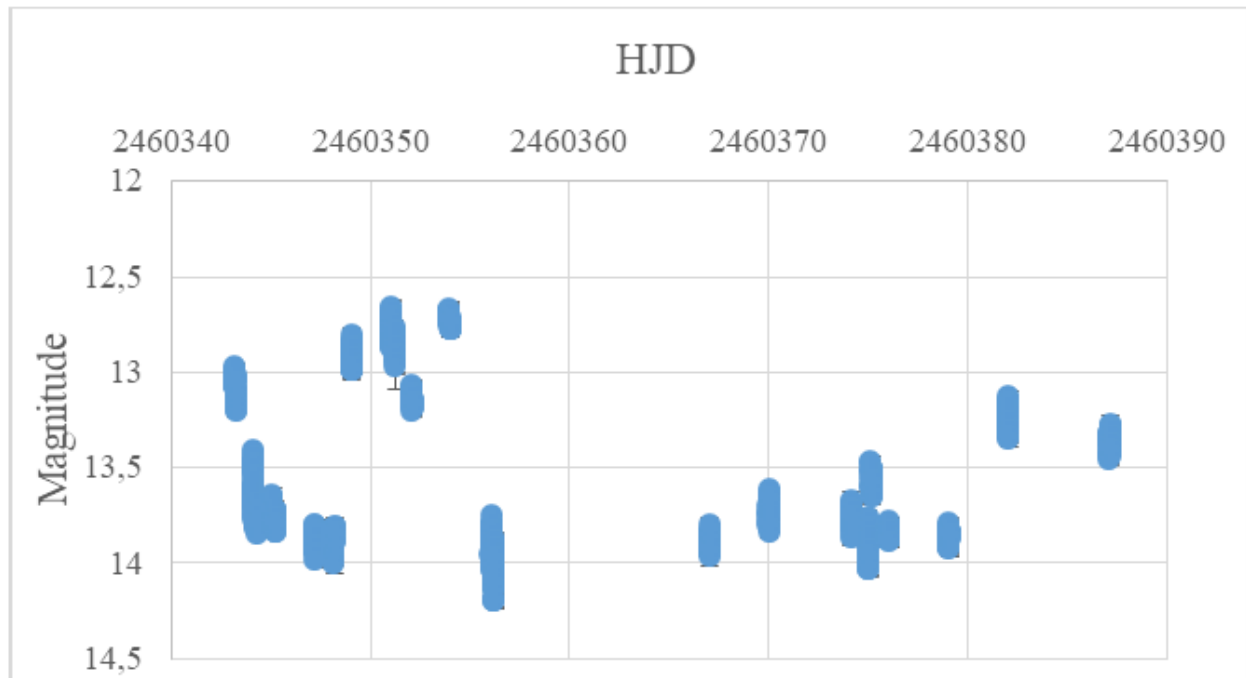


Fig. 1. Light curve of the YZ Cnc star

References:

1. Samus N.N., Kazarovets E.V., Durlevich O.V., Kireeva N.N., Pastukhova E.N., General Catalog of Variable Stars: Version GCVS 5.1, Astronomy Reports, 2017, vol. 61, No. 1, pp. 80-88 {2017ARep...61...80S}.
2. AAVSO database [electronic resource] / AAVSO – Electronic. text data – Access mode: <https://www.aavso.org>, free
3. Zasov A.V., Postnov K.A. General astrophysics. 3rd ed. corr. and additional – Fryazino: Century 2. 2016. – 576 p.
4. Kolbin A.I., Nikolaeva E.A. CCD photometry of variable stars / A.I. Kolbin, E.A. Nikolaev. – Kazan: Kazan. univ., 2023. – 74 p. Access mode: https://kpfu.ru/staff_files/F204820941/phot.pdf
5. Samus N. N. Variable stars, Textbook for the course “Astronomy” [Electronic resource] - Access mode: <http://heritage.sai.msu.ru/ucheb/Samus/index.html>